Origin of the Mertz Drift,
George V Basin, East Antarctica

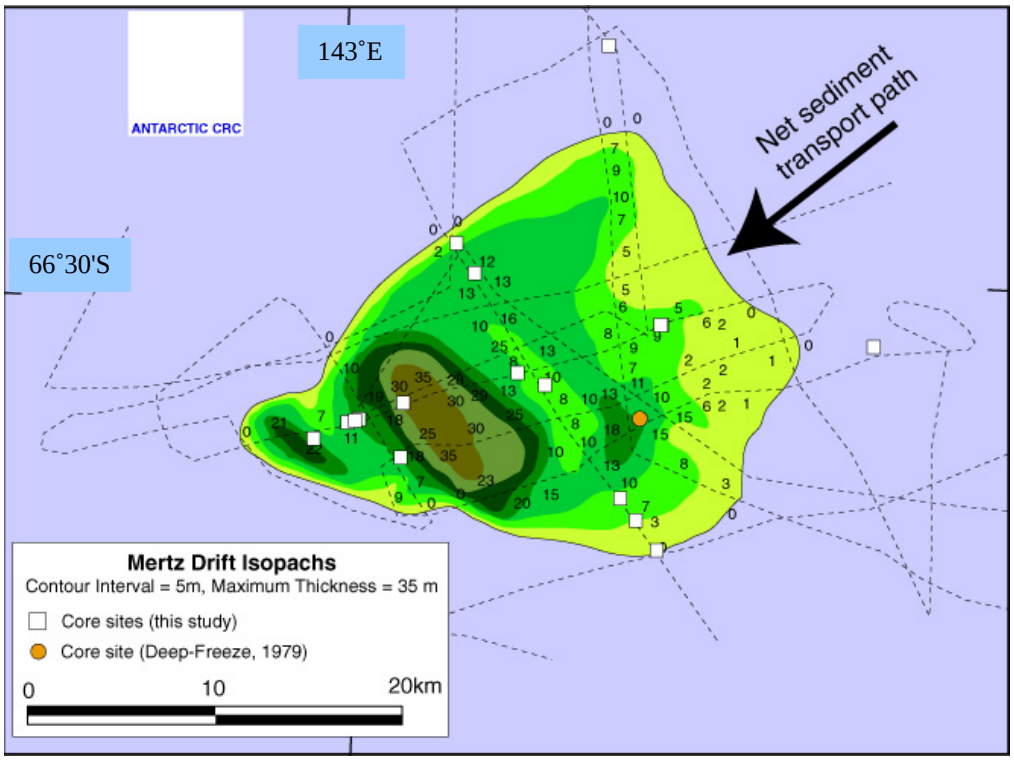

by

Robin J. Beaman B.Sc. (James Cook University)

A thesis submitted in partial fulfillment of the requirements of
the Bachelor of Antarctic Studies with Honours at
the Institute of Antarctic and Southern Ocean Studies (IASOS),
University of Tasmania.

November 2000

Declaration

I hereby declare that this thesis contains no material which has been accepted for the award of any other degree or diploma in any tertiary institution. To the best of my knowledge and belief, the thesis contains no material previously published or written by another person, except where due reference is made in the text of the thesis.

Robin J. Beaman

Abstract

During February-March 2000, a joint Italian/Australian marine geoscience expedition (Project WEGA) discovered and cored a large drift deposit, named the Mertz Drift. The drift is about 390 km^2 in area, and lies in the western end of the George V Basin, East Antarctica. I document a study of the Mertz Drift as the deposit contains an important high-resolution record of palaeoenvironment changes during the Holocene. X-radiographs of cores, visual core logs and multi-sensor core logger data are used to distinguish facies in the cores. A comparison of facies from all cores, radiocarbon ages, thin section analysis and seafloor photographs of the Mertz Drift allowed interpretation of five different facies into four generalised phases of environmental history. A diamicton corresponds to sub-ice shelf, water-lain till deposited during the Last Glacial Maximum, and underlies the Mertz Drift. Unconformably overlying the diamicton is a massively bedded siliceous mud and diatom ooze (SMO) with a high proportion of ice-rafted debris. This unit represents a period of glacial retreat of the ice shelf and a transition to an open marine environment, commencing about 14,000 yr BP and lasting for about 9000 years. A thick succession of laminated and cross laminated SMO follows, deposited during a mid-Holocene climate optimum from 5000 to 3000 yr BP. Overlying the Mertz Drift as a drape is a massively bedded fine sand/SMO with a high proportion of ice-rafted debris, deposited from 3000 yr BP to present. This drape reflects modern oceanographic conditions commencing from a time of climatic deterioration. This study found seasonal changes in diatom assemblages within lamination couplets with mean deposition times of between 2.6 to 4.3 years. Two currents are believed responsible for the construction of the drift. Upwelled Circumpolar Deep Water transports fine grained sediments southwards towards the inner shelf, and deep, high salinity Shelf Water flows northwesterly along the George V Basin, focusing sinking sediments into a drift deposit. A relative reduction of sea ice cover during a climatic optimum is believed to be a key factor for longer periods of upwelled Circumpolar DeepWater over the outer shelf. This leads to a surge in bottom currents and the concentration of greater volumes of sediment into the drift. This study has important implications for oceanographers as the results suggest a non-steady-state of Antarctic Bottom Water production during the Holocene.

Acknowledgements

I would like to thank sincerely my three supervisors for making this enjoyable project possible: Dr Andrew McMinn (IASOS) for offering guidance at crucial times; Dr Leanne Armand (IASOS) for the great support and critique of the thesis; and Dr Peter Harris (Antarctic CRC) for the interesting discussions and making the valuable data available to me in the first place.

I would also like to thank the various scientists who offered insights into their field of work: Dr Karen Gowlett-Holmes (CSIRO) for helping identify benthic fauna from photographs; Dr Nathan Bindoff and Guy Williams (Antarctic CRC) for explaining the complexities of Antarctic water masses; Dr Pat Quilty (Geology) for identifying foraminifera in the thin sections; Dr Rob Massom (Antarctic CRC) for the use of his satellite images of the Mertz Glacier region; and Dr Tom Trull (Antarctic CRC) for explaining productivity and carbon export in the Southern Ocean.

Thank you to Simon Stephens for preparing the thin section samples, and Lisette Robertson, Suenor Woon and Dr Fiona Taylor for assistance in obtaining the X-radiographs of the WEGA cores.

To the great members of the IASOS Bachelor of Antarctic Studies (Honours) 2000 intake, thank you very much for your excellent company, intelligence and experience shared this year. Australia's future science and education is in good hands.

I dedicate this thesis to the patience and moral support given me by my partner Nerida Gray who sacrificed much to join me in Hobart for this year.

Table of Contents

List of Figures and Tables

Tables **Page**

Acronyms and Abbreviations

AABW	Antarctic Bottom Water
AAT	Australian Antarctic Territory
ACC	Antarctic Circumpolar Current
ASW	Antarctic Surface Water
BP	Before Present
CDW	Circumpolar Deep Water
CRC	Cooperative Research Centre
DF79	'Operation Deep Freeze' 1979
EWD	East Wind Drift
GEBCO	General Bathymetric Chart of the Ocean
HSSW	high salinity Shelf Water
IRD	ice-rafted debris
ISW	ice Shelf Water
LGM	Last Glacial Maximum
MCDW	Modified Circumpolar Deep Water
RV	Research Vessel
SMO	siliceous mud and diatom ooze
SW	Shelf Water
TOC	Total Organic Carbon
US	United States of America
WEGA	Wilkes Land Glacial History
WW	Winter Water

Chapter 1. Introduction

1.1 Introduction

In February-March 2000, an Antarctic marine geoscience expedition, led by Drs P.T. Harris from the Antarctic CRC and G. Brancolini from the National Institute for Oceanography and Experimental Geophysics, discovered and mapped a large shelf sediment drift deposit that was named the Mertz Drift. It is similar to deep sea pelagic drift deposits in morphology and structure, however, it is composed of biosiliceous ooze and located within a 850 m depression at the western end of the George V Basin, East Antarctica.

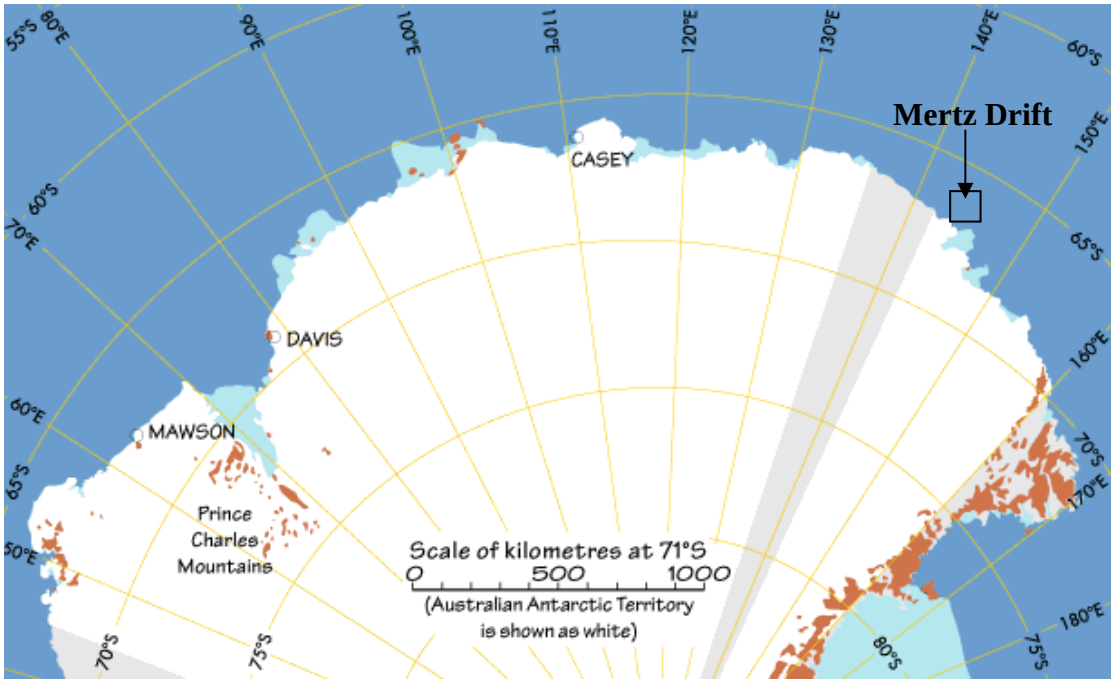

Figure 1.1 Map of East Antarctica showing study site within box (source: Australian Antarctic Division 2000).

The discovery was part of the joint Italian/Australian Research Cruise to study Wilkes Land Glacial History (Project WEGA) aboard the Research Vessel *Tangaroa*. The aim of the WEGA project was to collect detailed sedimentary records from the Terre Adélie and George V Land continental margin, for which little data presently exist. Using multi-channel seismic and chirper seafloor imagery, the research team

mapped the deposit which covered about 390 km^2. The drift is over 30 m thick, with dimensions of about 30 km east to west and 22 km north to south.

Sediment cores collected from the Mertz Drift revealed laminated, olive-green, siliceous mud and diatom ooze (SMO) overlying a glacial-marine diamicton. While the lower SMO sediments are laminated, there is a 20 to 50 cm thick sandy drape at the surface over the whole of the drift. The laminae possibly reflect annual seasonal changes in productivity (Domack 1988). The sandy drape suggests that a recent (late-Holocene) change in the depositional environment had occurred, possibly related to changes in the extent of the nearby Mertz Glacier tongue, current regime and/or the persistence of sea ice over the shelf area (Harris 2000). *Therefore, a study of the origin of the Mertz Drift became the purpose of this thesis, as the deposit could possibly contain an important high-resolution record of palaeoenvironment changes during the Holocene*.

A detailed study of the Mertz Drift complements the aims of the WEGA project, which was to determine the extent of the ice sheet during the Last Glacial Maximum (LGM) along this section of the shelf. Knowledge of the extent of the LGM ice sheet could thus provide ice boundary conditions for modelers. Another aim of the project was to collect sedimentary records for comparison with the Dome C ice core onshore. The correlation of sedimentary and glacial records would contribute to the understanding of temporal and spatial constraints of the glacial/interglacial stages and Quaternary palaeoclimatic fluctuations. The comparison of sedimentary and glacial records would also permit the linkage of atmospheric processes and the response of the marine system (Antarctic CRC 2000).

1.2 Previous Studies

The first collections of sediments in this region were during Douglas Mawson's 1911-14 Australasian Antarctic Expedition to Commonwealth Bay. The crew of the vessel *Aurora* obtained eight samples of the seafloor during depth soundings in the area. Within the George V Basin, sediments were primarily siliceous oozes composed of sponge spicules, diatoms and radiolaria. In general, the

biosiliceous component of sediments was found to increase below a depth of 550 m (Domack and Anderson 1983).

The next marine geological study to the area was not until 1978/79 during 'Operation Deep Freeze' (DF79) by the US Icebreaker *Glacier*. This expedition obtained seismic profiles and sediment cores in five north/south transects across the continental shelf off George V Land. The Mertz Drift site was sampled during this survey with core 12 (hereafter named core DF79-12) obtained from the southeast part of the deposit. Using a single line of 12 kHz seismic data, Domack (1988) recorded rather uniform and draped layers of fine grained, siliceous-rich sediments that thickened to about 40 m at the western end of the George V Basin (Figure 1.2). Domack (1988) postulated that the thicker SMO sediments should contain a greater proportion of gravity flow muds (turbidites) than the uniform and draped layers recovered in core DF79-12.

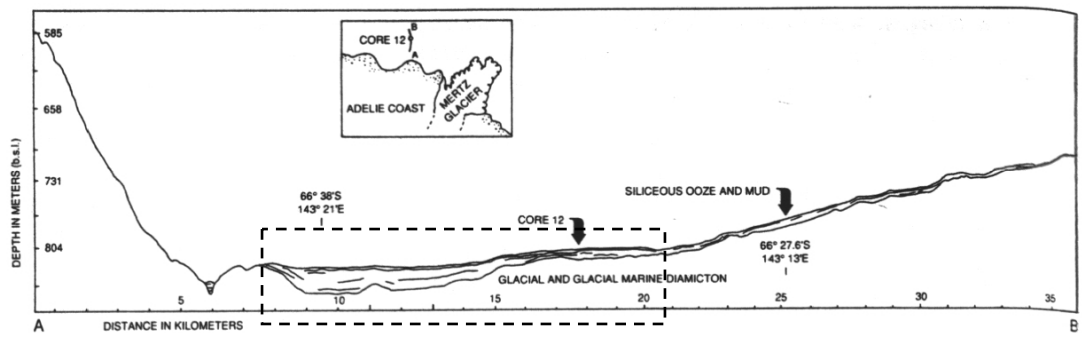

Figure 1.2 A north/south cross section through the western end of the George V Basin revealed by 'Operation Deep Freeze' 1979 (DF79) 12 kHz seismic profile (source: Domack *et al.* 1989). Note the position of core DF79-12, and the thickening of siliceous mud and diatom ooze (SMO) within dashed box indicating the Mertz Drift.

X-radiographs of core DF79-12 revealed sedimentary structures with horizontal laminations, cross laminations, and massive units. SMO facies overlie an erosional contact with glacial-marine diamicton at the base of the core (Domack 1988). Thus, deposition postdated a period of widespread glaciation on the shelf and is Holocene in age (Domack *et al.* 1989). Domack (1988) proposed that impinging Circumpolar Deep Water (CDW) removes fine grained sediment from outer shelf banks and transports it towards the coast to be deposited within inner shelf basins (Figure 1.3). Seasonal fluctuations in sea ice may also explain the development of

laminated intervals within the SMO facies, as individual laminae were found to have different assemblages of diatoms (Domack 1988). Radiocarbon ages from core DF79-12 revealed that the timing of the last glacial advance off George V Land was attributed to a mid-Holocene glacial expansion of the Mertz Glacier tongue, which was synchronous with a warming event of 7000 to 4000 yr BP (Domack *et al.* 1989). Domack *et al.* (1991) admitted that the timing of the transition to open marine conditions within the George V Basin was uncertain, and longer cores from this basin would help resolve the complete Holocene record in this area.

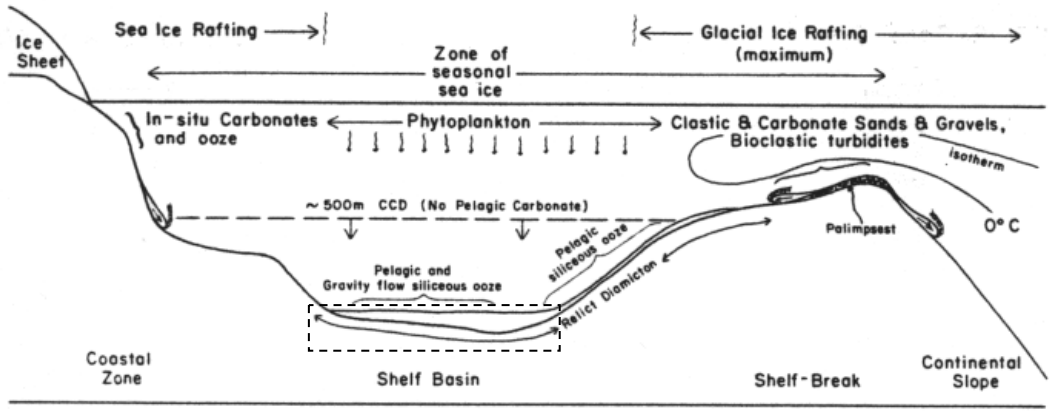

Figure 1.3 Depositional model for Antarctic glacial-marine environment on the continental shelf (source: Domack 1988). Seasonal phytoplankton blooms, winnowed fine grained sediments transported from the outer shelf banks by upwelling ocean currents and gravity flows contribute to the siliceous ooze deposited within the basin. Note the Mertz Drift would lie within the dashed box of this model.

There was then a twenty-year gap until the next marine geology survey to sample the George V Basin, which was the recent WEGA expedition that discovered and mapped the Mertz Drift (Figure 1.4). Brancolini and Harris (2000) labeled it a true 'drift' deposit since these sediments exhibit a patchy distribution, large-scale bedforms, contain foreset bedding and display a depositional architecture indicative of a 'confined drift' as defined by Faugeres *et al.* (1999). Confined drifts occur in relatively small basins or troughs, and often in tectonically active basins that account for their topographic confinement. The gross seismic character of a confined drift is similar to mounded, elongate drifts having distinct boundary channels along the margins (Faugeres *et al.* 1999).

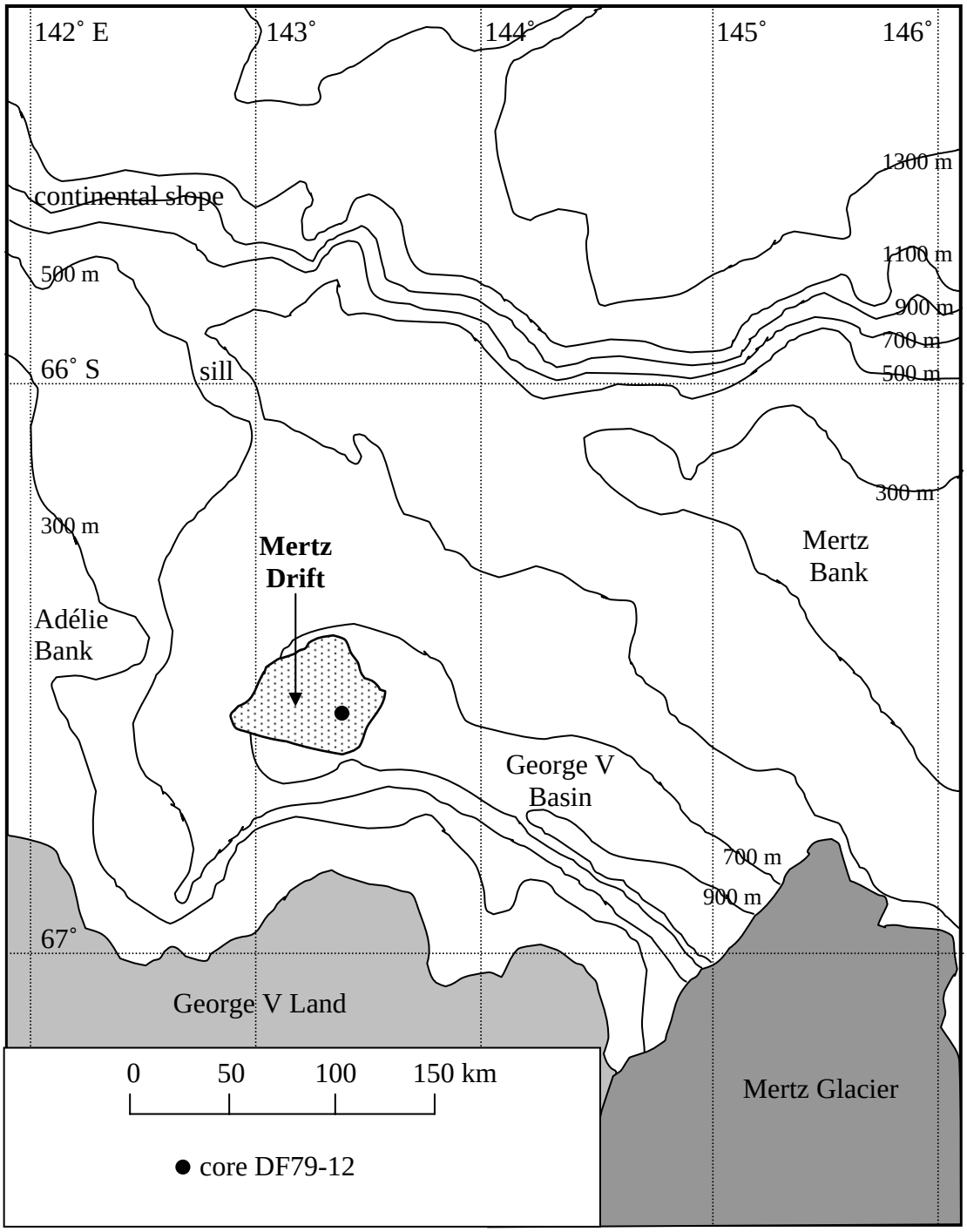

Figure 1.4 Map of the continental shelf off George V Land - Mertz Glacier region (modified from: Brancolini and Harris 2000). Note the position of the Mertz Drift in the western arm of the George V Basin at a depth of approximately 850 m.

A significant observation of the WEGA expedition is that the drift thinned to the north into an acoustically-transparent veneer. This observation implies that the drift is sourced from the outer continental shelf, with sediment transported landwards, across the shelf and into the 850 m deep inner basin (Brancolini and Harris 2000). It is possible that the cooling and sinking of Circumpolar Deep Water (CDW) is responsible for this current, however, the water current processes that have created the Mertz Drift are unclear (Brancolini and Harris 2000). The morphology of the deposit is a characterised by a horizontally broad, thin sediment about 5 metres thick on the east side of the drift that gradually thickens towards the west into a large lobe of about 35 metres. The drift then becomes horizontally narrow and thins to the west of the large lobe into a channel before increasing into a second 20 metre thick smaller lobe at the far west side of the deposit (Figure 1.5).

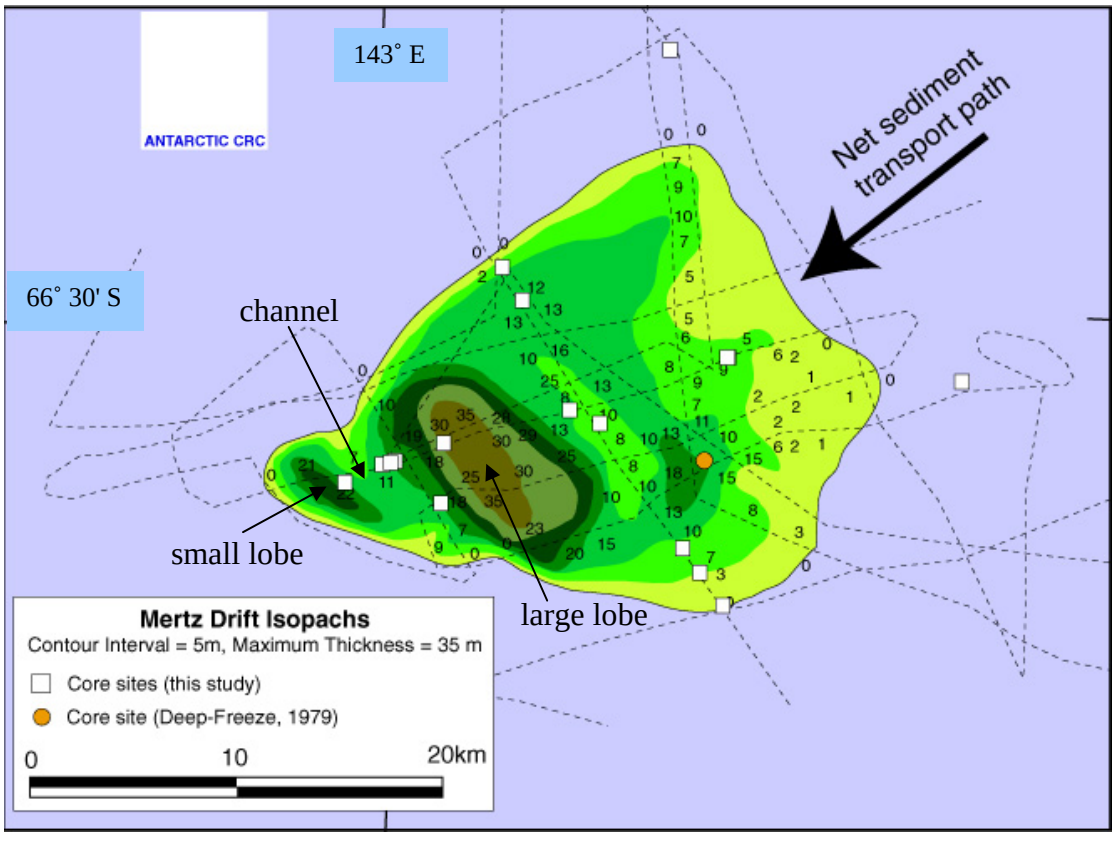

Figure 1.5 Mertz drift isopach map compiled from 3.5 kHz and deep tow chirper data (source: Brancolini and Harris 2000). Contour intervals = 5 m thickness. Numbers refer to spot thickness obtained from seismic profiles. Pecked lines refer to actual ship track. Black arrow is inferred net sediment transport path.

1.3 Aims and Hypotheses

This thesis has three main aims. The first is to produce facies descriptions using visual core logs, multi-sensor core logger data and sedimentary structures revealed by X-radiographs of cores recovered from the Mertz Drift. This is in order to discover if there is an overall facies succession within the deposit, and whether the drift has some underlying pattern of deposition. The second aim is to use radiocarbon age data to explain the timing of any facies succession, and whether or not the Mertz Drift sediments do record a high resolution of palaeoenvironment change during the Holocene. A third aim is to conduct a microscope study of Mertz Drift sediments using thin sections. Analysis may reveal the source of biosiliceous material, and whether sediments are a hemipelagic drape, current lain or from gravity flows.

Based upon the depositional model for the Antarctic glacial-marine environment by Domack (1988) and the findings by Brancolini and Harris (2000), the following hypotheses are proposed:

a. Mertz Drift sediments largely result from cyclical, high productivity diatom blooms due to annual seasonal changes in sea ice cover.

b. Mertz Drift sediments are concentrated and reworked by episodic, deep basin currents.

c. Mertz Drift sediments contain a high resolution record of bottom current intensity during the Holocene, and hence palaeoenvironment, off George V Land.

1.4 Outline of Thesis

Chapters One through Two of this thesis are directed towards providing an introduction to the subject and region. Chapter One introduces the limited findings from expeditions to the George V Basin and the geomorphology of the Mertz Drift.

Chapter Two describes the regional setting of the coast and continental shelf off George V Land, and describes the complex physical features of the area that may have had an impact on the formation of the Mertz Drift. Chapter Three outlines the data utilised in the study and the methods employed therein.

Chapter Four concentrates on sedimentology, and describes in more detail the results of core DF79-12 and Antarctic glacial-marine facies models. The results of facies descriptions from the WEGA cores are presented in this chapter. Chapter Five focuses on palaeoclimatology, discussing radiocarbon dating and its use in Antarctic Late Pleistocene-Holocene palaeoenvironment studies. The timing of post-LGM retreat of ice sheets and climate change is summarised for East Antarctica and George V Land. The results of radiocarbon dating of WEGA cores are displayed in this chapter. Chapter Six presents the results of thin section analysis. Chapter Seven is the discussion of overall facies succession and sedimentation history of the drift. A model of the formation of the Mertz Drift is shown. The conclusions drawn from this study and further research directions are given in Chapter Eight.

Chapter 2. Regional Setting

2.1 Introduction

This chapter on the regional setting of George V Land and the adjacent continental shelf seeks to explain the complex physical processes that may have an impact on the formation of the Mertz Drift. The coastline bounded by George V Land is first defined. The glacial setting is then described which includes the Mertz Glacier, ice walls of the coast and icebergs. The meteorological setting is presented with an explanation of Antarctic maritime weather and katabatic winds. This is followed by a description of sea ice and the Mertz polynya. The limited waves, swell and tidal information obtained from this area are then presented. The unusual bathymetry of the continental shelf off George V Land is described. This is followed by definitions of the currents and water masses around Antarctica, and descriptions of water masses discovered over the continental shelf off George V Land.

2.2 George V Land

Historical records of Wilkes Land indicate a number of identifying names for the coastline at different longitudes. Sedimentological research papers record the coastline adjacent to the Mertz Drift as George V Land (originally King George V Land), whereas oceanographic papers record the coast here as Adélie Land. However, as shown in Figure 2.1, the French Antarctic Territory, Terre Adélie (Adélie Land), is bounded between longitude 136˚ and 142˚ east (Joyner 1988). George V Land lies to the east of longitude 142˚ east. As the majority of research papers name the coastline in this region George V Land, in the vicinity of the Mertz Drift at longitude 143˚ east, then this name will be adopted for consistency.

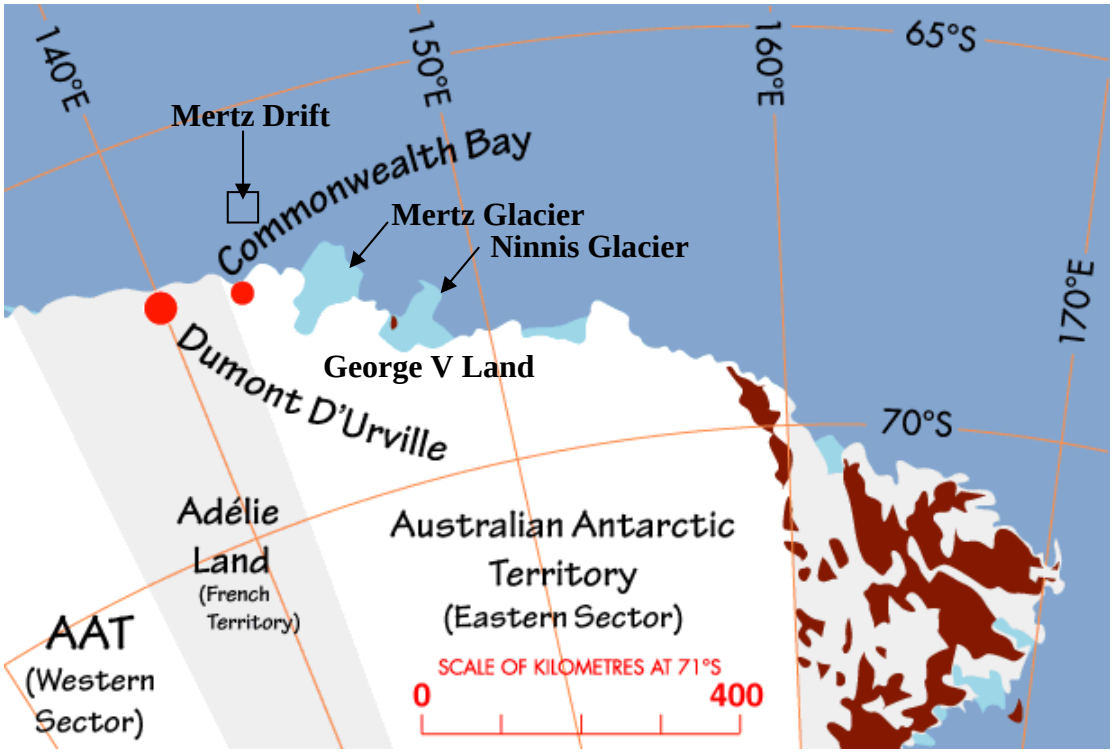

Figure 2.1 Map of the Australian Antarctic Territory (AAT), Adélie Land (in grey sector) and George V Land east of longitude 142˚ east (source: Australian Antarctic Division 2000). Note the study site within the box.

2.3 Glacial Setting

The coast of George V Land is dominated by the edge of an ice-covered plateau that rises to a height of over 1219 m at a distance of 64 km inland (Domack and Anderson 1983). The area includes some 390 km of coastline that has a total drainage basin of 145,000 km^2. Most of the coastline consists of ice cliffs that are mostly sediment free. Glacial drainage along the ice cliffs is probably sufficiently slow that wave erosion keeps pace with the rate of advance (Domack and Anderson 1983). Most of the ice drainage of George V Land occurs within a relatively small segment of the coastline through the Mertz and Ninnis Glaciers, named after Dr Xavier Mertz and Lieutenant Ninnis who died in 1913 as part of Douglas Mawson's Far-eastern Sledging Party (Mawson 1997). Of these two glaciers, the Mertz Glacier Tongue projects in a southwest to northeast direction approximately 150 km from the coast over the continental shelf (Figure 2.2), and is probably grounded on the shallow seafloor to the north.

Comparisons between various coastline surveys during the 20th century reveal that the calving front of the Mertz Glacier Tongue fluctuates in the order of tens of kilometres (Domack and Anderson 1983).

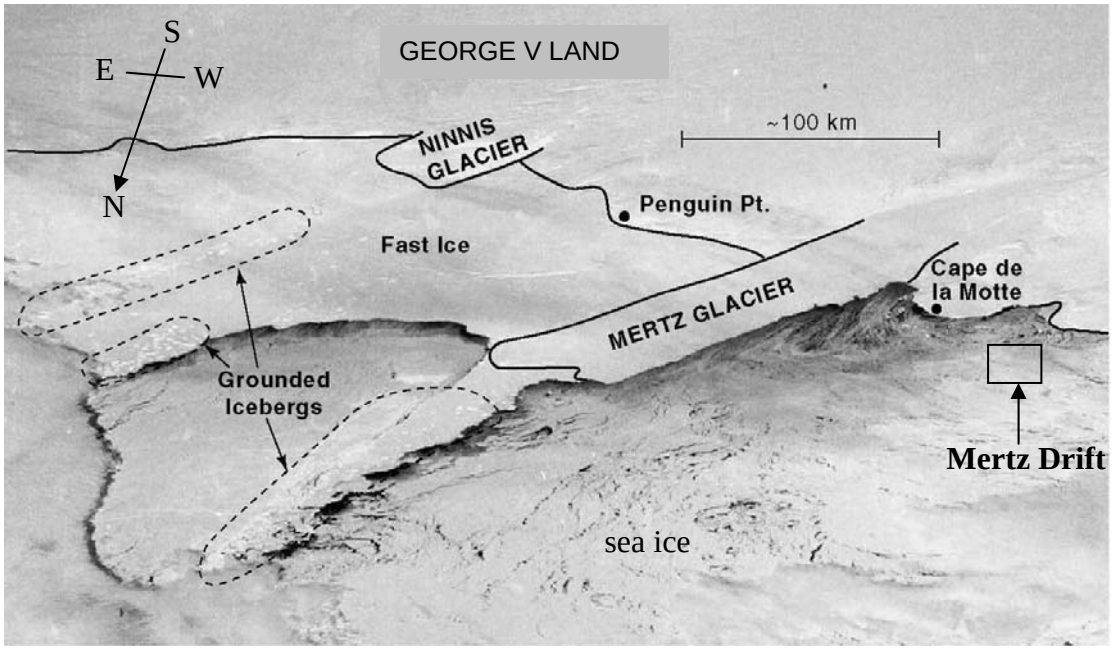

Figure 2.2 Oblique, southward-looking view of George V Land. (source: NASA Space Shuttle). The photograph shows sea ice in the foreground with the position of the Mertz and Ninnis Glaciers and coastline drawn in the background. Note the study site within the box.

Sediment-laden icebergs calved from the Mertz Glacier have dimensions of up to tens of km^2 (Anderson *et al.* 1980). The observed drift of icebergs from the Mertz and Ninnis Glaciers is to the west following the westerly-flowing surface currents (East Wind Drift; Domack and Anderson 1983). A line of grounded icebergs is found in the same southwest to northeast orientation as the Mertz Glacier Tongue (refer Figure 2.2). During winter, fast ice connects these icebergs to the glacier, creating a continuous zone of ice from the coast to the shelf break east of about longitude 146˚ east (Bindoff and Williams, submitted).

2.4 Meteorological Setting

The weather of Antarctica is dominated by a relatively simple tropospheric circulation system. The pressure decreases poleward from mid-latitudes, producing strong westerly winds (Walton 1987). Large temperature gradients between the cold

continent and the relatively warm ocean continually create low-pressure areas (cyclones) that travel eastward or southeastward with the prevailing wind. The concentration of cyclones forms a low-pressure trough between latitude 60˚ to 65˚ south. The maritime Antarctic weather thus consists of a continual succession of cyclonic storms on a time scale of two to three days, interspersed with short periods of finer weather resulting from intervening high pressure ridges (Walton 1987). South of this trough the mean pressure increases, producing easterly winds at low altitudes. The coastal zone has a higher proportion of clear days and remains relatively mild during summer under the influence of the nearby ocean. During winter, however, sea ice forms and air temperature falls much lower under radiative cooling (Walton 1987).

Near the base of coastal escarpments and mountain ranges, katabatic winds may form that have almost no relationship with the overall pressure field and resultant winds. These katabatic winds are still not well understood, however, it is thought that at the edges of the escarpment where the terrain slope increases, wind becomes more gravity-driven, overcoming the Coriolis effect (Walton 1987). In the vicinity of George V Land, the katabatic winds are channeled down the Antarctic Plateau through the valleys created by the Mertz and Ninnis Glaciers (Parish and Bromwich 1987). Katabatic winds in this region are the strongest recorded anywhere in Antarctica (Massom *et al.* 1998). For example, while close to the George V Land coastline, the WEGA research team experienced very strong katabatic winds gusting to Force 11, accompanied by very rough seas from 22 to 24 February 2000 and low temperatures to -15˚C (Brancolini and Harris 2000).

2.5 Sea Ice and Polynyas

Variability in the sea ice regime around Antarctica is fundamentally linked to the meteorology. Within the sea ice, polynyas may form as areas of open water or thin ice up to 0.3 m thick where new ice is removed by winds and ocean currents as it forms (Massom *et al.* 1998). Particularly rapid sea ice formation and export occurs where strong and persistent katabatic winds emerge from the continent via valleys, often associated with outlet glaciers. Polynyas in such locations are thought to be sites

of significant water mass modification due to the high salt flux into the ocean as a response to enhanced ice growth (Massom *et al.* 1998). Using passive microwave data, the mean area of the Mertz polynya is 23,300 km^2, with its maximum extent in October (Massom *et al.* 1998). It lies beside the Mertz Glacier Tongue and extends as far west as longitude 143˚ west (Figure 2.3). The strong katabatic winds flowing in the vicinity of the Mertz Glacier are thought to contribute to the formation and maintenance of this polynya, as winds continually remove sea ice allowing more to be formed (Massom *et al.* 1998).

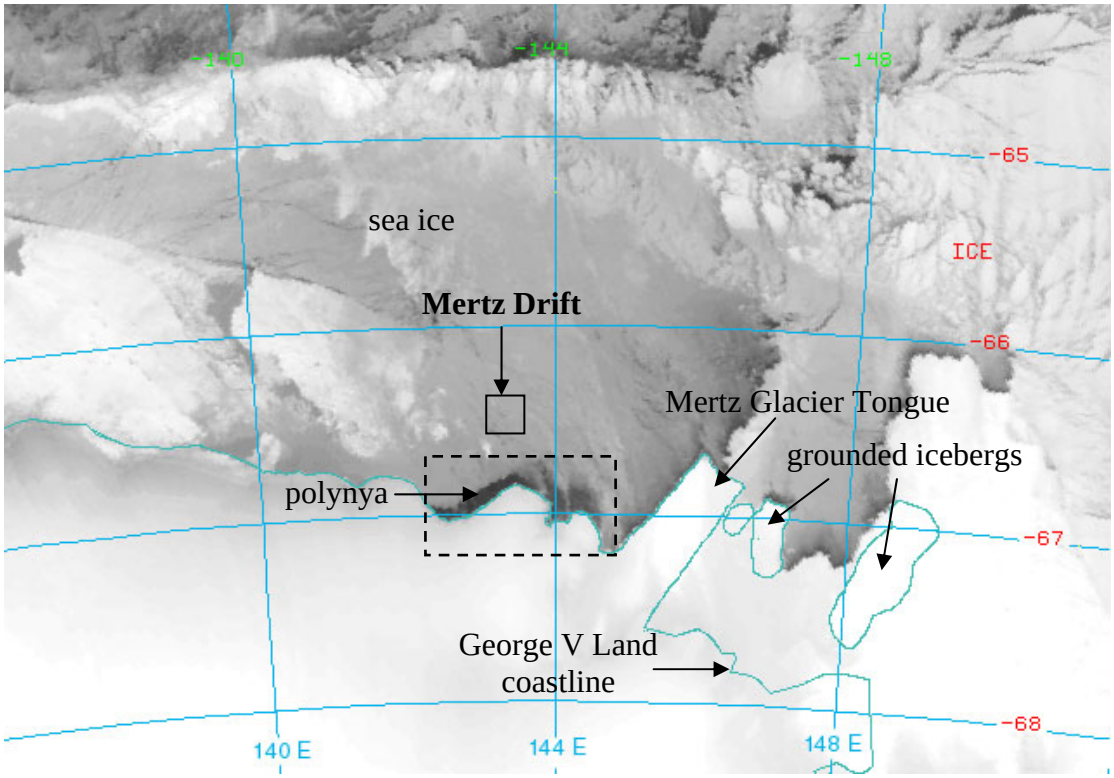

Figure 2.3 Advanced Very High Resolution Radiometer channel 4 image of the Mertz Glacier Tongue and associated polynya (source: Australian Bureau of Meteorology 14 June 1999). Dark patch inside dashed box is Mertz polynya indicating open water within sea ice. Note Mertz Drift study area inside small box.

2.6 Bathymetry

The continental shelf off George V Land is deep with an average shelf break depth of 500 m and approximately 180 km wide (Domack 1982; Wright *et al.* 1983). The physiography of the shelf is dominated by the George V Basin (also called the Adélie Depression or the Mertz-Ninnis Trough), which is a linear, inner shelf basin that parallels the coast (Figure 1.4). This basin, like other East Antarctic shelf basins,

is steep sided and joined to the shelf-break by a U-shaped valley that is fjord-like (Harris and O'Brien 1996). These deep basins and valleys are believed to have a structural origin as a result of rifting of Australia with Antarctica during the Tertiary period then sculpted by successive ice advances during the Pleistocene (Domack *et al.* 1980; Hampton *et al.* 1987). The George V Basin reaches its deepest point of over 1100 m in the vicinity of the Mertz Glacier, and then trends in a west-northwest for approximately 300 km (General Bathymetric Chart of the Ocean - GEBCO map data 1997). The Mertz Drift lies at the western arm of this linear basin at a depth of approximately 850 m. There is a ridge at about longitude 144˚ east that separates this western arm of the basin from the deeper east section (Harris 2000). A trough or sill 500 m deep connects the George V Basin to the continental slope at position 66˚ south, 143˚ east, and approximately 150 km north of the Mertz Drift. This sill is bounded to the east by the shallow 200 m deep Mertz Bank and to the west by the similar flat-topped 200 m deep Adélie Bank.

2.7 Waves, Swell and Tides

Published wave and swell data from the coast of George V Land are limited, so the following information relies predominantly upon data from the WEGA expedition that surveyed the area from February to March 2000. Brancolini and Harris (2000) noted that while winds were often high (speed range 0 - 60 kn; mean speed 16 kn), it was predominantly from the south, and the short fetch and deep water inhibited wave height (height range 0 to 3 m; mean height 0.5 m). Likewise, swell was predominantly generated from the south (mean period 7 sec; height range 0 to 4.5 m; mean height 2 m). In addition, new ice forming in the south of the area at the onset of winter may have further inhibited wave and swell formation.

The tide on the George V Land continental shelf is diurnal, i.e. predominantly one high water and one low water each day, with a maximum tidal range of 1.8 m (Australian National Tide Tables 2000). Harris and O'Brien (1996) state that the depth of the East Antarctic shelf and the presence of sea ice over much of the year restricts the effects of swell and waves in reworking shelf sediments. Similarly, the microtidal

range (< 2 m) along the coast indicates that tidal currents play only a minor role in shelf sediment dynamics.

2.8 Currents and Water Masses

The waters of the Southern Ocean have a special importance to oceanographers because of the variety of water masses produced and the ability for these waters to spread throughout the world as bottom water (Whitworth *et al.* 1998). Ocean currents are also the dominant energy type responsible for the physical reworking of sediments along the East Antarctic margin (Harris and O'Brien 1996). Because of the variety of water masses produced south of the Polar Front, definitions will mostly follow those in the review by Whitworth *et al.* (1998).

The wind-driven Antarctic Circumpolar Current (ACC) flows eastward, exchanging waters among the Southern Ocean basins. This current includes Circumpolar Deep Water (CDW), and is believed to be the critical water mass because it is involved in the formation of all others (Whitworth *et al.* 1998). CDW is considered in two layers: the upper, with an oxygen minimum and nutrient maximum, is entrained within the ACC; the lower, with a salinity maximum, can be found south of the ACC where it frequently meets the Antarctic continental shelf. Both upper and lower layers of CDW are warmer than the cold surface waters that overlie it. Vertical and lateral mixing in the slope and shelf regions can convert the lower layer CDW to other water masses. This mixing is enhanced by the East Wind Drift (EWD) that moves in a westerly direction around the Antarctic continent driven by the polar easterly winds (Whitworth *et al.* 1998).

Whitworth *et al.* (1998) used a temperature, salinity and density diagram to define Antarctic water masses (Figure 2.4). The upper boundary of CDW is the density value 1028.03 kg/m^3. The lower boundary of CDW is defined by the density value of 1028.27 kg/m^3. On the shelf, it is possible for CDW to mix with the overlying Antarctic Surface Water or with the underlying Shelf Water and has been given the term Modified Circumpolar Deep Water (MCDW). It is considered to be

colder and fresher than the regional CDW, however the boundary between the two is vague (Whitworth *et al.* 1998).

Overlying CDW, and with density lower than 1028.03 kg/m^3, is Antarctic Surface Water (ASW). Because of its location at the air/sea/ice interface, ASW is the most variable in properties of all Antarctic water masses. Its salinity is less than about 34.45 $^0/_{00}$ and its temperatures ranges from 2˚ C to - 2˚ C. In summer, Antarctic Surface Water is sometimes called Winter Water (WW) since it is a remnant of the isothermal winter mixed layer (Whitworth *et al.* 1998; Wong *et al.* 1998).

Underlying CDW is Antarctic Bottom Water (AABW), which has a density of less than 1028.27 kg/m^3 and is warmer than -1.7˚ C. AABW is believed to be created in a two-stage process. First, MCDW mixes with Shelf Water to produce water seen at the bottom of the shelf edge, then this water sinks along the slope, entraining the warmer, saltier CDW to produce AABW (Whitworth *et al.* 1998).

Water denser than 1028.27 kg/m^3 and colder than minus 1.7˚ C is called Shelf Water. This water mass could result from two processes: (1) from salt rejected from winter sea ice formation being trapped within basins, and (2) from the onshelf mixing of MCDW, which is cooled in winter (Wong *et al.* 1998).

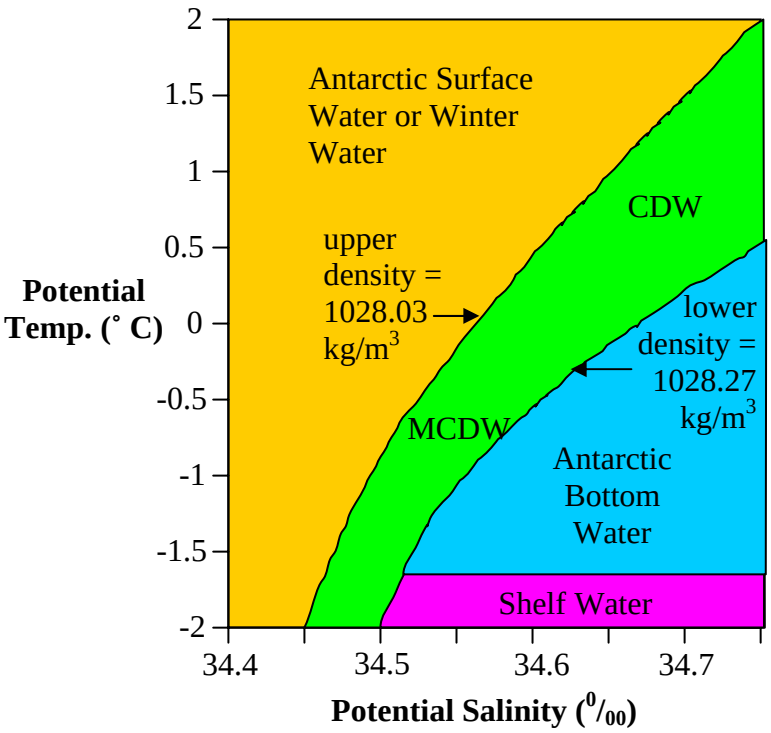

Figure 2.4 A potential temperature, salinity and density diagram that defines Antarctic water masses (modified from: Whitworth *et al.* 1998). CDW = Circumpolar Deep Water; MCDW = Modified Circumpolar Deep Water.

The search for Antarctic Bottom Water (AABW) from the continental shelf off George V Land led Rintoul (1998) to conclude that a cold, fresh, high oxygen and dense variety of AABW (his Adélie Land Bottom Water) originated from the sill connecting the George V Basin to the continental slope. A more recent Australian winter oceanographic expedition to the Mertz Glacier polynya area found four distinct water masses near the Mertz Glacier (Bindoff and Williams, submitted):

(1) A relatively warm, fresh and oxygen-poor Modified Circumpolar DeepWater (MCDW) flowed in a predominantly southwesterly direction in tongues over the Mertz Bank towards the coast, and in depths of up to 500 m (Figure 2.5).

(2) Over the George V Basin was a large volume of relatively homogenous and non-stratified Winter Water (WW). The WW was derived from the MCDW when it was cooled by the atmosphere and gained brine through interaction with the Mertz

polynya. WW extended to depths of about 500 m and flowed towards the Mertz Glacier and westward following the coast (Figure 2.5).

(3) Underlying the WW in the deepest parts of the basin was a strongly stratified, dense, oxygen rich, high salinity Shelf Water (HSSW). Through the ocean-atmosphere interaction at the polynya, water masses were converted from MCDW into WW and HSSW by cooling and the addition of brine (Bindoff and Williams, submitted). Rintoul (1998) concluded that the HSSW in the George V Basin was the source of the Antarctic Bottom Water flowing off the shelf (Figure 2.5).

(4) Bindoff and Williams (submitted) also discovered a supercooled and freshened variety of Shelf Water called ice Shelf Water (ISW). Both WW and HSSW water masses were modified by their interaction under the Mertz Glacier to become ISW. This water mass occurred in depths to 500 m and flowed westerly, following the coastline (Figure 2.5).

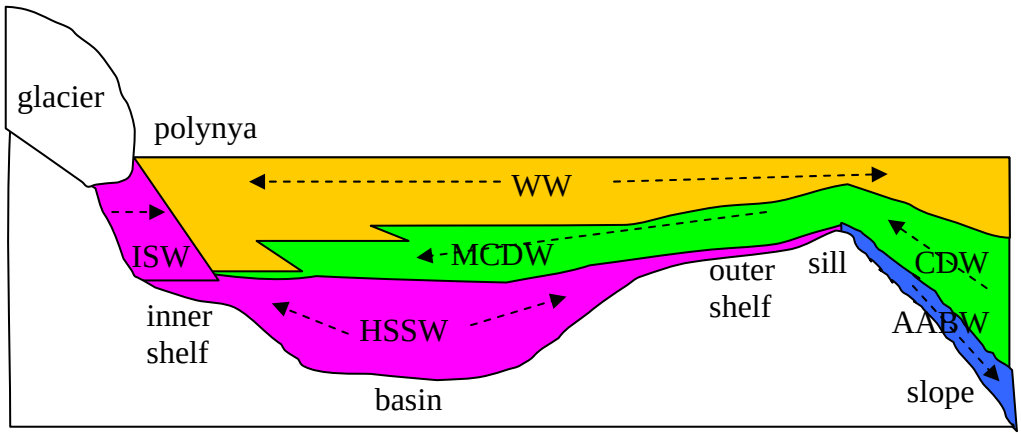

Figure 2.5 Cross section through the continental shelf in the vicinity of the Mertz Glacier showing relative positions of water masses (modified from: Bindoff and Williams, submitted). Colours of water masses match those of Figure 2.4. Arrows infer direction of flow across the shelf. Water masses are: Circumpolar Deep Water (CDW); Modified Circumpolar Deep Water (MCDW); Winter Water (WW); high salinity Shelf Water (HSSW); ice Shelf Water (ISW); Antarctic Bottom Water (AABW).

Chapter 3. Materials and Methods

3.1 Introduction

This chapter sets out the sources of data for the present project. It includes a map and tables of the positions of the sediment cores collected by the WEGA expedition used in this study. Area, volume and carbon content statistics for the Mertz Drift are first explained. One aim of this thesis was to determine if the drift has some underlying pattern of deposition. Facies descriptions of each Mertz Drift core were produced using X-radiographs, visual core logs and multi-sensor core logger data, and the methods are detailed below. X-radiographs also permitted counts of ice-rafted debris (IRD) gravel content within each core in order to determine patterns of IRD deposition in relation to facies. Seafloor photographs of the Mertz Drift are examined to provide clues to the modern environment of deposition. Another aim of the thesis was to use radiocarbon age data to explain the timing of any facies succession through sediment accumulation rates. Radiocarbon dates are also used to calculate the mean time period of deposition of laminae couplets of several cores. A third aim of this thesis was to examine thin sections of sediments under microscope, in the method described below, to determine whether samples were deposited as a hemipelagic drape, current lain or from gravity flows.

3.2 Sources of Data

Data for the present study are derived from the results of the joint Italian/Australian WEGA research expedition during February to March 2000 aboard the RV *Tangaroa*. The expedition collected 18 piston and gravity cores from 16 sites on the deposit, in two cross-drift transects (Figure 3.1). Sediment sampling equipment consisted of a one tonne core head, with up to 6 m barrel lengths, configured as either a gravity or piston corer. A Shipek grab was also deployed independently at several stations to sample the upper 10 cm of sediment. Cores were logged visually onboard the Tangaroa for colour, sedimentary structures, ice-rafted debris (IRD), presence of burrows, grain size and fossils. Cores were also logged using a non-destructive Geotech Model 36 multi-sensor core logger for bulk density, magnetic susceptibility

and P-wave velocity. Cores were refrigerated in approximately one metre long sections after being split into an archived (unsampled) and sampled halves. While on site, seabed photographs were taken using a Benthos model 372A underwater camera and a model 383 flash (Brancolini and Harris 2000).

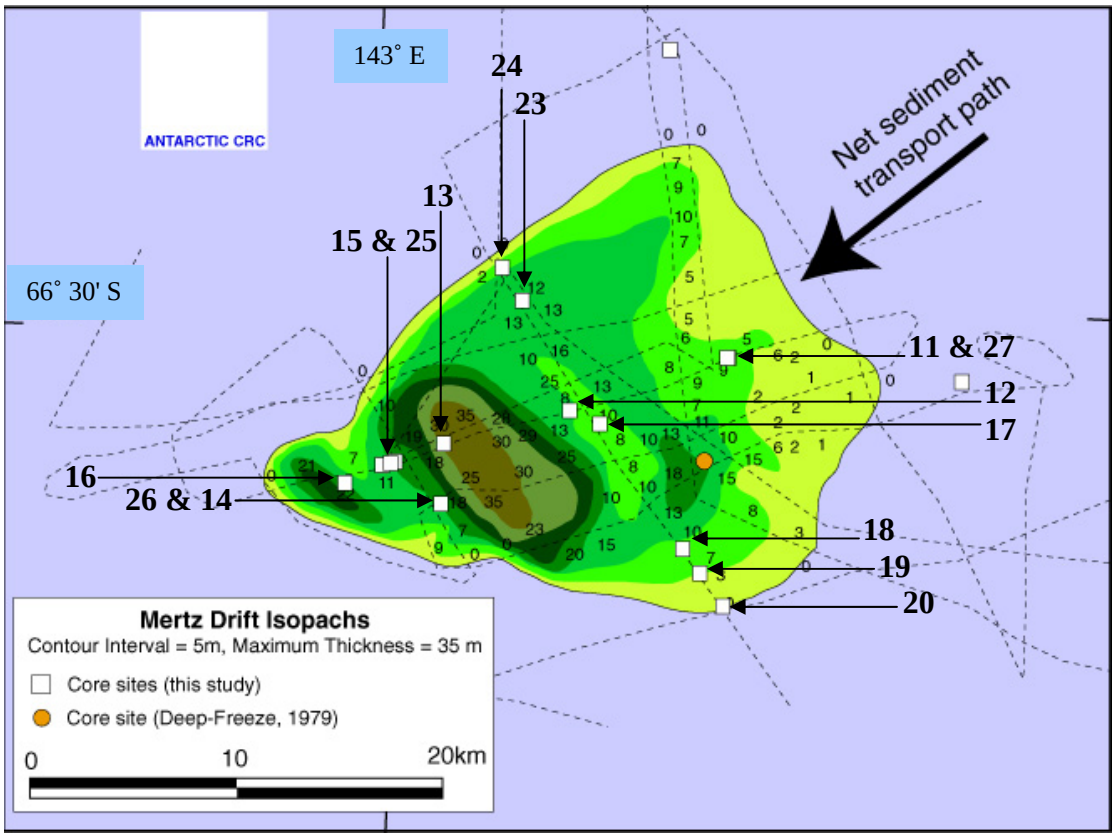

Figure 3.1 Isopach map of the Mertz Drift showing station numbers (in bold) in relation to sediment core sites (small white squares) (source: Brancolini and Harris 2000). Unnumbered small white boxes outside of the Mertz Drift are WEGA sediment core sites excluded from the present study.

Table 3.1 lists the positions and depths of cores obtained from the Mertz Drift in order of station number. Mertz Drift cores are grouped in Table 3.2 according to their relative proximity to one another, and given a name according to their position on the drift for ease of comparison. It should be noted that the high concentration of cores collected from the Mertz Drift is unusual in the history of deep sea coring, allowing much comparison between adjacent cores. Of these groups, only core 16PC01 on the small lobe did not have an immediately adjacent core.

Station Number	Latitude south	Longitude east	Depth (metres)	Core Name
11	66˚ 31'.21	143˚ 23'.03	794	GC02, GC03
12	66˚ 32'.57	143˚ 12'.64	837	GC04
13	66˚ 33'.43	143˚ 04'.32	840	GC05
13	66˚ 35'.00	143˚ 04'.19	863	GC06
14	66˚ 33'.91	143˚ 01'.13	871	GC07
15	66˚ 33'.97	143˚ 00'.32	880	GC08, GC09
16	66˚ 34'.44	142˚ 57'.87	855	PC01
17	66˚ 32'.94	143˚ 14'.62	830	PC02
18	66˚ 36'.18	143˚ 20'.04	815	PC03
19	66˚ 36'.80	143˚ 21'.13	840	PC04
20	66˚ 37'.64	143˚ 22'.70	795	PC05
23	66˚ 29'.75	143˚ 09'.55	833	PC09
24	66˚ 28'.89	143˚ 08'.20	819	PC10
25	66˚ 33'.98	143˚ 00'.33	843	PC11
26	66˚ 33'.93	143˚ 00'.88	870	PC12
27	66˚ 31'.22	143˚ 22'.95	793	PC13

Table 3.1 Position and depth of Mertz Drift stations occupied and cores collected during the WEGA research expedition.

Core Groups	Position on Drift
11GC02, 11GC03 27PC13	east
18PC03 19PC04 20PC05	south
12GC04 17PC02	centre
23PC09 24PC10	north
13GC05 13GC06	large lobe
14GC07 26PC12	large lobe edge
15GC08, 15GC09 25PC11	channel
16PC01	small lobe

Table 3.2 Mertz Drift cores grouped according to their relative proximity to each other.

3.3 Area, Volume and Carbon Content

Area and volume statistics are determined to allow comparisons of the Mertz Drift against other Antarctic drift deposits. Using the isopach map and scale of Figure 1.5, the area and volume of each isopach thickness interval was calculated using a grid scale of 2 mm^2 is equivalent to 206,611 m^2 (Chapter 4). This volume figure was then used to calculate the carbon content of the drift, as these deposits may play a significant role in the carbon cycle of the Antarctic continental shelf (Harris *et al.* 1999). Calculations utilised the methods of Harris *et al.* (1999), which required equations for:

(1) volume of solids = (volume of deposit) x 40%.
Where 40% is the value used in Harris *et al.* (1999) for ratio of solids/seawater.

(2) mass of solids = (calculated volume of solids) x 2600 kg/m^3.
Where 2600 kg/m^3 is the value used in Harris *et al.* (1999) for the mass of solids/volume of solids.

(3) carbon content = (calculated mass of solids) x 1.5%.
Where 1.5% is the percentage of total organic carbon in core DF79-12 (Domack *et al.* 1989). At the time of writing this thesis, total organic carbon of WEGA sediments had yet to be processed.

3.4 X-radiographs

Using the archived half of the cores, X-radiographs were undertaken at Rush, Taylor and Partners Diagnostic Radiologists in Hobart using a Siemans Polyphos 50 machine. Siliceous mud and diatom ooze (SMO) sediments required an average power of 46 kilovolt (kV) and time of 32 milliAmpsec (mAs) to reveal the internal structure. The more dense diamicton unit underlying the SMO required an average of 66 kV and 32 mAs. Black and white photographs were produced from the negatives of the X-radiographs, and photo reproductions of each core were constructed on 100 x 70 cm boards with a downcore cm scale.

3.5 Facies Classification

The X-radiographs of each Mertz Drift core were examined closely for sedimentary structures. These included the presence of laminations or cross laminations, convoluted or massive structures (Chapter 4). The presence of burrows within X-radiographs of the cores was also recorded. Burrows were observed within X-radiographs as generally horizontal, dark-toned, ragged lines (Harris 2000). Where sedimentary structures were identified in the X-radiographs, comparison was made with the visual core logs and multi-sensor core logger data for accuracy, particularly when trying to identify the presence of burrows and sedimentary structures that were obscured by poor X-radiographs. Information on sedimentary structure and sediment type revealed by visual core logs, multi-sensor core logger data and X-radiographs were then incorporated into a facies classification modified from Domack (1988). Facies classification for each Mertz Drift core is presented in facies interpretation logs (Appendix A). The proportion of the different facies observed in X-radiographs of cores is presented in a table in order to determine any overall patterns of deposition. The proportion of burrows observed in each facies is also given in a table to help in identifying patterns of deposition within the Mertz Drift.

3.6 Ice-rafted Debris (IRD) Gravel Content

Using the X-radiographs for each Mertz Drift core, IRD granules (2-4 mm) and pebbles (4-64 mm) were counted for each 5 cm interval down core . Granule and pebble counts were then combined into the classification 'gravel' as total gravel content. For each core, gravel content, representing the number of grains per 5 cm interval, are presented in graphs alongside facies interpretation logs (Appendix A). IRD gravel within the glacial-marine diamicton at the base of a number of cores was not counted as this project focussed upon IRD deposition patterns within SMO sediments only. Gravel content from each Mertz Drift core was used to calculate the overall gravel content percentage for each facies (Chapter 4).

3.7 Seafloor Photographs

The use of photographs to reveal the benthic community is useful as they assist in interpreting the modern environment of deposition. Clues may be given as to whether Mertz Drift sediments are presently being concentrated and reworked by deep basin currents, a hypothesis of this study. Fauna and features are identified for several seafloor photographs representative of the Mertz Drift surface, and related to habitat information where possible (Chapter 4).

3.8 Radiocarbon Ages

In the laboratory, 63 samples were taken of various Mertz Drift grab samples, piston and gravity cores for radiocarbon dating at the Institute of Geological and Nuclear Sciences, Lower Hutt, New Zealand. The conventional radiocarbon age results obtained were corrected for contamination by older sediments and reservoir effect to bring the core-tops to modern age (Chapter 5). The practice amongst marine sediment workers is to subtract the core-top radiocarbon age from the remainder of down core radiocarbon ages (Cunningham *et al.* 1999, McMinn 2000). The corrected ages of Mertz Drift cores 13GC05, 13GC06 and 26PC12 were graphed against depth in KaleidaGraph Version 3.5, and a linear regression and correlation coefficient were calculated for each graph. The slope calculated for linear regression of each plot was then used to produce average sediment accumulation rates. These rates were compared against the facies within the cores to determine if there were any underlying sedimentation patterns within the Mertz Drift.

3.9 Laminations

Domack (1988) proposed that laminae possibly reflect annual seasonal changes in productivity. An aim of this project was to calculate the mean deposition time for lamination couplets to test the hypothesis that Mertz Drift sediments largely result from cyclical, high productivity diatom blooms due to annual seasonal changes in sea ice cover. This calculation relied upon X-radiographs to observe and measure the thickness of lamination couplets within the cores. Lamination couplets were

defined as a pair of light and dark-toned lines within X-radiographs. It was important first to test the validity of the X-radiographs to record laminations accurately as the images essentially display internal, three-dimensional sedimentary structures as two dimensions. Therefore, a comparison was made of the number of lamination couplets per 10 cm interval recorded on visual core logs for cores 13GC05 and 13GC06 compared to the number revealed by X-radiographs for the same 10 cm interval (Chapter 5). Only intervals of lamination couplets that were clear within the X-radiographs were used in the comparison. Graphs of visual versus X-radiograph lamination couplet counts were produced in KaleidaGraph Version 3.5, and a linear regression and correlation coefficient calculated for each graph.

X-radiographs of cores 13GC05 and 26PC12 were then examined in closer detail to reveal the mean number of lamination couplets per cm and the mean couplet thickness in cm. The mean couplet thickness (in cm) was multiplied by the average sediment accumulation rate (in yr/cm) from these two cores to reveal the mean time period for lamination couplets (in years; Chapter 5).

3.10 Thin Section Analysis

Four block samples of core 26PC12 were extracted for thin section analysis under microscope (Chapter 6). Analysis may reveal the source of biosiliceous material, and whether sediments are a hemipelagic drape, current lain or from gravity flows. Block samples were obtained from the core at depths: 8.5-11.5, 162-165, 227-230.5 and 237-240.5 cm. Samples were freeze dried, placed in an oven and left for two days at 60˚C until all water had evaporated. Samples were then put in a dessicator under vacuum, and an epoxy resin (AralditeM/Hardener HY956 - 10g/1.7g) introduced to impregnate and cover the samples. Samples were released from the dessicator and allowed to harden over four hours. After samples had hardened, the blocks were flattened with a 400 grid diamond grinding surface and glued to glass slides. The glass-mounted blocks were then sectioned at 20 µm and polished so as to reveal sediment microstructure for analysis under microscope.

Analysis of thin sections was initially a comparison against the facies interpretation log of core 26PC12 to determine the facies of the samples. The overall style of deposition of the thin sections was compared against the equivalent depth within X-radiographs of core 26PC12. This was in order to determine if there was any correlation between the textural differences in the thin section and structures observed in the X-radiographs. Thin sections were analysed under stereo and compound microscopes to detect finer-scale qualitative differences in the microstructure. No attempt was made to conduct a quantitative analysis of diatom species due to the late preparation of thin sections and lack of time. Photomicrographs were taken of important features of the thin sections to highlight points within the analysis.

Chapter 4. Sedimentology

4.1 Introduction

This chapter is in two parts. The first part describes the previous sedimentology results from 'Operation Deep Freeze' 1979 (DF79) in greater detail, in particular those of core DF79-12 which penetrated the southeast part of the Mertz Drift. Core DF79-12 provides a comparison against the findings of this project using the cores from the WEGA research expedition. Antarctic glacial-marine facies and continental shelf surficial sediment facies are also described that will allow comparison of Mertz Drift sediments with Antarctic polar glacial sequences. The second part presents the sedimentological results of this project. This includes area, volume and carbon content statistics, facies classification and ice-rafted debris (IRD) gravel content of Mertz Drift cores, and the results of seafloor photograph descriptions to interpret the modern environment of deposition. The chapter concludes with a summary of these results.

4.2 Previous Sedimentology Studies

4.2.1 Core DF79-12

Core DF79-12 penetrated approximately 600 cm of laminated siliceous mud and diatom ooze (SMO) before striking a weakly stratified, glacial-marine diamicton (Domack and Anderson 1983). Facies classification based upon sedimentary structures revealed by X-radiographs were varied (Domack 1988), and included laminations, discontinuous laminae, cross laminae, massive beds, diamicton and the presence of IRD (Figure 4.1). The overall facies succession of DF79-12 illustrated in Figure 4.1 revealed diamicton at 600 cm followed by about 130 cm of sediment providing poor X-radiographs then massive beds with relatively high IRD content to about 330 cm. Massive beds were overlain predominantly by laminations with minor cross laminae and massive intervals to about 70 cm. The upper 70 cm of core DF79-12 was mostly discontinuous laminae and laminations.

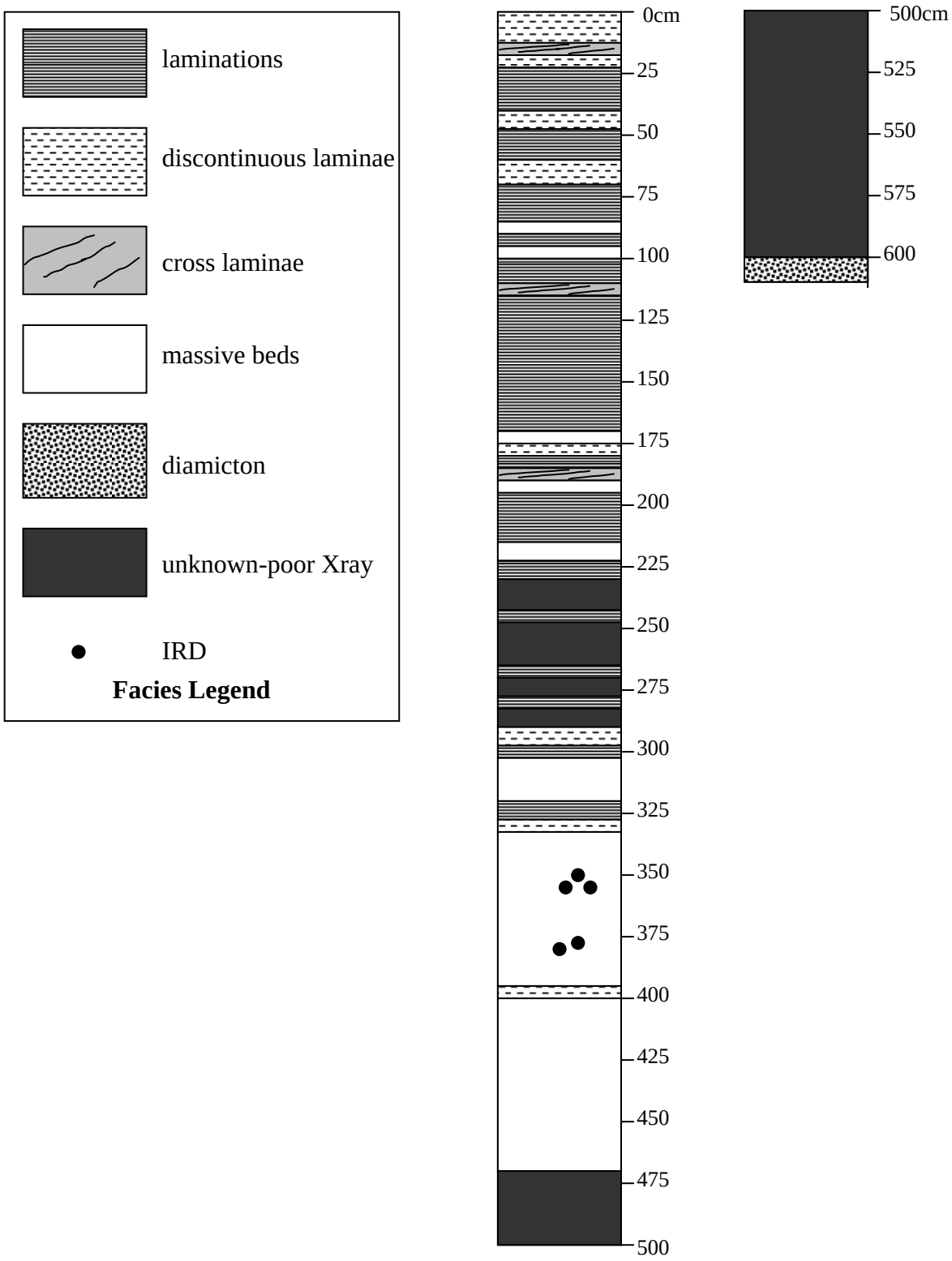

Figure 4.1 X-radiograph facies interpretation log and legend for core DF79-12 (modified from: Domack 1988).

Detailed sediment analysis of core DF79-12 revealed variations in the terrigenous sand through the core (Figure 4.2). There is a significant increase in sand percentage in the upper 60 cm of the core corresponding with the discontinuous laminae and laminations observed in the upper 70 cm of Figure 4.1. There is also an increase in sand percentage in the lower 200 cm of the core, overlying the diamicton. This corresponds approximately with the predominantly massive beds of Figure 4.1. The IRD content in core DF79-12 is low, however, gravel content in core DF79-13 (a similarly laminated SMO core located approximately 27 km north of core DF79-12 within George V Basin) showed that increases in IRD gravel fraction correlate well with peaks in sand percentage (Domack *et al.* 1989). Sediment analysis revealed that the least terrigenous sand was found within the mostly laminated and cross laminated SMO intervals between 400 and 60 cm where biogenic sedimentation dominated (Domack *et al.* 1989).

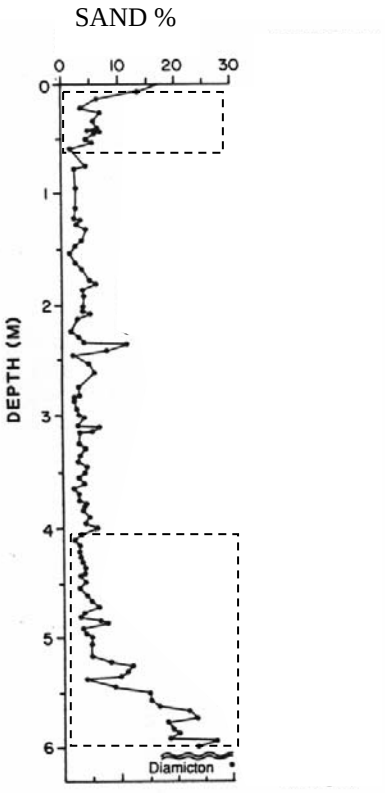

Figure 4.2 Downcore variation in percentage sand for core DF79-12 (source: Domack *et al.* 1989). Note the relative increase in sand % within the dashed boxes.

The deposition of biogenic sediments was interpreted by Domack and Anderson (1983) to have occurred soon after recession of the glacial ice from the shelf (refer Chapter 5 for detail on timing), as evidenced by the contact between diamicton and overlying SMO. There was a change from proximal ice tongue sedimentation at the base of the core (diamicton) to open marine sedimentation above (SMO; Domack *et al.* 1989). The transition between proximal and distal ice tongue was recorded by an upward reduction in fine grained sand and an increase in biogenic material within the 600 to 400 cm interval. As the glacier melted upon retreat, increased winnowing of relict glacial-marine sediments by impinging Circumpolar Deep Water (CDW) on the outer shelf was believed to be largely responsible for transporting the fine sand, silt and clay into the basin (Domack and Anderson 1983). Domack (1988) stated that sediment gravity flows, meltwater plumes and aeolian transport may also be a source of transport for sediments into the basin. Yet Domack (1988) noted a lack of evidence for sediment gravity flows within the basin, but speculated that the thickest part of the George V Basin (Mertz Drift) should contain a greater proportion of gravity flow muds than the uniform and draped layers recovered in core DF79-12.

Domack (1988) proposed a model explaining the laminated SMO within deep basin cores, in which areas that undergo seasonal fluctuations in sea ice cover contribute significant quantities of biogenic detritus to the bottom after high productivity, diatom blooms within the open water photic zone. Initial analysis of diatom flora within individual laminae of core DF79-12 revealed strong contrasts in species diversity and size. Epontic (sea ice habitat) diatoms dominated within one of each laminae couplet (Domack 1988). Therefore, layers may represent initial pelagic flux from melting sea ice followed by productivity during the rest of summer represented by open water diatoms. The lack of pelagic carbonate within these sediments, such as planktonic foraminifera, was most likely related to carbonate dissolution at depths below 500 m (Domack 1988).

4.2.2 Glacial-Marine Facies

In this present study it is important to consider the diamicton and SMO sediments within the WEGA expedition cores and core DF79-12 within the wider perspective of Antarctic glacial-marine facies. This enables comparisons with Antarctic polar glacial sequences. Antarctic glacial-marine sediments fall roughly into three groups (Anderson *et al.* 1983):

(1) Transitional glacial-marine facies. This facies is a dominantly massive, unsorted diamicton with some stratification, similar to lodgment tills (Figure 4.3). This facies contains a low-diversity, marine fossil assemblage, indicating deposition in an environment where conditions were unsuitable for most marine organisms. The facies is interpreted as having been formed under an ice shelf, and grades seawards into muds and oozes. Basal debris, melted out beneath the shelf, is deposited on the seafloor with minor marine fossils.

(2) Compound glacial-marine facies. This facies includes mud and diatomaceous oozes with only minor IRD, and is classified as compound due to the mixture of glacial and marine components (Figure 4.3). These are the most widespread sediments on the Antarctic seafloor today, blanketing the shelf in depths greater than about 300 m. This facies is interpreted as having been formed in a deep (> ~300 m) open marine environment, where biogenic sedimentation dominates over terrigenous sediment supply from glaciated coastlines or icebergs.

(3) Residual glacial-marine facies. This facies is confined to shallow (< ~300 m) outer shelf banks in an open marine environment (Figure 4.3). Deposits consist of unsorted gravel and sand, and possibly minor silt and clay after most of the fines have been winnowed by marine currents, leaving residual sediments. This facies also contains substantial carbonate material such as bryozoa, mollusc, echinoderms, coral fragments and foraminifera.

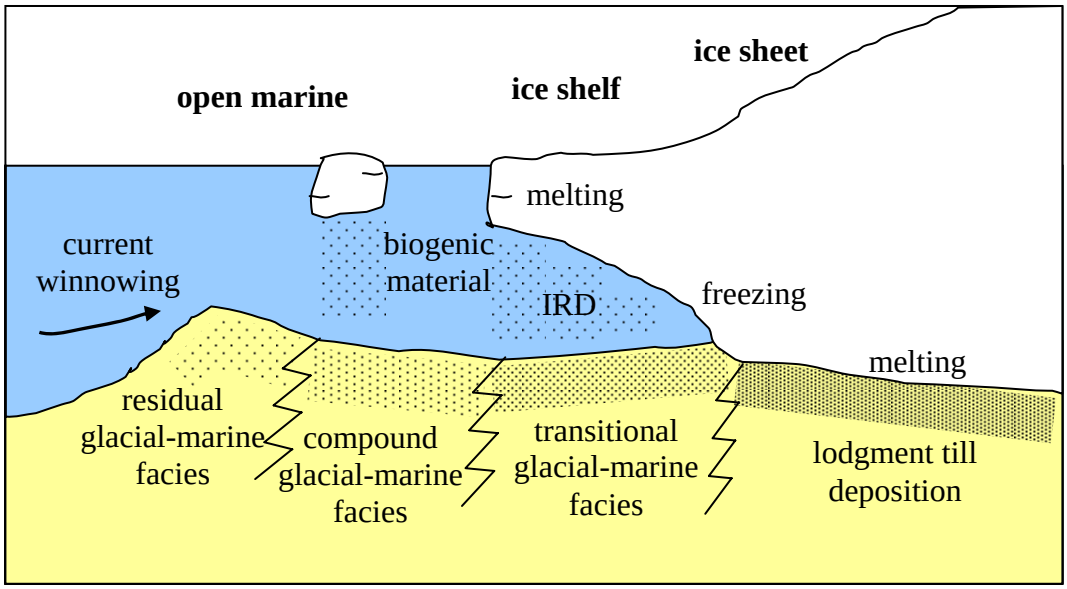

Figure 4.3. Model of Antarctic glacial-marine environments and facies (modified from: Anderson *et al.* 1983). Transitional glacial-marine facies consist of basal debris melted from beneath ice shelves and minor marine fossils. Compound glacial-marine facies comprise mostly biogenic material and minor IRD. Residual glacial-marine facies are sediments remaining after ocean currents have winnowed and removed fine grained material.

4.2.3 Surficial Sediment Facies

Since the relatively simple, Antarctic shelf-wide, glacial-marine sedimentation model was proposed by Anderson *et al.* (1983), much work has been done to refine depositional models that can be applied to the wide range of settings in Antarctica (Domack and Harris 1998). Most revised models have only targeted specific depositional environments such as facies successions resulting from ice shelf retreat (Domack and Harris 1998, Harris and O'Brien 1998), or marine sedimentation at a calving ice wall margin (Ashley and Smith 2000). The most common contribution in facies descriptions has come from workers describing surficial sediments around the Antarctic continental shelf. This is not surprising given the relative ease of obtaining sediments in grab samples compared to deep water cores, or the use of technology such as sidescan sonar and the newer multibeam echosounders to remotely sense images of the seafloor.

Surficial sedimentary facies over the continental shelf off George V Land were described based upon the lithology of sediments in cores obtained during

Operation Deep Freeze 1979. Domack (1988) classified surface sediments into carbonate and siliceous facies. Carbonate facies occurred in two distinct zones on the continental shelf: a nearshore region bordering the ice sheet at depths shallower than approximately 250 m containing *in situ* and reworked accumulations of calcareous shell material; and on the upper continental slope and on the outer shelf adjacent to shallow banks. Siliceous facies occurred as shelf basin sediments below approximately 500 m. This classification contributed to the Domack (1988) depositional model for Antarctic glacial-marine environment on the continental shelf (refer Chapter 1 - Figure 1.3).

The first part of this chapter has discussed the sedimentological results from core DF79-12, and described Antarctic glacial-marine facies and surficial sediments within the George V Basin. This information provides a baseline for the results of this project, presented in the second part of the chapter.

4.3 Results

The sedimentological results commence with area, volume and carbon content statistics, which are essential for comparison against other drift deposits. Carbon content is calculated as these deposits may play a significant role in the carbon cycle of the Antarctic continental shelf (Harris *et al.* 1999). An aim of this thesis was to determine if the Mertz Drift has some underlying pattern of deposition. This part of the chapter will explain how facies were classified within Mertz Drift cores and the general pattern of appearance. Ice-rafted debris (IRD) gravel content is also measured within cores to ascertain whether there are patterns of deposition in the drift. Seafloor photographs are discussed to help determine the modern environment of deposition.

4.3.1 Area, Volume and Carbon Content

An estimation of the area and volume of each sediment isopach (i.e. vertical columns) is given in Table 6.1. These results indicate the Mertz Drift has an area of approximately 390 km^2 and a volume of 5 km^3. The greatest areal coverage over the drift (111.074 km^2) is observed where the isopach thickness is 0-5 m. However, in

terms of volume contribution to the whole drift it is relatively low (0.555 km^3). The greatest contribution to volume is found where isopach thickness is 10-15 m (1.622km^3), yet here, area is similar to the 0-5 m isopach coverage (108.120 km^2).

Isopach Thickness (m)	Area (km^2)	Volume (km^3)
0-5	111.074	0.555
5-10	96.157	0.962
10-15	108.120	1.622
15-20	23.884	0.478
20-25	18.120	0.453
25-30	17.417	0.523
30-35	13.926	0.487
total	**388.698**	**5.080**

Table 4.1 Mertz Drift area and volume.

Calculations of carbon content utilised the approximate volume of 5 km^3 determined from the total volume calculated in Table 6.1. The estimate of carbon content of the Mertz Drift is 78 Mt, when derived from the following calculations:
(1) volume of solids = 5 km^3 x 40% = 2 km^3
(2) mass of solids = 2 km^3 x 2 600 kg/m^3 = 5200 million tonnes (Mt)
(3) carbon content = 5200 Mt x 1.5% = 78 Mt

4.3.2 Facies Classification

Examination of the X-radiographs of the Mertz Drift cores indicates an improved classification scheme is required when compared to Domack's (1988) X-radiograph interpretation of core DF79-12 (Figure 4.1). This was achieved by incorporating information such as the sedimentary structures revealed by the X-radiographs, and the grain size variations recorded in visual logs and multi-sensor core logger data. The Domack (1988) 'discontinuous laminae' facies was not used because of the difficulty in observing a difference between any discontinuous laminae and massively bedded sedimentary structure within X-radiographs of Mertz Drift cores. Sediments containing observed discontinuous laminae were classified within 'massively bedded siliceous mud and ooze' (SMO) facies in this study.

Five distinct facies are recognised and classified into: massively bedded SMO; massively bedded fine sand/SMO; laminated SMO; cross laminated SMO; and diamicton. Facies interpretation logs of all Mertz Drift cores are presented as figures within Appendix A in order of station number. A facies interpretation legend is given in Appendix A (Figure A1). The facies interpretation logs include intervals where sedimentary structures were not obvious due to dark X-radiographs (~ 7% of core X-radiographs). Facies interpretation logs in Appendix A also record the burrows observed within each core. The presence of facies within cores and the approximate percentage of facies from all cores is given in Table 4.2. Table 4.3 records the approximate percentage of burrows occurring in facies from all cores. The presence of facies within cores, the percentage of facies and percentage of burrows in facies is tabled to assist in determining any patterns of deposition within the Mertz Drift.

Cores	massively bedded SMO	massively bedded fine sand/SMO	laminated SMO	cross laminated SMO	diamicton
11GC02	x	x			
11GC03	x	x	x	x	
12GC04	x	x	x		
13GC05	x	x	x	x	
13GC06	x	x	x	x	
14GC07	x	x	x	x	
15GC08	x	x	x		
15GC09	x		x		
16PC01	x	x	x	x	
17PC02	x	x	x	x	x
18PC03	x	x	x	x	
19PC04	x	x	x	x	x
20PC05	x	x			x
23PC09	x	x	x	x	
24PC10	x	x			x
25PC11	x		x		
26PC12	x	x	x	x	x
27PC13	x	x	x	x	x
~ %	**33**	**10**	**48**	**4**	**5**

Table 4.2 Presence (x) of facies and approximate percentage of each facies from all Mertz Drift cores. Note 48% of all cores is laminated SMO, or the highest proportion of facies overall.

	massively bedded SMO	massively bedded fine sand/SMO	laminated SMO	cross laminated SMO	diamicton
~ %	60	24	16	0	0

Table 4.3 Approximate percentage of burrows occurring in each facies from all Mertz Drift cores. Note 60% of all burrows occurs in massively bedded SMO facies, or the highest proportion of burrows overall.

The following descriptions define the facies classification applied in this study, discuss the overall presence within cores, and provide images of X-radiographs as examples:

(1) Massively bedded SMO. This facies is the equivalent of Domack's (1988) 'massive beds'. X-radiographs displayed convoluted or no discernible (massive) sedimentary structure (Figure 4.4). Visual core logs often recorded these intervals with mottles. Burrows were often seen within the X-radiographs. Approximately 60% of all burrows observed within Mertz Drift cores appeared in this facies (Table 4.3).

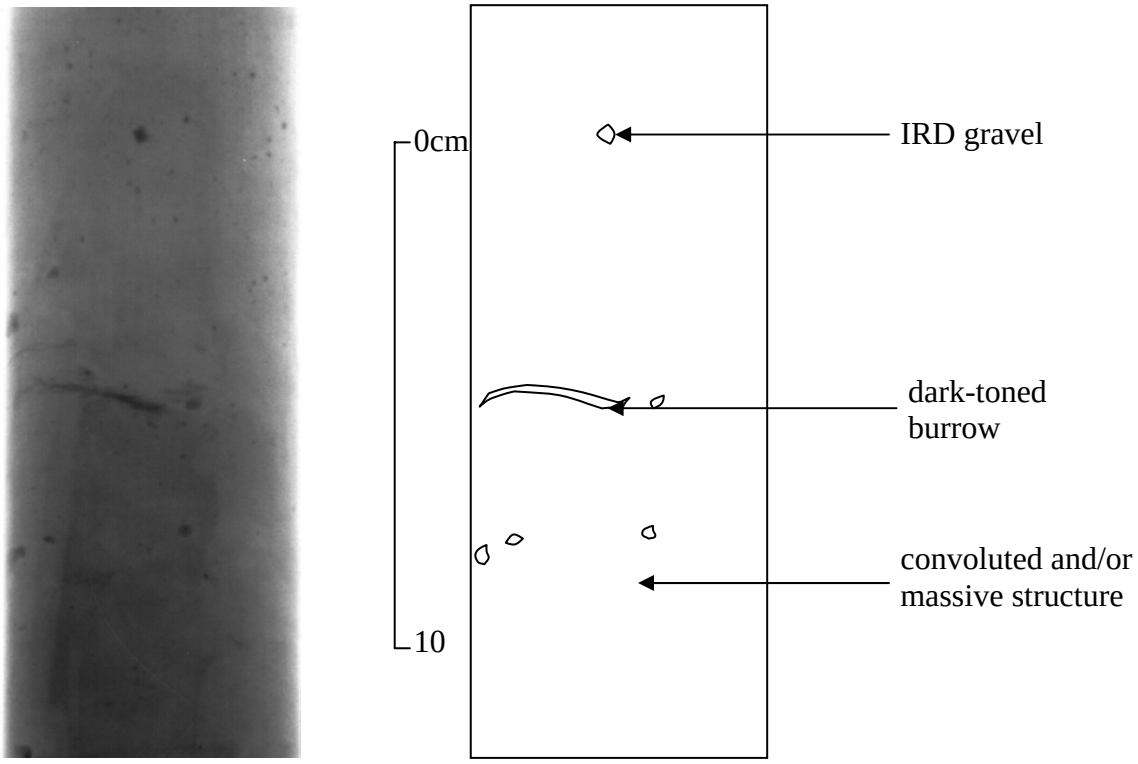

Figure 4.4 X-radiograph example and line drawing of massively bedded SMO facies within core 26PC12 (depth 393-408 cm).

Massively bedded SMO represents approximately 33% of all Mertz Drift cores, or the second most common facies (Table 4.2). This facies was observed in all cores studied (Table 4.2). This facies conforms to the compound glacial-marine facies of Anderson *et al.* (1983), as it comprises a mixture of glacial and marine components.

(2) Massively bedded fine sand/SMO. Domack (1988) did not provide a classification for this facies. Within massively bedded fine sand/SMO, X-radiographs of Mertz Drift cores reveal sedimentary structure as convoluted or massive (Figure 4.5). This facies is similar to the previously described massively bedded SMO except that numerous sand grains may be seen as dark-toned (dense) material in X-radiographs. Ice-rafted debris (IRD) gravel and dark-toned mottles, which may be sponge spicules according to the visual observation logs, are often observed in the X-radiographs. Burrows are also relatively numerous with approximately 24% of all burrows appearing in this facies (Table 4.3).

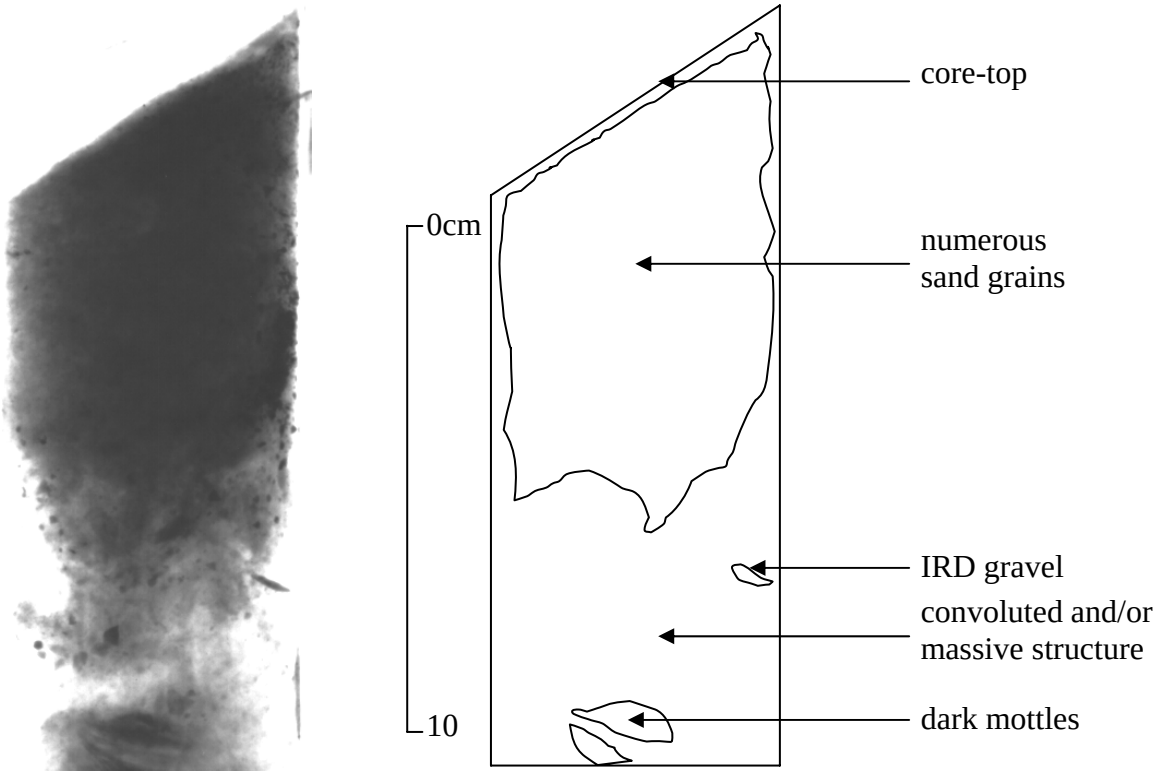

Figure 4.5 X-radiograph example and line drawing of massively bedded fine sand/SMO facies from core 16PC01 (depth 0-15 cm). Note: dark mottles may be sponge spicules.

Massively bedded fine sand/SMO represents approximately 10% of all Mertz Drift cores (Table 4.2). This facies is observed in 16 of the 18 recovered cores (Table 4.2). Cores with no evidence of this facies expression were cores 15GC09 and 25PC11, from the channel between the large and small lobes of the drift. Massively bedded fine sand/SMO also conforms to the compound glacial-marine facies of Anderson *et al.* (1983).

(3) Laminated SMO. This facies is the equivalent of Domack's (1988) 'laminations'. Laminated SMO facies are revealed by distinct horizontal dark- and light-toned laminae within the X-radiographs of Mertz Drift cores (Figure 4.6). Burrows are not as numerous with only approximately 16% of all burrows observed within this facies (Table 4.3).

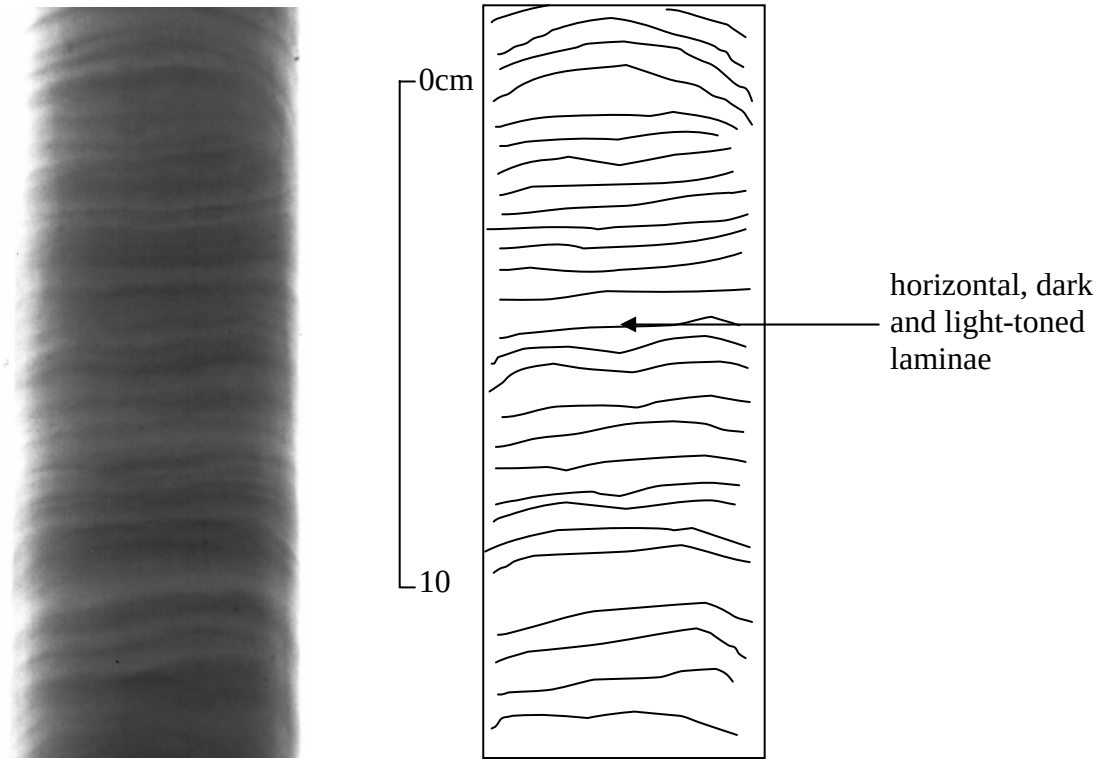

Figure 4.6 X-radiograph example and line drawing of laminated SMO facies within core 17PC02 (depth 164-179 cm). In this 15 cm section, dark-toned laminae have an approximate mean thickness of 2.7 mm; light-toned laminae have a mean thickness of 3.1 mm

Laminated SMO comprises approximately 48% of all Mertz Drift cores, and was the predominant sedimentary structure discernible within X-radiographs (Table 4.2). All Mertz Drift cores, except cores 11GC02, 20PC05 and 24PC10, were

observed with this facies (Table 4.2). Of these three exceptions, cores 20PC05, to the south of the drift, and 24PC10, to the north of the drift, lie at the periphery of the deposit where the isopach map of Figure 3.1 records sediment thickness at less than 1 m. Laminated SMO conforms to the Anderson *et al.* (1983) compound glacial-marine facies.

(4) Cross laminated SMO. This facies is the equivalent of Domack's (1988) 'cross laminae'. X-radiographs of cross laminated SMO display foresets and lateral accretion surfaces (Figure 4.7). Cross laminated SMO intervals commonly exhibit features that appear to be lateral accretion surfaces inclined at about 25˚, overlain by parallel foreset laminae. Occasionally, laminae are wavy or laterally discontinuous, or appear to be climbing ripples. Burrows are not observed in any cross laminated SMO facies (Table 4.3).

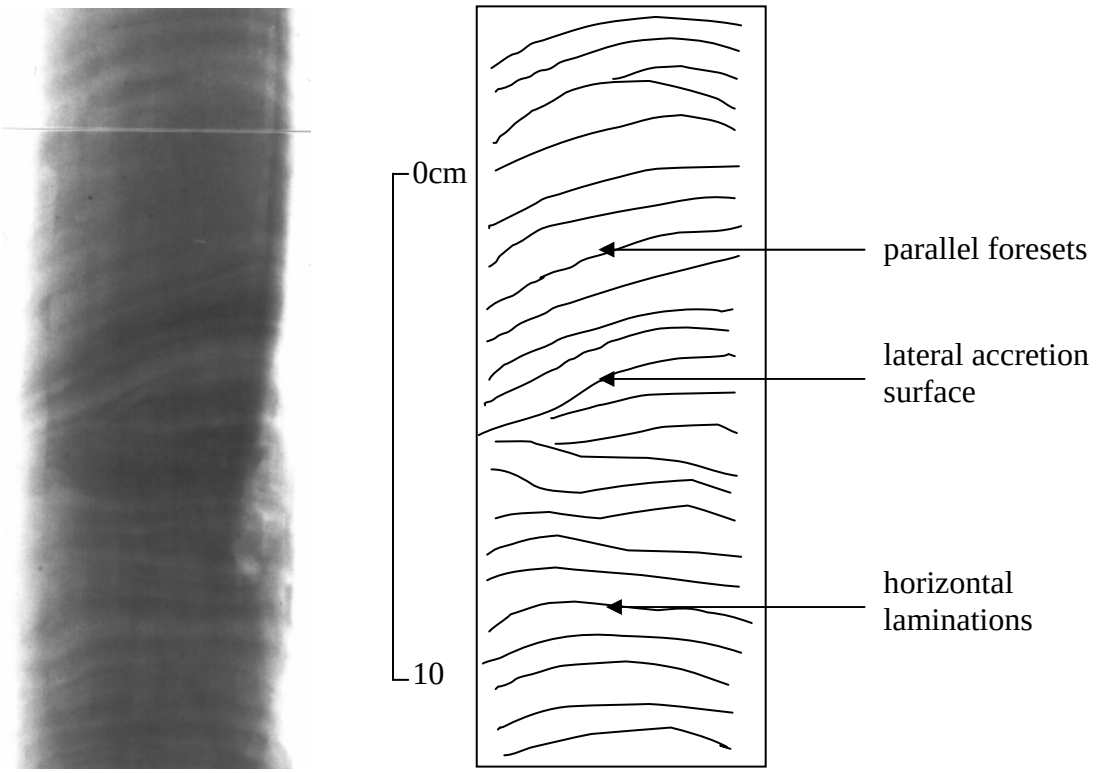

Figure 4.7 X-radiograph example and line drawing of cross laminated SMO facies from core 17PC02 (depth 91-106 cm).

Cross laminated SMO was the least common facies in Mertz Drift cores, representing approximately 4% of all cores (Table 4.2). This facies was observed in 11 of the 18 cores, most commonly in the longer piston cores (Table 4.2). Cross

laminated SMO occurs as intervals of about 7 cm thickness usually within the laminated SMO facies. This facies corresponds to the Anderson *et al.* (1983) compound glacial-marine facies.

(5) Diamicton. Domack (1988) also classified this facies 'diamicton'. Diamicton consists of massively bedded muddy gravel, observed in X-radiographs as very dark (dense) grains (Figure 4.8). Burrows were not observed within this facies (Table 4.3).

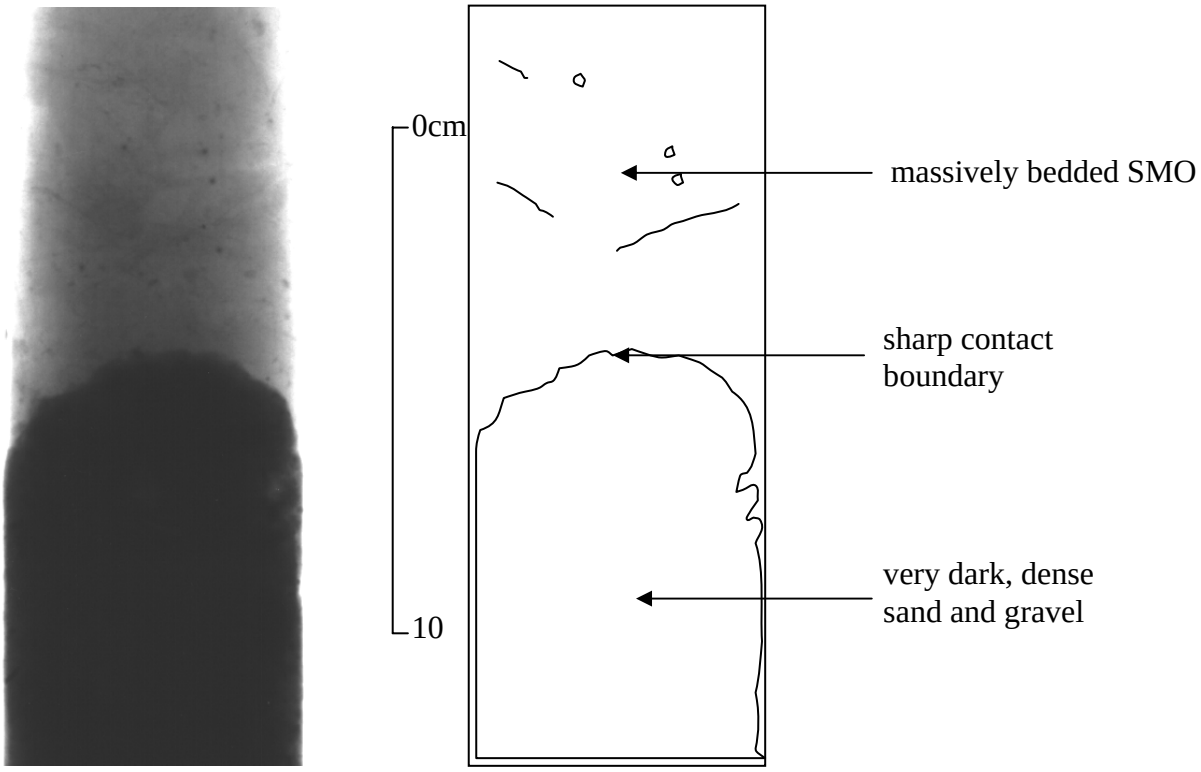

Figure 4.8 X-radiograph example and line drawing of diamicton facies from core 26PC12 (depth 486-501 cm).

Diamicton represents approximately 5% of all Mertz Drift cores (table 4.2). Diamicton only occurred within six piston cores that were sufficiently long to penetrate through the drift (Table 4.2). This facies matches the transitional glacial-marine facies of Anderson *et al.* (1983).

4.3.3 Ice-rafted Debris (IRD) Gravel Content

IRD gravel content at 5 cm intervals down each Mertz Drift core is recorded as graphs alongside the facies interpretation logs presented in Appendix A. The number of IRD gravel particles within each facies (except diamicton) is given in Table 4.3. Approximately 51% of all IRD gravel occurs in massively bedded SMO, which contain the highest proportion of gravel overall. A similarly high proportion of IRD gravel is found in massively bedded fine sand/SMO with approximately 30% of all IRD occurring in this facies. Despite laminated SMO being the largest proportion of Mertz Drift cores, only about 18% of all IRD gravel occurs in this facies. Cross laminated SMO recorded the least amount of gravel overall with about 1% of all IRD occurring in this facies.

Cores	massively bedded fine sand/SMO	massively bedded SMO	laminated SMO	cross laminated SMO
11 GC02	7	3		
11 GC03	6	2	2	1
12 GC04	14			
13 GC05		4	2	
13 GC06	1	1	10	
14 GC07	12			
15 GC08	3	19	1	
15 GC09		15	8	
16 PC01		9	5	
17 PC02	13	4	1	
18 PC03		7	8	1
19 PC04	17	23	15	1
20 PC05		19		
23 PC09	25	1	21	
24 PC10	8	35		
25 PC11		52	3	
26 PC12	2	30	5	
27 PC13	34	16	5	1
Sum (%)	**142 (30.1)**	**240 (50.8)**	**86 (18.2)**	**4 (0.9)**

Table 4.3 Table of IRD gravel content within each facies of each core, with the sum occurrence and percentage of all IRD within each facies. Note that massively bedded SMO has approximately 51% of all IRD, the highest proportion overall.

An example of the relative differences in IRD gravel content between facies is recorded in the gravel content graph of core 27PC13, from the east side of the drift (Figure 4.9). A peak of four gravel particles per 5 cm occurs within the massively bedded SMO at the bottom of the core. Within the predominantly laminated SMO and cross laminated SMO in the middle of the core is relatively low gravel content (one to two particles per 5 cm interval). At the top of core 27PC13, peaks of up to six gravel particles per 5 cm interval occur within the massively bedded fine sand/SMO.

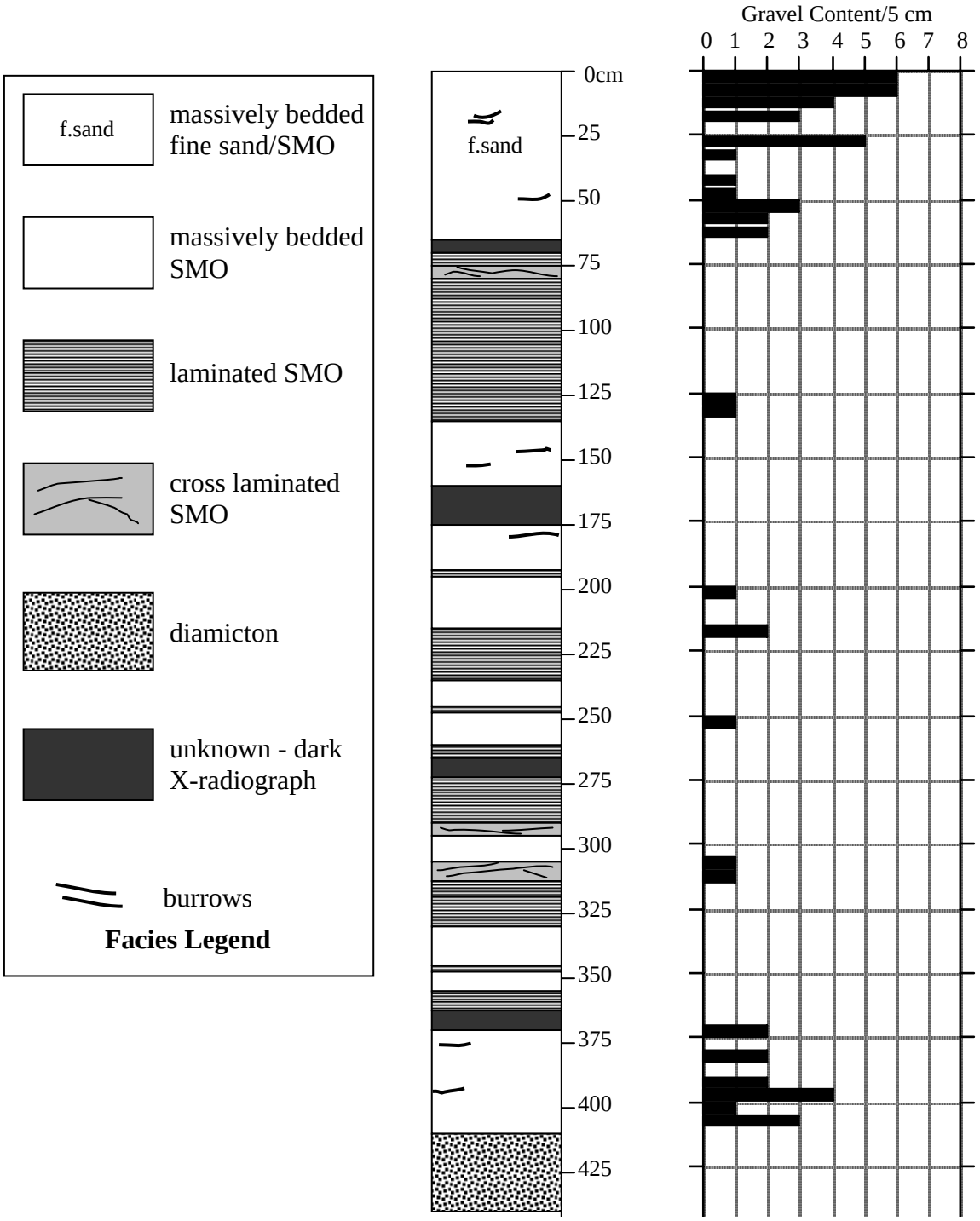

Figure 4.9 Graph of gravel content opposite the facies interpretation log of core 27PC13. Facies legend on the left.

4.3.4 Seafloor Photographs

Of the six stations photographed over the Mertz Drift during the WEGA research expedition, only station number 24, at the very north of the drift revealed clear photographs of the seafloor. The remaining photographs were too obscured by turbidity in the water column to be useful. The two photos of station 24 are shown in Figures 4.10 and 4.11.

Figure 4.10 Photograph of seafloor at station 24 in 819 metres of water (source: Brancolini and Harris 2000). Note the current tilted 20 cm long Sea pen (centre) and particles reflecting camera flash in the water column (top of photo).

Figure 4.11 Photograph of seafloor at station 24 in 819 metres of water (source: Brancolini and Harris 2000). Note the two large spherical glass sponges and angular ice-rafted cobble behind (centre-right). Smaller organisms in foreground may be golfball sponges with irregular projections. Sea pen in far backgound (top-right).

The organisms observed in the photographs are described as epibenthic suspension feeders that filter material entrained within the water column due to strong currents (Arntz and Gallardo 1994; Edgar 1997). The spherical, stalked sponges belong to the Class Hexactinellida. These sponges are mostly deepwater with exquisite glasslike skeletons (Buchsbaum *et al.* 1987). They are highly adapted to soft sediments but require some hardened material for attachment such as a rock or sponge spicule mat (Gowlett-Holmes 2000). Sea pens belong to Class Anthozoa Order Pennatulacea, and live with the stalk embedded in mud. The featherlike upper portion of the colony bears feeding polyps that capture tiny animals swept along in seabottom currents (Buchsbaum *et al.* 1987). Descriptions of seafloor photographs are summarised in Table 4.4. The substrate observed within the photographs is siliceous facies from Domack's (1988) surfical sedimentary facies classification. However, the substrate most likely represents massively bedded fine sand/SMO facies in this present study.

Station 24	Latitude 66˚ 28'.89 south	Longitude 143˚ 08'.20 east	Water depth 819m
Silty mud and ooze with current tilted solitary sea pen.			
Station 24	**Latitude 66˚ 28'.89 south**	**Longitude 143˚ 08'.20 south**	**Water depth 819m**
Silty mud and ooze and ice-rafted cobble. Biota are glass sponges, golfball sponges and a sea pen.			

Table 4.4 Location and summary of seafloor photograph descriptions of Station 24 on the Mertz Drift.

4.4 Summary of Results

In summary, the Mertz Drift has an area of approximately 390 km^2 and a volume of 5 km^3. Carbon content of the drift is 78 million tonnes (Mt).

The five facies identified in Mertz Drift cores in relation to the Domack (1988) classification and modified classification of this study are:

(1) Massively bedded SMO. Observed as 33% of all Mertz Drift cores, and recorded in all cores. Approximately 60% of all burrows observed appeared in this facies. Massively bedded SMO has the most IRD gravel content at 51% of all IRD gravel occurring in this facies.

(2) Massively bedded fine sand/SMO. Represented approximately 10% of all Mertz Drift cores, and is found in 16 out of 18 cores. Approximately 24% of all burrows occur in this facies. Massively bedded fine sand/SMO also has a large proportion of gravel content at 30% of all IRD gravel present in this facies.

(3) Laminated SMO. Comprised approximately 48% of all Mertz Drift cores, and is the most common facies observed. This facies is in 15 out of 18 cores. Despite being the predominant facies overall, only 16% of all burrows appear within this facies. Laminated SMO recorded only 18% of all IRD gravel overall.

(4) Cross laminated SMO. Represented approximately 4% of all Mertz Drift cores, and is the least common facies recorded. This facies is in 11 out of 18 cores. Burrows

were not seen in any cross laminated SMO facies. Cross laminated SMO recorded the least amount of IRD gravel content at 1% of all IRD in this facies.

(5) Diamicton. Observed in approximately 5% of all Mertz Drift cores. Diamicton only occurred within six cores that were sufficiently long to penetrate through the Mertz Drift. Burrows were not observed within this facies. IRD gravel content was not quantified in diamicton.

Seafloor photographs at one site record sponge communities and Anthozoa on the Mertz Drift. This benthos is adapted for growing on soft sediments, and consists of epibenthic suspension feeders that filter material swept along by strong currents. The substrate represents massively bedded fine sand/SMO facies.

Chapter 5. Palaeoclimatology

5.1 Introduction

Chapter Five discusses palaeoclimatology, in particular the timing and glacial development of East Antarctica since the Last Glacial Maximum (LGM). Information on glacial history will provide a baseline from which to compare the results of the radiocarbon age data from the Mertz Drift cores. Thus, this chapter is in two parts. Part one begins with a brief overview of radiocarbon dating and its use in Antarctic marine cores. A general view of the timing of post-LGM glacial development of East Antarctica is presented. This first part also discusses the geographic limits of the last glacial advance off George V Land, and the radiocarbon age results of 'Operation Deep Freeze' 1979 (DF79), in particular, the ages obtained from core DF79-12. The results of ages from core DF79-12 have been used to constrain the timing for the retreat of the Mertz Glacier over the George V Basin.

The second part of this chapter presents the results of radiocarbon dating samples from the Mertz Drift cores. Sediment accumulation rates are calculated for cores 13GC05, 13GC06 and 26PC12, and are compared against the facies within the cores to determine if there are any underlying sedimentation patterns within the Mertz Drift. The laminations observed within X-radiographs and visual core logs of cores 13GC05 and 13GC06 are compared against one another for accuracy, then the mean deposition time is calculated for lamination couplets in cores 13GC05 and 26PC12. The reason for calculating the mean deposition time for lamination couplets is because an hypothesis of this study is that Mertz Drift sediments largely result from diatom blooms due to annual seasonal changes in sea ice cover. The mean deposition time thus assists in determining whether lamination couplets have an annual cyclicity. A summary of the Mertz Drift results concludes Chapter Five.

5.2 Palaeoclimatology

5.2.1 Radiocarbon Dating

The timing of glacial and climatic events since the Last Glacial Maximum (LGM) in Antarctica is determined primarily through radiocarbon or carbon-14 dating (Ingolfsson *et al.* 1998). Therefore, an understanding of the problems and limitations of this dating technique is important before interpretations of dates can be made. Radiocarbon dating uses carbon-14 obtained from terrestrial and aquatic mosses, marine materials like mollusc shells, foraminifera, phytoplankton carbon and marine mammal bones (Ingolfsson *et al.* 1998). Antarctic deep marine sediments lack calcite due to the dissolution of calcium carbonate, yet they contain significant amounts of organic carbon that may be used for radiocarbon dating (Domack *et al.* 1989).

The carbon-14 content of all marine organisms is affected by the 'reservoir effect', which produces marine species with apparent radiocarbon ages older than they really are (Berkman and Forman 1996). In Antarctic living marine species, the reservoir effect commonly exceeds 1000 years, which is much older than marine species from other parts of the world (Berkman and Forman 1996). An effect of this scale is believed to arise from the depletion of carbon-14 in oceanic surface water around Antarctica, and relates to the antiquity of the carbon pool in the Southern Ocean (Berkman *et al.* 1998). The depletion of carbon-14 results in modern radiocarbon ages for Antarctic marine samples that appear too old (Verkulich and Hiller 1994; Cunningham *et al.* 1999). To correct radiocarbon ages obtained from shallow marine fossils, which may contain sufficient calcium carbonate for dating, a reservoir correction value is subtracted from the obtained radiocarbon age (Berkman and Forman 1996; Berkman *et al.* 1998). A number of researchers use a circum-Antarctic reservoir correction value of 1000 to 1300 years (Baroni and Orombelli 1991; Ingolfsson *et al.* 1998), but this correction value may vary regionally (Berkman and Forman 1996).

When dating deep Antarctic marine sediments, the lack of calcium carbonate or large marine fossils requires dating organic carbon, and using a standard reservoir

correction value has not always resulted in bringing marine sediment core-tops to the modern age (Cunningham *et al.* 1999; McMinn 2000). This is possibly due to plankton harvesting anomalously 'old' surface waters mixed with glacial meltwater (Domack *et al.* 1989) or at the seafloor through reworking of older sediment by glacial advance and contamination of the modern sediments (Harris *et al.* 1996). The practice amongst marine sediment workers is to subtract the core-top radiocarbon age from the remainder of downcore radiocarbon ages (Cunningham *et al.* 1999; McMinn 2000). This methodology assumes an age offset due to the reservoir effect and that contamination is constant through time. Neither of these assumptions may be accurate in providing true corrected ages (Cunningham *et al.* 1999).

5.2.2 Post-LGM Glacial Development of East Antarctica

The timing of the Last Glacial Maximum (LGM) around Antarctica is believed to have coincided with the timing of lowest global sea levels around 20,000-18,000 years Before Present (yr BP; Ingolfsson *et al.* 1998). Current opinion suggests that as the Northern Hemisphere continental ice sheets retreated and global sea level began to rise about 18,000 years ago, the outlet glaciers along the East Antarctic continental shelf were also forced to retreat landward (Harris and O'Brien 1998). Using a marine sediment core from Prydz Bay (core sections 1R-3R Ocean Drilling Program Leg 119, Site 740A), the timing of glacial retreat showed siliceous mud and diatom ooze (SMO) was initially deposited after 10,700 yr BP, thus dating the time of ice shelf retreat past the core site (Domack *et al.* 1991). Harris and O'Brien (1998) also confirm that the onset of open marine conditions after the LGM occurred about 10,000 yr BP on the outer shelf off Mac.Robertson Land, near Prydz Bay. A facies succession from SMO to terrigenous sediment and back to SMO within Prydz Bay was interpreted as evidence of a surge in the outlet system of the Lambert Glacier synchronous with a mid-Holocene warming event (Domack *et al.* 1991).

Given the paucity of data from marine sediments along the Antarctic continental shelf, evidence for the timing of post-LGM glacial retreat is more numerous from studies on land (Ingolfsson *et al.* 1998). These include studies of glacial morphology (Goodwin 1996; Colhoun 1997), lake sediments (Roberts and

McMinn 1999; Roberts *et al.* 2000), raised beaches (Baroni and Orombelli 1991; Berkman *et al.* 1998) and fossil penguin rookeries (Heine and Speir 1989; Emslie *et al.* 1998). In the review and broad synthesis of East Antarctic glacial history since the LGM, Ingolfsson *et al.* (1998) applied a standard 1300 year reservoir correction to all radiocarbon ages (Figure 5.1).

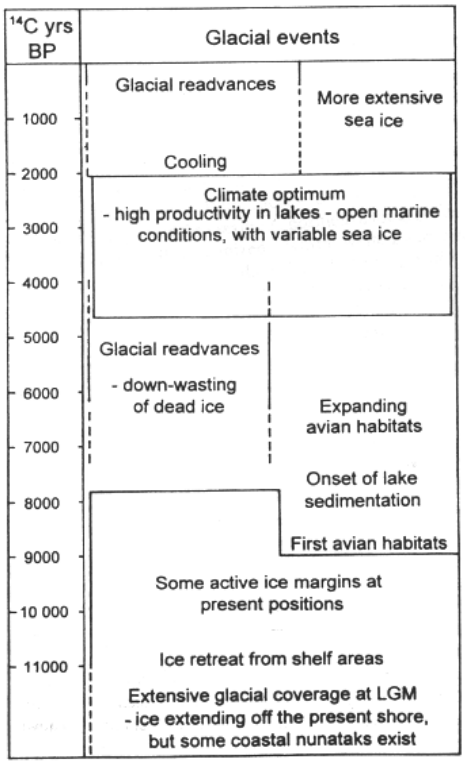

Figure 5.1 Broad synthesis for glacial and climatic development in East Antarctica since the LGM (source: Ingolfsson *et al.* 1998). The LGM is believed to have occurred 20,000-18,000 yr BP (Ingolfsson *et al.* 1998).

Ingolfsson *et al.* (1998) found that all land based studies of East Antarctica inferred relatively moderate ice thickness during the LGM, with ice extending off the present shore, but not far onto the shelf. Ice retreat from the shelf areas was underway by 13,000 to 10,000 yr BP (Berkman *et al.* 1998; Ingolfsson *et al.* 1998). The oldest deglaciation dates show freshwater and avian habitats developed in coastal areas between 12,000 to 8000 yr BP (Ingolfsson *et al.* 1998; Roberts and McMinn 1999). Indications of a minor mid-Holocene glacial readvance from 6200 yr BP are reported from glaciers in the Bunger Hills (Colhoun 1997).

There is evidence for a mid-Holocene climate optimum from about 4700 to 2000 yr BP (Berkman *et al.* 1998; Ingolfsson *et al.* 1998). This period was warmer, wetter and had less sea ice than the present (Ingolfsson *et al.* 1998). Baroni and Orombelli (1991) call this same period a 'penguin optimum' when areas of land along the coast of Victoria Land in the Ross Sea became free of ice. A distinct climatic deterioration occurred after 2000 yr BP, again with colder, drier conditions, and more sea ice (Ingolfsson *et al.* 1998; Roberts *et al.* 2000). There followed a subsequent warming to the current warmer climate to present (Ingolfsson *et al.* 1998; Roberts *et al.* 2000). The data also show minor fluctuations of the ice margins over the past few hundred years, possibly correlating with Little Ice Age advances in the Northern Hemisphere (Fitzsimons and Colhoun 1995; Goodwin 1996; McMinn 2000).

5.2.3 Limits of Glacial Advance off George V Land

A variety of methods was used to reconstruct ice flow paths and the geographic limits of the ice sheet during the last glacial advance off George V Land (refer next section 5.2.4 for details on timing). Domack *et al.* (1989) identified lateral and terminal moraines upon the outer shelf using seismic profiles. These submarine moraines partly encircled the deep, inner shelf basins and intervening banks of the continental shelf off George V Land where the Mertz and Ninnis Glacier Tongues dominate ice drainage. Relict glacial tills were also molded into fluted surfaces that reflected ice flow direction (Domack *et al.* 1989). Another method was to study the mineralogy of relict glacial and glacial-marine sediments from the continental shelf in order to determine the source terrain from the geology known along the coast (Domack 1982). Using the various methods to reconstruct ice flow paths, Domack *et al.* (1989) proposed that during the last glacial advance, ice flow over the continental shelf was from southeast to northwest (Figure 5.2), in contrast to the northeast ice flow presently with the Mertz and Ninnis Glacier Tongues.

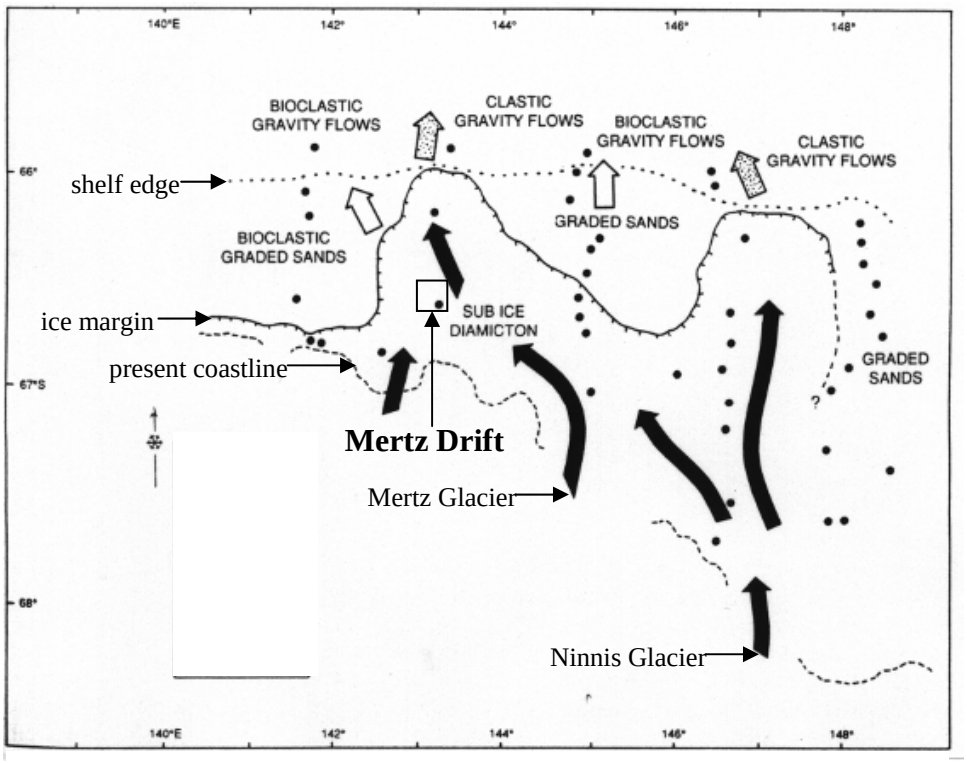

Figure 5.2 Late Pleistocene-Holocene reconstruction for the George V Land ice margin (source: Domack *et al.* 1989). Dark arrows = ice flow paths; white arrows = transport direction for bioclastic sands; and dotted arrows = transport directions for coarse clastics. Note the Mertz Drift study site within the box.

Figure 5.2 exhibits an expanded Mertz Glacier grounded on the outer shelf north of the Mertz Drift during the last glacial advance. The stratified muddy diamicton found at the bottom of core DF79-12 was interpreted to have been deposited as subglacial till in quiescent marine conditions in the deepest part of the basin while the expanded Mertz Glacier Tongue was above it (Domack 1982; Domack *et al.* 1991).

5.2.4 Carbon-14 Ages in Core DF79-12

Bulk organic carbon samples from core DF79-12 were obtained for radiocarbon dating (Table 5.1). A linear regression of uncorrected radiocarbon dates belonging to core DF79-12 revealed a sediment accumulation rate of about 340 cm/kyr (Domack *et al.* 1989). When the sediment accumulation rate was extrapolated to the core-top of DF79-12, a surface age of about 5500 yr BP was produced. The extrapolated surface age correlated well with the uncorrected age of a surface sample taken from core DF79-9 (a core obtained on the Adélie Bank some 80 km to the west

of core DF79-12) at 5020 yr BP (Domack *et al.* 1989). Thus, the corrected ages in core DF79-12 are radiocarbon ages minus 5020 years (Domack *et al.* 1991).

Sample No.	Core	Depth (cm)	Description	Radiocarbon Age (yr BP)	Corrected Age (yr BP)
AA6428	12	103-104	SMO	6000 +/- 90	980
AA6429	12	150-151	SMO	6130 +/- 95	1110
AA1970	12	203-204	SMO	6430 +/- 80	1410
AA6430	12	398-400	SMO	6900 +/- 75	1880
AA6431	12	478-480	SMO	7450 +/- 80	2430
AA1971	12	549-550	SMO	7350 +/- 80	2330

Table 5.1 Uncorrected and corrected radiocarbon ages from core DF79-12 (Sample Nos. AA1970 and AA1971 from: Domack *et al.* 1989; Sample Nos. AA6428, AA6429, AA6430 and AA6431 from: Domack *et al.* 1991).

Domack *et al.* (1991) used the corrected ages to interpret a transition from proximal ice-tongue to open marine conditions, which demonstrated the last glacial advance off George V Land was mid-Holocene in age. They stated that the LGM in the George V Basin was associated with the outlet systems (Mertz and Ninnis Glacier Tongues) rather than the main ice sheet itself. The timing of the last glacial advance was attributed to a mid-Holocene glacial expansion of the Mertz and Ninnis Glacier Tongues synchronous with a warming event of 7000 to 4000 yr BP (Domack *et al.* 1991). Domack *et al.* (1989) previously noted that other Antarctic marine sediment studies revealed that post-LGM sea level rise and glacial retreat around Antarctica were much earlier than the mid- to late-Holocene glacial retreat interpreted from core DF79-12. Domack *et al.* (1991) admitted that the timing of the transition to open marine conditions within the George V Basin was uncertain, and longer cores from this basin would help complete the Holocene record in this area.

The first part of this chapter has discussed the timing and glacial development of East Antarctica since the LGM. The geographic extent and timing of the last glacial advance over the George V Basin has also been discussed. This information provides a baseline for the radiocarbon age results of this study, which are presented in the second part of the chapter.

5.3 Results

One of the aims of this study was to use radiocarbon age data to explain the timing of any facies succession, and whether the Mertz Drift sediments do record a high resolution of palaeoenvironment change during the Holocene. The results of radiocarbon age data from samples obtained from Mertz Drift cores are presented. Sediment accumulation rates are calculated for cores 13GC05, 13GC06 and 26PC12, then compared against facies interpretation logs of the cores in order to determine if there are any underlying sedimentation patterns. Lamination couplets observed within X-radiographs and visual core logs of cores 13GC05 and 13GC06 are compared against one another for accuracy, then mean deposition time is calculated for lamination couplets in cores 13GC05 and 26PC12. The mean deposition time is calculated in order to determine whether lamination couplets have an annual cyclicity. An annual cyclicity may prove one of the hypotheses for this study - that Mertz Drift sediments largely result from diatom blooms due to annual seasonal changes in sea ice cover.

5.3.1 Radiocarbon Ages

Twenty-five radiocarbon ages had been received from the Institute of Geological and Nuclear Sciences, New Zealand. An additional radiocarbon age was received from Geochron Laboratory, Massachusetts, USA. Table 5.2 documents uncorrected radiocarbon and corrected ages. Note that errors are additive for corrected age. Uncorrected radiocarbon ages are also displayed next to the facies interpretation logs of Mertz Drift cores presented within Appendix A.

Lab No.	Core	Depth (cm)	Description	Radiocarbon Age (yr BP)	Corrected Age (yr BP)
NZA11851	13GC05	0-1	f.sand/SMO	3155 +/- 70	0 +/- 70
NZA11892	13GC05	15-16	SMO	5653 +/- 60	2498 +/- 130
NZA11893	13GC05	100-101	SMO	5881 +/- 60	2726 +/- 130
NZA11924	13GC05	200-210	SMO	6 024 +/- 55	2869 +/- 125
NZA11925	13GC05	292-293	SMO	6 542 +/- 70	3387 +/- 140
NZA11926	13GC06	0-1	f.sand/SMO	2 736 +/- 55	0 +/- 55
NZA11927	13GC06	42-43	SMO	5 822 +/- 65	3086 +/- 120
NZA11928	13GC06	100-101	SMO	6 078 +/- 60	3342 +/- 115
NZA11929	13GC06	200-201	SMO	6 352 +/- 55	3616 +/- 110
NZA11837	14GC07	0-1	f.sand/SMO	2 272 +/- 55	0 +/- 55
NZA11838	14GC07	70-71	SMO	7 970 +/- 60	5698 +/- 115
NZA11839	15GC09	0-1	SMO	2 690 +/- 55	0 +/- 55
NZA11840	15GC09	20-22	SMO	5 828 +/- 55	3138 +/- 110
NZA11841	17PC02	0-1	f.sand/SMO	2 431 +/- 55	0 +/- 55
NZA11842	17PC02	45-46	SMO	5 927 +/- 60	3496 +/- 115
NZA11843	17PC02	514-515	diamicton	27 020 +/- 200	24,589 +/- 255
NZA11835	25GB13	0-1	f.sand/SMO	2 835 +/- 65	not applicable
GX26788	25PC11	145-147	SMO	3 120 +/- 40	no surface age
NZA11844	25PC11	398-399	SMO	7 668 +/- 55	no surface age
NZA11836	26GB14	0-1	f.sand/SMO	2 780 +/- 55	not applicable
NZA11845	26PC12	0-1	f.sand/SMO	2 241 +/- 55	0 +/- 55
NZA11846	26PC12	99-100	SMO	5 414 +/- 55	3173 +/- 110
NZA11847	26PC12	199-200	SMO	6 115 +/- 65	3874 +/- 120
NZA11848	26PC12	299-300	SMO	6 266 +/- 70	4025 +/- 125
NZA11849	26PC12	399-400	SMO	7 152 +/- 60	4911 +/- 115
NZA11850	26PC12	482-483	SMO	15 469 +/- 70	13,228 +/- 125

Table 5.2 List of Mertz Drift samples utilised for radiocarbon dating.

(1) Uncorrected Radiocarbon Ages. The material dated ranges in age from 2241 yr BP from the top of core 26PC12, on the large lobe edge, to a maximum age of 27,020 yr BP for diamicton from core 17PC02, in the centre of the Mertz Drift. The only sample taken near the SMO-diamicton boundary is from the base of 26PC12 (482-483 cm), and returned an uncorrected age of 15,469 yr BP. Eight sampled core-tops (0-1 cm) revealed uncorrected radiocarbon ages of between 2241 yr BP from core 26PC12 to 3155 yr BP from core 13GC05. The eight core-top ages produced a mean surface radiocarbon age of 2643 yr BP with a standard deviation of +/- 290 years.

(2) Corrected Ages. The corrected ages listed in Table 5.2 utilise only the age from each core-top and not the mean core-top (surface) correction. Only core 25PC11, from the channel, did not have a core-top age and thus a corrected age. It should be noted that any samples from stations 15 and 25, in the channel, are suspect as

recovery of sediments from this part of the drift were quite poor due to the high water content and slumping within the cores. Of the cores corrected, 13GC05 and 13GC06, from the large lobe, 17PC02 in the centre of the drift and possibly 15GC09, in the channel, constrain the massively bedded fine sand/SMO drape over the Mertz Drift, as samples were obtained just below this layer (Harris 2000). These corrected ages are 2498, 3086, 3496 and 3138 yr BP, respectively. Thus, the fine sand/SMO layer has a mean age of 3055 yr BP (standard deviation = +/- 358 years). Using the limited corrected ages available, the SMO-diamicton facies boundary previously mentioned lies between 13,228 and 24,589 yr BP.

(3) Corrected Age versus Depth Graphs. Only cores 13GC05 and 13GC06, on the large lobe, and core 26PC12, from the large lobe edge, had sufficient corrected age samples to produce graphs of age versus depth. A linear regression and correlation coefficient was calculated for each graph. The slope of the linear regression allows calculation of average sediment accumulation rates for these cores.

The graphs of corrected age versus depth for cores 13GC05 and 13GC06 (Figures 5.3 and 5.4 respectively) demonstrate similar and fairly consistent trends of sediment accumulation rates. Comparison with the facies interpretation logs of cores 13GC05 and 13GC06 (refer Appendix A - Figures A.5 and A.6) revealed predominantly laminated SMO between the radiocarbon sample positions. Linear regression analysis indicates good age versus depth correlation (R = 0.96; R = 0.99 respectively, where R = 1 is a perfect fit and R = 0 is a poor fit).

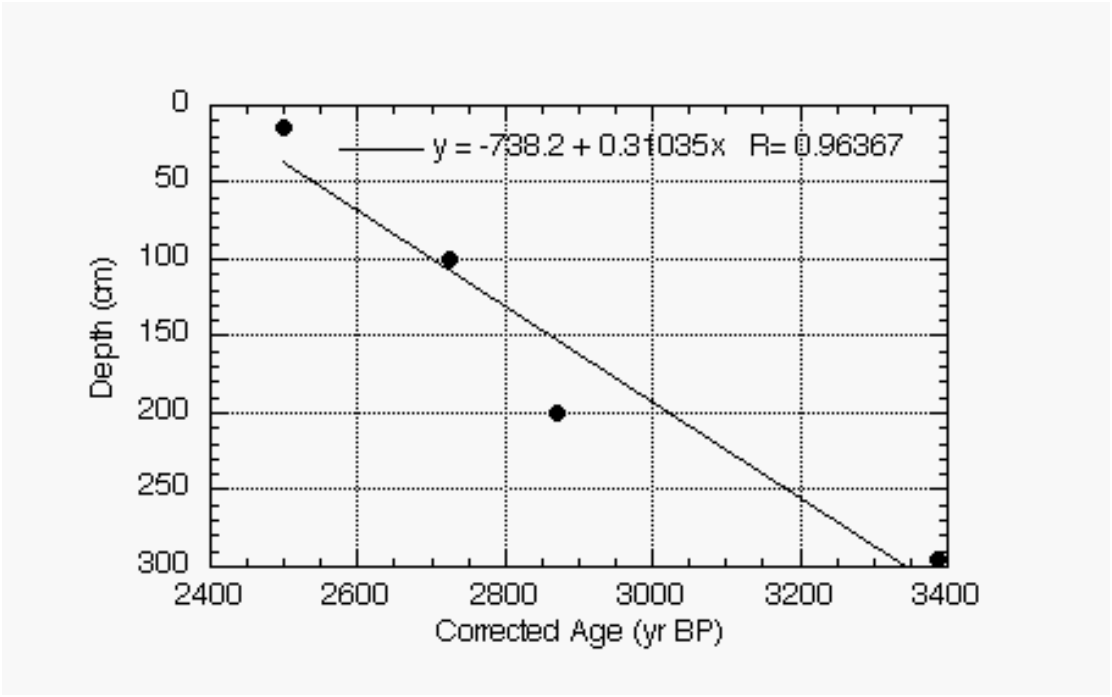

Figure 5.3 Graph of corrected age versus depth for core 13GC05 (samples 15-16, 100-101, 200-210 and 292-293 cm). Linear regression: Depth = -738.2 + 0.31035 x Corrected Age; Correlation coefficient: R = 0.96367.

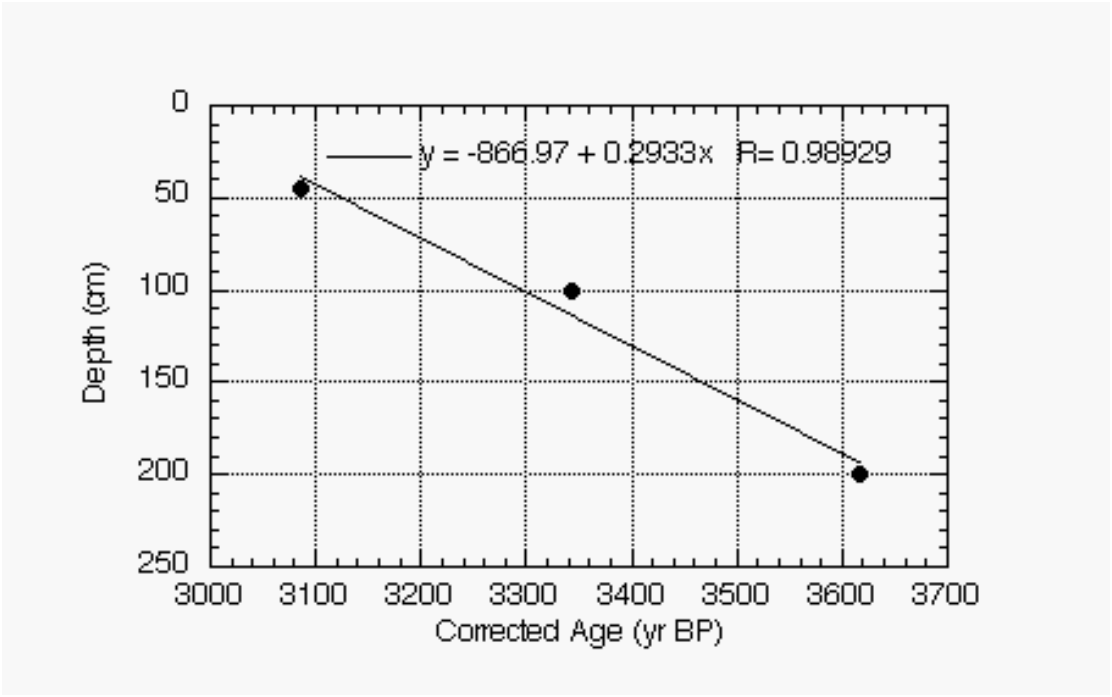

Figure 5.4 Graph of corrected age versus depth for core 13GC06 (samples 42-43, 100-101 and 200-201 cm). Linear regression: Depth = -866.97 + 0.2933 x Corrected Age; Correlation coefficient: R = 0.98929.

Initial analysis of a graph of corrected age versus depth of core 26PC12 indicated that the sediment accumulation rate between the bottom two samples (399-400 cm and 482-483 cm) was much lower than average accumulation rates for the samples above 399 cm (Figure 5.5). A comparison with core 26PC12 facies interpretation log revealed predominantly massively bedded SMO between 399 to 483 cm while mostly laminated SMO was above 399 cm (refer Appendix A - Figure A.18). The conclusion is that sediment accumulation rates vary between facies. To calculate linear regressions (sediment accumulation rates) for the two different facies within the samples obtained from core 26PC12, two graphs are presented, displaying corrected age versus depth for samples 99-100 to 399-400 (Figure 5.6) and samples 399-400 to 482-483 (Figure 5.7)

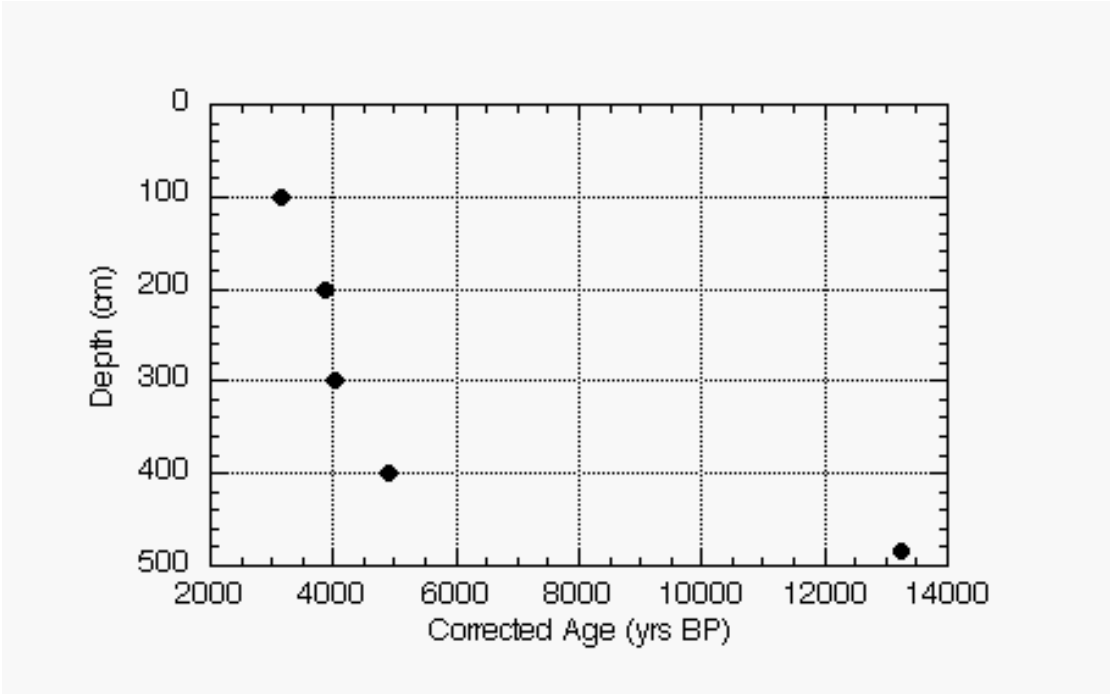

Figure 5.5 Graph of corrected age versus depth for core 26PC12 (samples 99-100, 199-200, 299-300, 399-400 and 482-483 cm). Note the different slopes (sediment accumulation rates) between samples 99-100 to 399-400 cm and 399-400 to 482-483 cm.

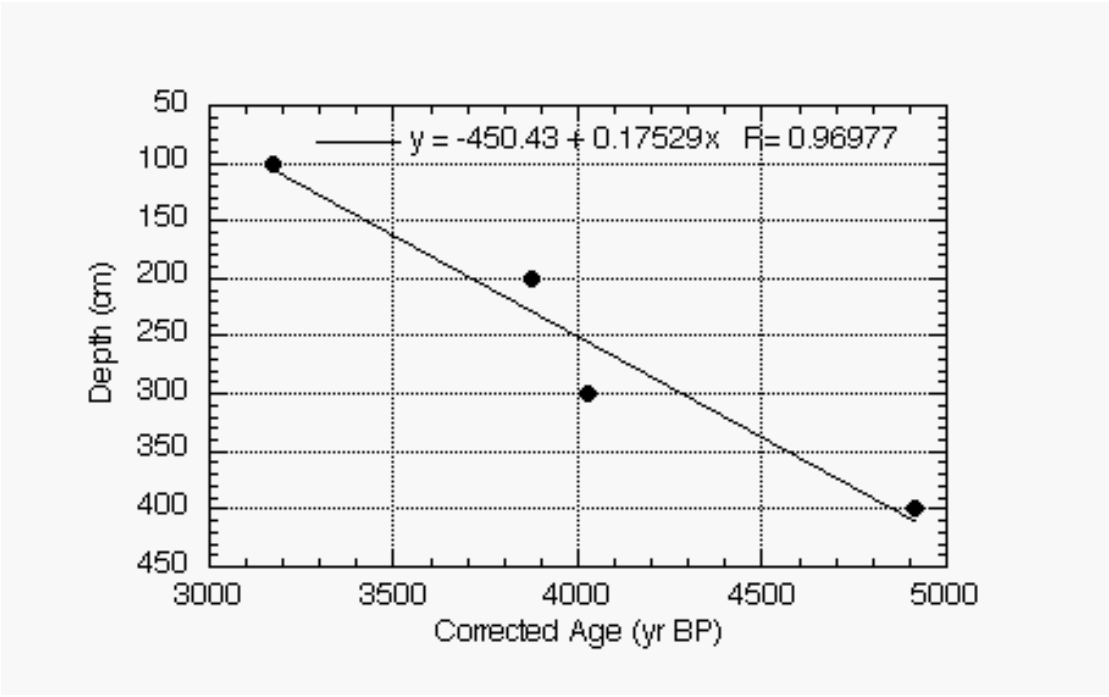

Figure 5.6 Graph of corrected age versus depth for core 26PC12 (samples 99-100, 199-200, 299-300 and 399-400 cm). Linear regression: Depth = -450.43 + 0.17529 x Corrected Age; Correlation coefficient: R = 0.96977. Note the relatively high sedimentation rate of about 0.66 cm/yr between samples 199-200 and 299-300 cm.

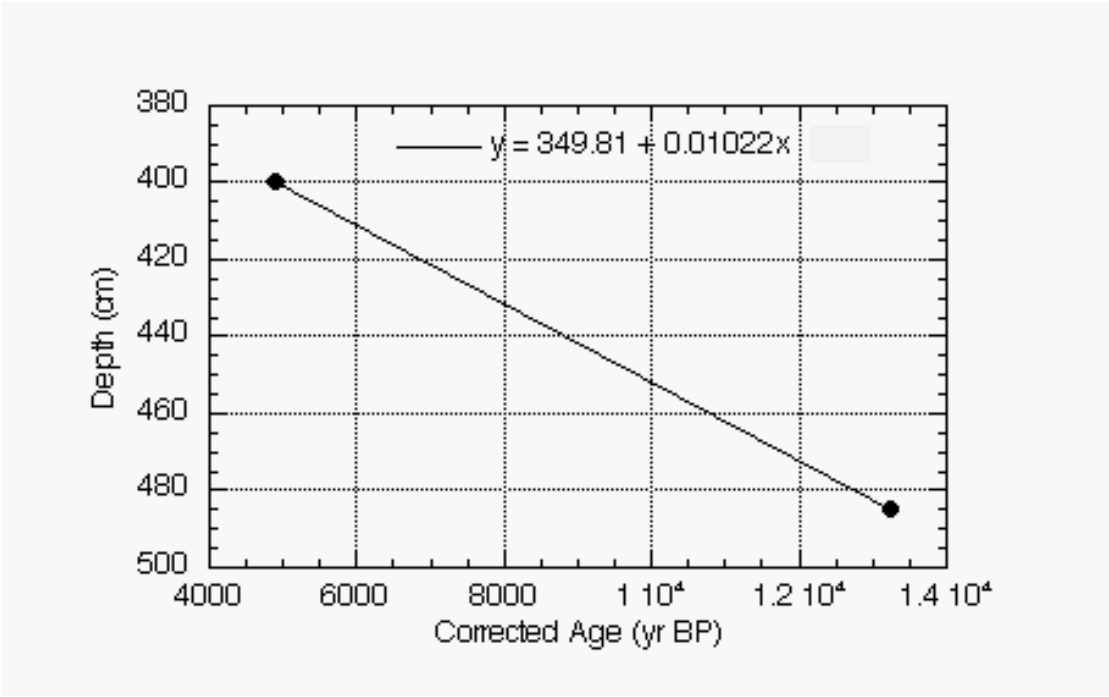

Figure 5.7 Graph of corrected age versus depth for core 26PC12 (samples 399-400 and 482-483 cm). Linear regression: Depth = 349.81 + 0.01022 x Corrected Age.

Figure 5.6 also demonstrates a fairly consistent trend of sediment accumulation rate within the predominantly laminated SMO facies, indicating a good age versus depth correlation (R = 0.97). In Figure 5.6, there is a relatively high sediment accumulation rate of about 0.66 cm/yr between samples 199-200 and 299-300 cm. This high accumulation rate corresponds with a section of core 26PC12 observed with three cross bedded SMO intervals.

(4) Sediment Accumulation Rates. From the slopes of the linear regressions calculated for the previous graphs, average sediment accumulation rates (cm/kyr then converted to cm/yr and yr/cm) are presented for the laminated SMO intervals of cores 13GC05, 13GC06 and 26PC12 (Table 5.3). Average sediment accumulation rates are also included from the cross bedded SMO and massively bedded SMO intervals of core 26PC12.

Core	Depth Interval (cm)	Facies	cm/kyr	cm/yr	yr/cm
13GC05	15-293	laminated SMO	310	0.310	3.22
13GC06	42-201	laminated SMO	293	0.293	3.41
26PC12	99-400	laminated SMO	175	0.175	5.71
26PC12	200-300	cross bedded SMO	662	0.662	1.51
26PC12	400-483	massive SMO	10	0.010	100.00

Table 5.3 Average sediment accumulation rates and predominant facies within cores 13GC05, 13GC06 and 26PC12.

The average sediment accumulation rates of Table 5.3 clearly show variability in deposition rates across the Mertz Drift. On the large lobe of the drift (cores 13GC06 and 13GC05), deposition of laminated SMO sediments was a high 293-310 cm/kyr respectively. On the edge of the large lobe (core 26PC12), deposition of laminated SMO is reduced to 175 cm/kyr. The section of core 26PC12 observed with three cross laminated SMO intervals reveals a relatively higher rate of deposition at 662 cm/kyr. At the bottom of core 26PC12, the massively bedded SMO appears to deposit at a relatively slow 10 cm/kyr.

In addition to the average sediment accumulation rates of Table 5.3, the massively bedded fine sand/SMO facies, found as a drape over the Mertz Drift, has an approximate sediment accumulation rate of 10 cm/kyr, based upon the average 30 cm thickness of the drape and the mean age of 3055 yr BP at the base of the facies. Thus, the average sediment accumulation rate of the massively bedded fine sand/SMO facies is comparable with that of the massively bedded SMO facies.

Based upon the average sediment accumulation rates, corrected ages were applied as an approximate 'best fit' to the facies interpretation logs and IRD gravel content graphs of cores 13GC05, 13GC06 and 26PC12 (Figures 5.8, 5.9 and 5.10 respectively).

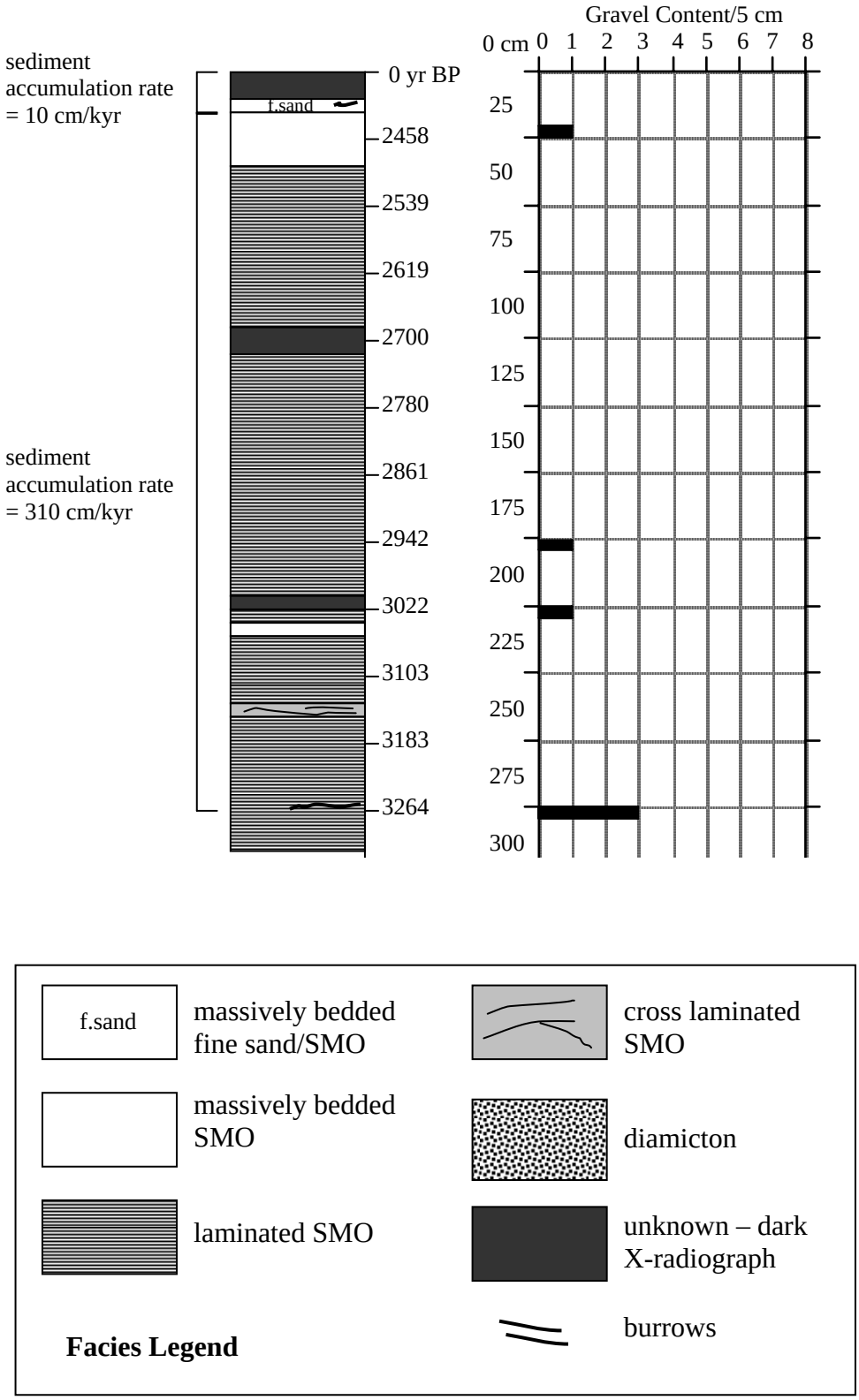

Figure 5.8 Corrected age for core 13GC05 facies interpretation log and corresponding graph of gravel content per 5 cm based on average sediment accumulation rates. The core is predominantly laminated SMO deposited between about 3200 to 2500 yr BP with correspondingly low gravel content. From about 2500 yr BP a massively bedded SMO was deposited with massively bedded fine sand/SMO in the top 15 cm of the core.

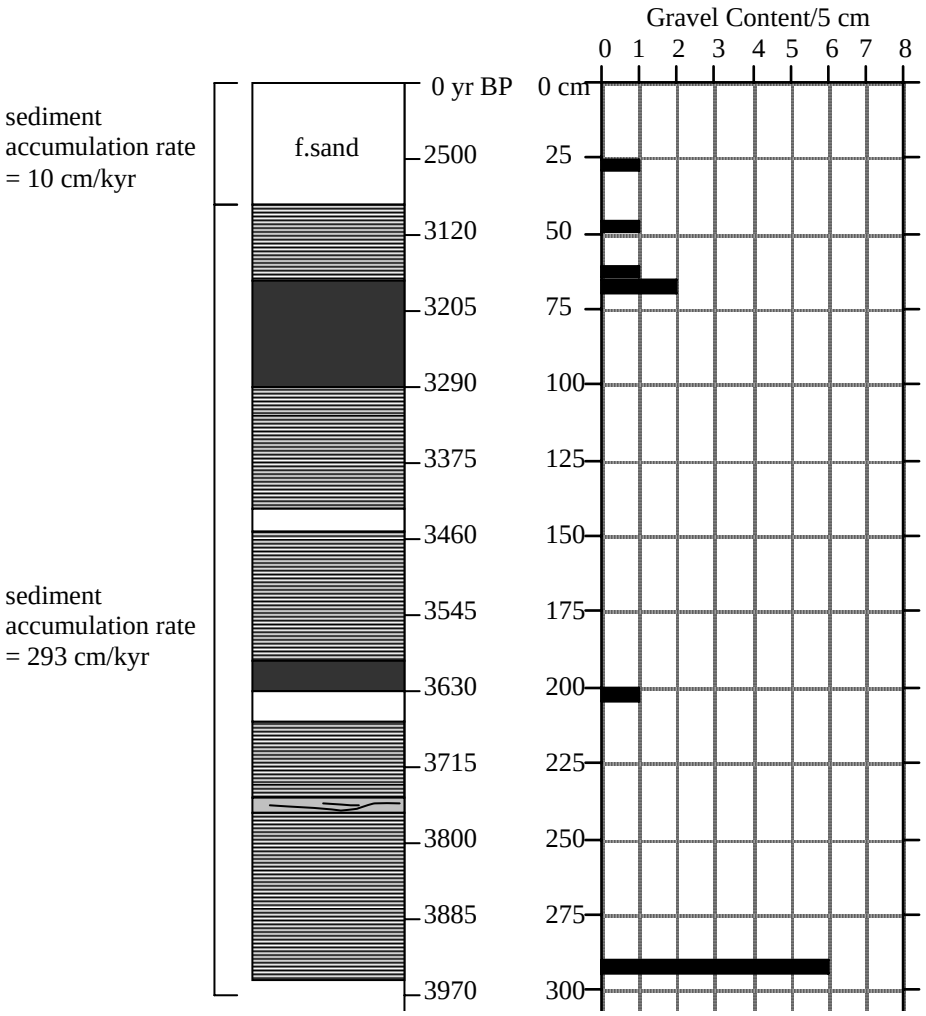

Figure 5.9 Corrected age for core 13GC06 facies interpretation log and corresponding graph of gravel content per 5 cm based on average sediment accumulation rates. Refer to Figure 5.8 for facies legend. The log displays predominantly laminated SMO deposited from about 3970 to 3080 yr BP. There is a correspondingly low gravel content except for a peak of 6 particles at about 3930 yr BP and a relative increase in gravel between about 3200 and 2500 yr BP. A massively bedded fine sand/SMO was deposited from about 3080 yr BP in the top 40 cm of the core.

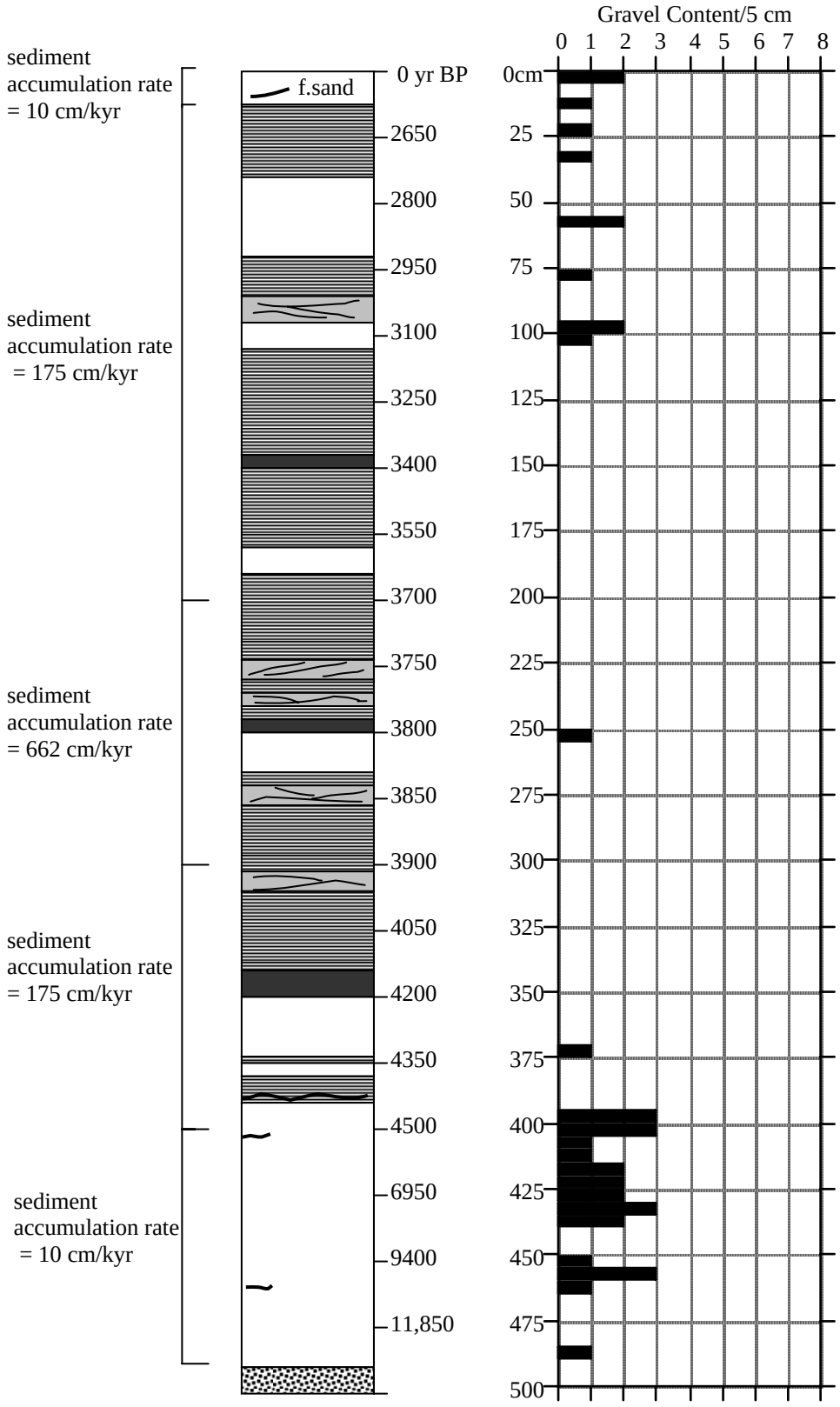

Figure 5.10 Corrected age for core 26PC12 facies interpretation log and corresponding graph of gravel content per 5 cm based on average sediment accumulation rates. Refer to Figure 5.8 for facies legend. Diamicton lies at the base of the core. A massively bedded SMO was deposited from about 14,000 to 4400 yr BP with a correspondingly high gravel content. Then a predominantly laminated SMO with minor intervals of cross laminated SMO was deposited between about 4400 and 2500 yr BP. Massively bedded fine sand/SMO was deposited from about 2500 yr BP to present. Gravel content is low for most of the laminated SMO facies then increases from about 3100 yr BP.

Figure 5.11 is presented as a summary of the average sediment accumulation rates (cm/kyr) and predominant facies within cores 13GC05, 13GC06 and 26PC12 in context to the overall distribution across the Mertz Drift.

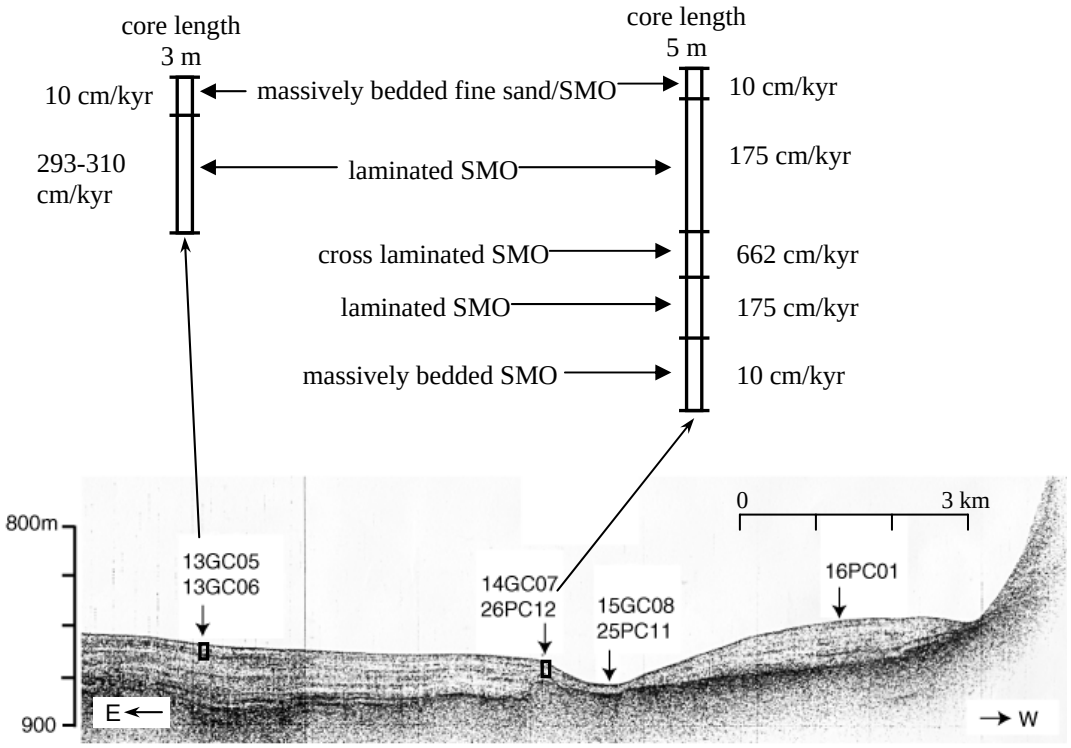

Figure 5.11 3.5 kHz seismic data along an east-west transect over the Mertz Drift with average sediment accumulation rates (cm/kyr) and predominant facies within cores 13GC05, 13GC06 and 26PC12 (source: Brancolini and Harris 2000). Note the large (left) and small (right) lobes separated by a channel (where cores 15GC08 and 25PC11 are located).

As cores 13GC05 and 13GC06 are positioned within approximately 1 km of each other, they allow a good comparison of chronostratigraphy between the cores. A cross bedded SMO interval occurs at approximately 240 cm in both cores, and is assumed to be deposited at the same time. However, core 13GC05 records this interval at about 3140 yr BP, and core 13GC06 records it at about 3740 yr BP, a 600 year difference. The 600 years may be a real difference or explained by the higher surface radiocarbon age of 3155 yr BP in core 13GC05 compared to the surface radiocarbon age of 2736 yr BP in core 13GC06, where both ages were used to correct the remaining radiocarbon ages in each core. The +/- errors of radiocarbon ages are additive when corrected, so errors in cores 13GC05 and 13GC06 are +/- 210 and 175 years respectively. The 600 year difference may explained by the combination of

variation in surface ages of the cores and the +/- errors in corrected radiocarbon ages. This comparison highlights the difficulties of correcting for the reservoir effect and contamination in Antarctic marine sediment cores.

In summary, massively bedded SMO facies was deposited between about 14,000 to 5000 yr BP, a time period of 9000 years. Laminated SMO facies was then deposited from about 5000 to 3000 yr BP. Massively bedded fine sand/SMO facies was deposited as a drape over the Mertz Drift from about 3000 yr BP to the present.

5.3.2 Laminations

An aim of this project was to calculate the mean deposition time for lamination couplets to test the hypothesis that Mertz Drift sediments largely result from cyclical, high productivity diatom blooms due to annual seasonal changes in sea ice cover. The calculation relies upon X-radiographs to count lamination couplets within cores. To test the validity of using X-radiographs to record the internal sedimentary structure of cores, a comparison was made of the number of lamination couplets per 10 cm interval recorded on visual core logs for cores 13GC05 and 13GC06, compared to the number revealed by X-radiographs for the same interval. Graphs of visual versus X-radiograph lamination counts are presented in Figures 5.12 and 5.13 respectively. In addition, a linear regression and correlation coefficient was calculated for each graph.

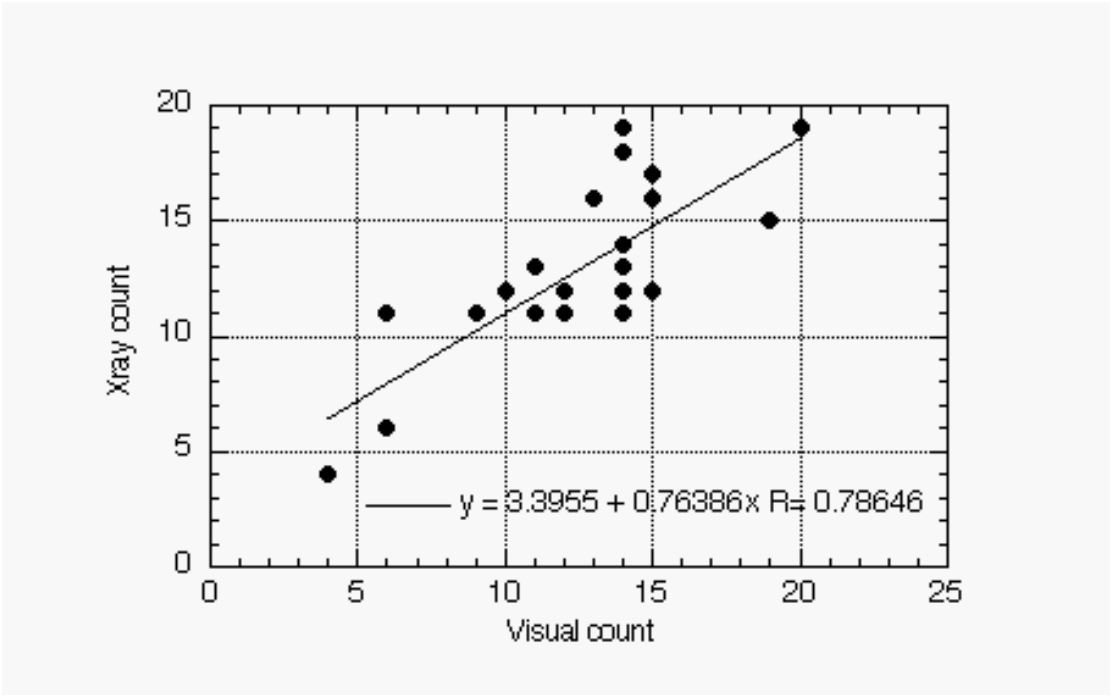

Figure 5.12 Graph of visual count versus X-radiograph count of lamination couplets within core 13GC05. Linear regression: X-radiograph count = 3.3955 + 0.76386 x Visual count; Correlation coefficient: R = 0.78646.

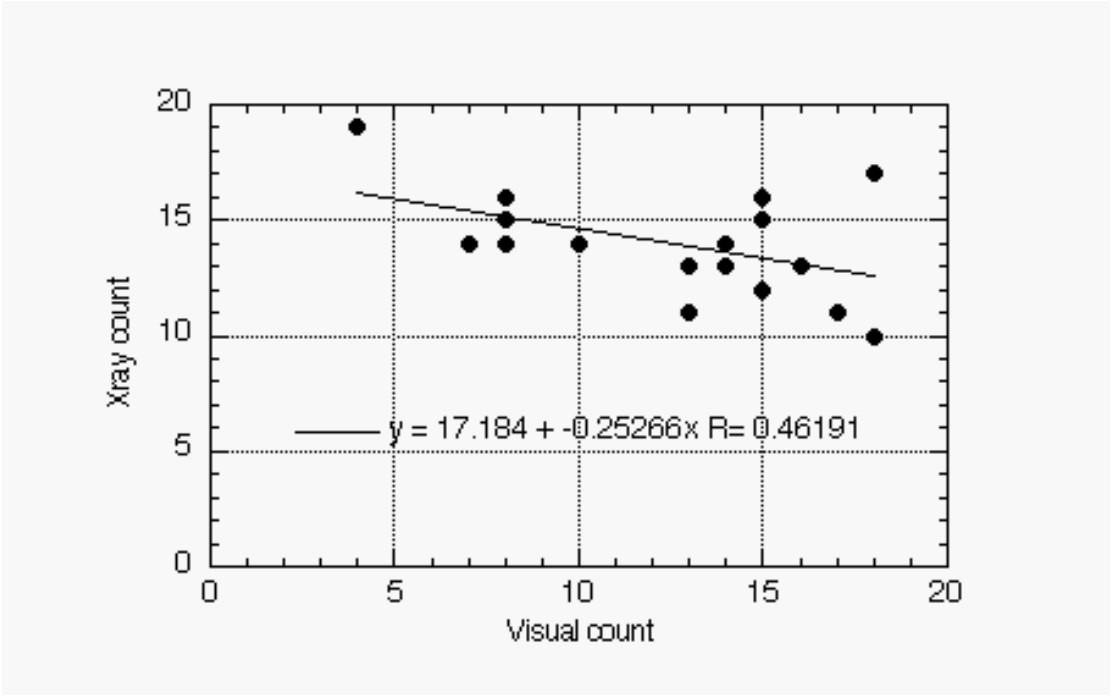

Figure 5.13 Graph of visual count versus X-radiograph count of lamination couplets within core 13GC06. Linear regression: X-radiograph count = 17.184 - 0.25266 x Visual count; Correlation coefficient: R = 0.46191.

Graphs of the visual versus X-radiograph lamination counts for cores 13GC05 and 13GC06 reveal differing trends. For Figure 5.12 (core 13GC05), the visual counts reasonably agree with the X-radiograph counts (R = 0.79). From the calculated linear regression of Figure 5.12, the X-radiograph counts approximately three more lamination couplets for every visual lamination couplet count, which may be interpreted as a slight overestimation. The overestimation of X-radiograph counts is possibly because of the ability of X-radiographs to record three dimensional sedimentary structures as two dimensions, whereas visual counts record only a two dimensional view of sedimentary structure from the surface of a split core.

In contrast to core 13GC05, the trend for core 13GC06 (Figure 5.13) is poor (R = 0.46). The visual counts do not agree with the X-radiograph counts. Hence, core 13GC06 was rejected for further laminae analysis as the X-radiographs of this core do not provide the confidence to count the number of laminations accurately, and then calculate the mean deposition time for lamination couplets.

Visual core logs from the WEGA expedition recorded the number of lamination couplets only in cores 13GC05 and 13GC06, the latter being rejected for further lamination analysis. The only other core possible for lamination analysis is core 26PC12, which did not have the number of lamination couplets recorded in a visual core log, and cannot be tested with the same method for accuracy of the X-radiographs to record laminations. However, the X-radiographs of core 26PC12 are of relatively high quality and sufficiently clear to use for further analysis. Therefore, to calculate the mean deposition time for lamination couplets, X-radiographs of cores 13GC05 and 26PC12 were examined in closer detail to reveal the mean number of lamination couplets per cm and the mean couplet thickness in cm (Tables 5.4 and 5.5 respectively).

Depth Interval (cm)	No. Lamination Couplets	No. Lamination Couplets/cm	Couplet Thickness (cm)
40-50	11	1.10	0.90
50-60	12	1.20	0.83
60-70	12	1.20	0.83
70-80	11	1.10	0.90
80-90	11	1.10	0.90
110-120	13	1.30	0.78
120-130	11	1.10	0.91
130-140	11	1.10	0.91
140-150	16	1.60	0.63
150-160	17	1.70	0.59
160-170	14	1.40	0.71
170-180	15	1.50	0.67
mean (SD)		**1.28 (0.21)**	**0.80 (0.12)**

Table 5.4 Table of lamination couplet detail within core 13GC05. SD = standard deviation. Note: the mean number of lamination couplets/cm = 1.28 and the mean couplet thickness = 0.80 cm.

Depth Interval (cm)	No. Lamination Couplets	No. Lamination Couplets/cm	Couplet Thickness (cm)
103-110	11	1.57	0.64
110-120	14	1.40	0.71
120-130	19	1.90	0.53
130-140	13	1.30	0.77
140-145	6	1.20	0.83
160-170	11	1.10	0.91
170-180	13	1.30	0.77
192-200	11	1.37	0.73
200-210	17	1.70	0.59
210-220	14	1.40	0.71
280-290	11	1.10	0.91
290-300	12	1.20	0.83
310-320	10	1.00	1.00
320-330	13	1.30	0.77
330-340	16	1.60	0.63
382-390	9	1.13	0.89
mean (SD)		**1.35 (0.24)**	**0.76 (0.12)**

Table 5.5 Table of lamination couplet detail within core 26PC12. SD = standard deviation. Note: the mean number of lamination couplets/cm = 1.35 and the mean couplet thickness = 0.76 cm.

As the laminated SMO facies sediment accumulation rate for core 13GC05 converts to 3.22 yr/cm (from Table 5.3), then the mean deposition time for lamination couplets in core 13GC05 = 3.22 yr/cm x 0.80 cm = 2.58 years. The laminated SMO facies sediment accumulation rate for core 26PC12 converts to 5.71 yr/cm (from

Table 5.3), therefore, the mean deposition time for lamination couplets in core 26PC12 = 5.71 yr/cm x 0.76 cm = 4.34 years. Thus, for core 13GC05, from the large lobe, and core 26PC12, from the edge of the large lobe, lamination couplets have a mean deposition time of between 2.6 to 4.3 years respectively. These values are approximate only because of the possibility of overestimating the number of lamination couplets within X-radiographs, and errors in calculating average sediment accumulation rates.

5.4 Summary of Results

Uncorrected radiocarbon ages for Mertz Drift samples ranged from 2241 yr BP from the surface of core 26PC12 to a maximum age of 27,020 yr BP for diamicton at the base of core 17PC02. A sample near the SMO-diamicton boundary of core 26PC12 recorded an uncorrected radiocarbon age of 15,469 yr BP. The mean surface radiocarbon age of the Mertz Drift is 2643 yr BP.

Corrected radiocarbon ages reveal the fine sand/SMO drape over the Mertz Drift commenced deposition at a mean age of 3055 yr BP. The SMO-diamicton boundary was deposited between 13,228 and 24,589 yr BP.

Graphs and linear regressions of corrected radiocarbon age versus depth for cores 13GC05, 13GC06 and 26PC12 demonstrated good age versus depth correlation, and high sedimentation rates (eg. 0.175-0.310 cm/yr) for samples taken from predominantly laminated SMO facies. Within core 26PC12, a relatively high sedimentation rate (eg. 0.662 cm/yr) between samples 199-200 and 299-300 cm corresponds with a section of the core observed with three cross bedded SMO intervals.

The average sedimentation accumulation rates show variability in deposition rates across the Mertz Drift and between facies. The average sediment accumulation rates calculated for facies are:

(1) Massively bedded fine sand/SMO - 10 cm/kyr.

(2) Laminated SMO - 175, 293 and 310 cm/kyr.

(3) Cross laminated SMO - 662 cm/kyr.
(4) Massively bedded SMO - 10 cm/kyr.

Comparison of ages between a similar cross bedded SMO interval at 240 cm depth in both cores 13GC05 and 13GC06 reveal a 600 year difference. The difference may explained by the combination of variation in surface ages of the cores and the +/- errors in corrected radiocarbon ages.

In summary, massively bedded SMO facies was deposited between about 14,000 to 5000 yr BP. Laminated SMO facies was then deposited from about 5000 to 3000 yr BP. Massively bedded fine sand/SMO facies was deposited as a drape over the Mertz Drift from about 3000 yr BP to the present.

A graph and linear regression of the visual versus X-radiograph lamination couplet counts for core 13GC05 reveal that visual counts agree reasonably with the X-radiograph counts. There may be a slight overestimation in counts of the number of lamination couplets revealed by X-radiographs. A linear regression of the visual versus X-radiograph lamination couplet counts for core 13GC06 suggest that visual counts do not agree with the X-radiograph counts.

Calculations of the mean deposition time of lamination couplets in cores 13GC05 and 26PC12 indicate periods of between 2.6 and 4.3 years respectively.

Chapter 6. Thin Section Analysis

6.1 Introduction

A hypothesis of this study is that Mertz Drift sediments largely result from cyclical, high productivity diatom blooms due to annual seasonal changes in sea ice cover. The aim of the project was then to conduct a microscope study of Mertz Drift sediments using thin sections, which may reveal the source of biosiliceous material, and whether sediments are a hemipelagic drape, current lain or from gravity flows. The first part of this chapter describes previous diatom studies of the surface sediments of the George V Basin collected during 'Operation Deep Freeze' 1979 (DF79), and the reports of downcore siliceous components of core DF79-12.

The second part of the chapter describes the results of thin section analysis of four block samples from core 26PC12. The depths from which thin sections were obtained are initially compared against the facies interpretation log of core 26PC12 to show where the thin sections are in relation to the facies in the core. The sedimentary structures of the thin sections, such as mottles and laminae, are then compared against the equivalent depth X-radiographs for any correlation between thin section and X-radiograph structures. Thin sections were analysed under stereo and compound microscopes to detect finer-scale qualitative differences in the microstructure. A summary of results is provided at the end of the chapter.

6.2 Previous Diatom Studies

6.2.1 Diatom Analysis in George V Basin

Leventer (1992) determined the modern distribution of diatoms in surface sediments from cores obtained during 'Operation Deep Freeze' 1979 (DF79), and related this assemblage data to environmental information. Concentrations of up to 250 million diatom valves/gram of sediment were found, particularly within the deeper parts of the George V Basin. A westerly increasing diatom abundance was observed within the basin (Figure 6.1). The relative increase in diatom abundance to

the west was attributed to the East Wind Drift (EWD) current, laterally transporting fine grained, diatomaceous material to the west, and also to the persistent sea ice cover east of longitude 147˚ east decreasing primary productivity.

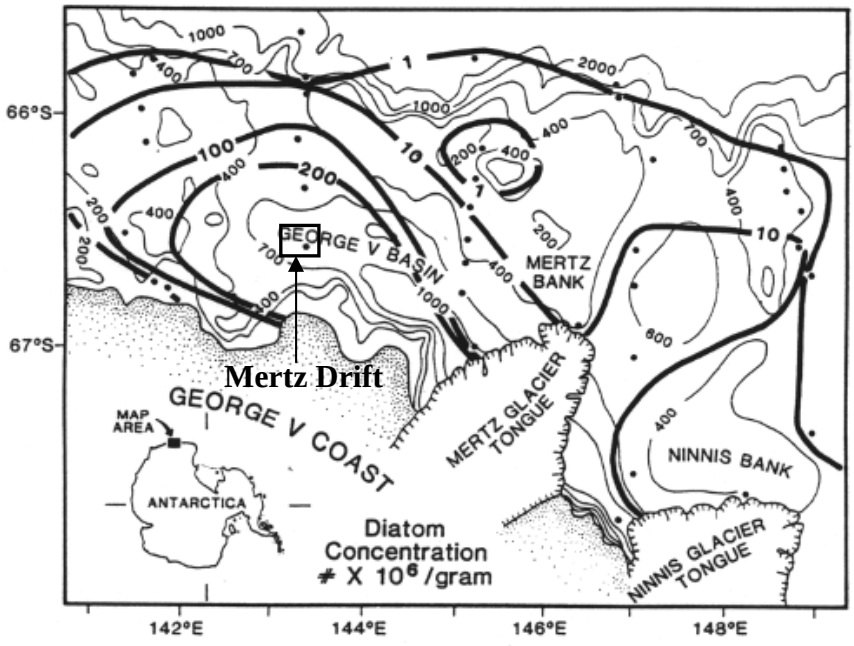

Figure 6.1. Absolute distribution of diatoms in surface sediments on the continental shelf off George V Land (source: Leventer 1992). Note the study site within the box. Mertz Drift surface sediment has a diatom concentration of 200 x 10^6/gram.

Within the George V Basin, the most abundant diatom species was *Fragilariopsis curta*, a small pennate form commonly found as a member of the sea ice community and a dominant component of ice edge blooms (Figure 6.2). There is an offshore decrease in this species and a relative increase in the more 'oceanic' species *Fragilariopsis kerguelensis*, indicating the decreasing influence of sea ice in an offshore direction.

Leventer (1992) concluded that the downcore variability in relative abundance of the two species, *Fragilariopsis curta* and *F. kerguelensis*, would be useful in understanding the history of sea ice versus open water production over the continental shelf off George V Land.

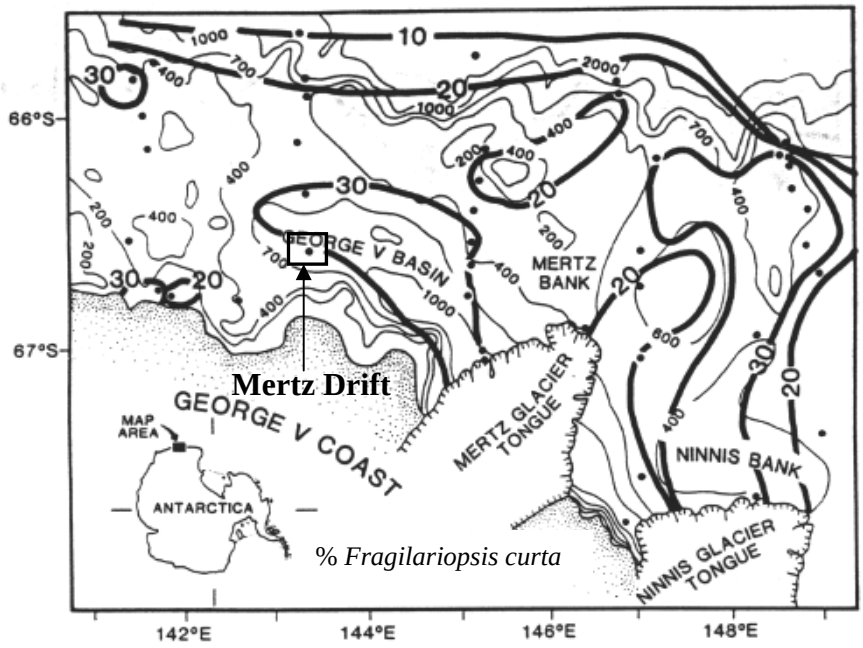

Figure 6.2. Relative concentration of *Fragilariopsis curta* in surface sediments on the continental shelf off George V Land (source: Leventer 1992). Note the study site within the box. Mertz Drift surface sediments have 20-30% *F. curta.*

6.2.2 Core DF79-12

Reports of the downcore siliceous components of core DF79-12 are quite limited, and are general in nature. Domack (1988) stated that the dominant biogenic constituents of siliceous mud and diatom ooze (SMO) facies consisted of planktonic diatoms, minor benthic diatoms, radiolarians, silicoflagellates and sponge spicules. Calcium carbonate, in the form of planktonic foraminifera, was almost completely lacking in sediments. Faecal pellets comprised up to 25% of the sediment, where they had yet to disintegrate in shallow portions of the core.

Initial analysis of diatom floras within individual laminae within core DF79-12 revealed strong contrasts in species diversity and size (Domack 1988). Laminae differed in that small sea ice diatoms, such as *Fragilariopsis curta*, dominated within one lamina of each lamination couplet. The relative dominance of sea ice diatoms to other diatoms in each couplet was interpreted as representing the initial pelagic flux of diatoms induced by melting sea ice, while the overlying lamina represented productivity during the remainder of the summer (Domack 1988). This interpretation led to the Domack (1988) productivity model (refer Chapter 1 - Figure 1.3) to explain

the development of laminated SMO facies within shelf basin sediments. In this model, areas that undergo seasonal fluctuations in sea ice cover contribute significant quantities of biogenic detritus to the seafloor. As sea ice melted, dense and short-lived sea ice diatoms would be quickly ‘fluxed’ to the bottom followed by diatoms produced during the remainder of summer. Domack (1988) concluded that it is not known whether the seasonal conditions of open water over the western end of George V Basin (i.e. Mertz Drift area) are due to wind-forced breakout of sea ice, and hence reducing the flux of diatoms to the seafloor, or melting, which may contribute significant biogenic detritus in the manner proposed in the productivity model.

The results of diatom distribution in the surficial sediments of George V basin and the limited results and interpretation of core DF79-12 have been discussed in the first part of this chapter. This information serves as a baseline against which the results from thin section analysis in this study will be compared.

6.3 Results

The following thin section analysis of four samples from core 26PC12 may help to resolve questions pertaining to the origin and physical processes involved in the deposition of Mertz Drift sediments. Analysis may reveal the source of biosiliceous material, and whether sediments are a hemipelagic drape, current lain or from gravity flows.

The depths from which thin sections were obtained are first compared against the facies interpretation log of core 26PC12 to show where the thin sections are in relation to the facies in the core. The sedimentary structures of the thin sections, such as mottles and laminae, are then compared against the equivalent depth X-radiographs for any correlation between thin section and X-radiograph structures. Photomicrographs of sediments in the thin sections are also presented to highlight important features. The microstructure of thin sections are qualitatively described for finer-scale features revealed by stereo and compound microscope.

6.3.1 Thin Section Facies

The facies interpretation log of core 26PC12 against the depths from which thin section samples were obtained is presented in Figure 6.3. Samples were taken from the following facies: massively bedded fine sand/SMO (8.5-11.5 cm); laminated SMO (162-165 cm); cross laminated SMO (227-230.5 and 237-240.5cm).

Thin sections were obtained from these facies to assist in confirming or denying the sedimentary structures observed in X-radiographs and visual core logs, as well as the interpretations of environment of deposition. Thin section samples were not obtained from massively bedded SMO or diamicton facies due to the lack of time available to process samples.

It should be noted that the processing of thin sections led to some shrinkage and desiccation of the sediments, which made comparison with the equivalent depth X-radiographs slightly difficult. Additionally, neither the X-radiographs and photographs of thin sections reproduced very well into this thesis due to the limitations of scanning and printer resolution. Line drawings of both X-radiographs and thin section photographs are provided to assist in comparisons of sedimentary structure.

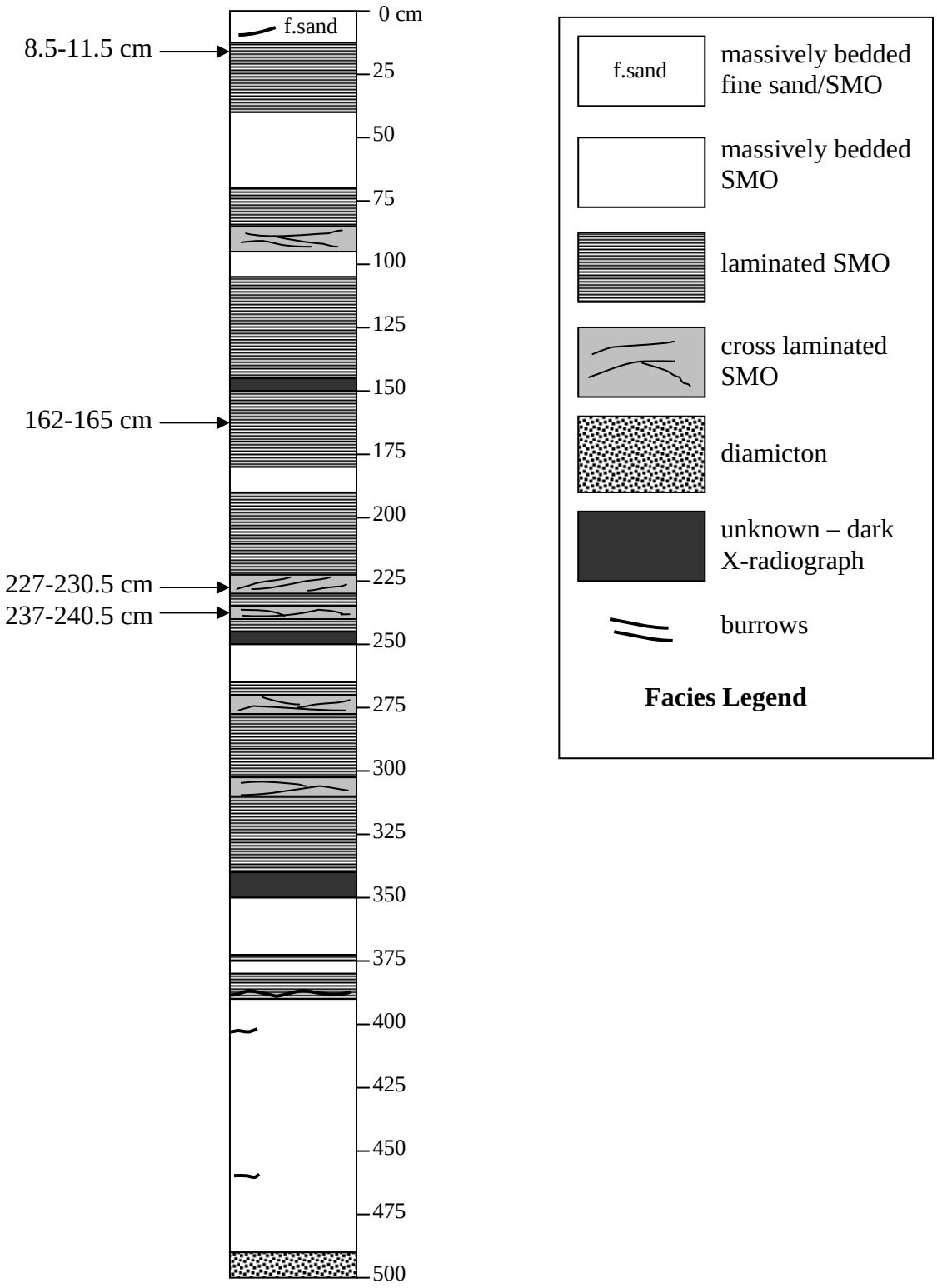

Figure 6.3 Four thin section sample depths against the core 26PC12 facies interpretation log. The sample at 8.5-11.5 cm is massively bedded fine sand/SMO. The sample from 162-165 cm is laminated SMO. Samples 227-230.5 and 237-240.5 cm are both cross laminated SMO facies.

6.3.2 Thin Section Analysis

(1) Massively bedded fine sand/SMO (sample depth 8.5-11.5 cm). Figure 6.4A&B displays the X-radiograph and thin section at the equivalent depth. The massively bedded fine sand/SMO in the X-radiograph shows dark-toned mottles, thin discontinuous laminae and the massive bedding characteristic of this facies. Within the thin section, even though there is some shrinkage and disruption of the sediments from processing the thin section, the same thin laminae and mottles can be seen, and are found to be concentrations of fine to very fine grained sand. The pockets of sand correlate with the darker-toned (dense) structures of the X-radiograph i.e. mottles and thin laminae. The majority of sediments are siliceous material such as diatoms and sponge spicules, which correlate with the light-toned parts of the X-radiograph.

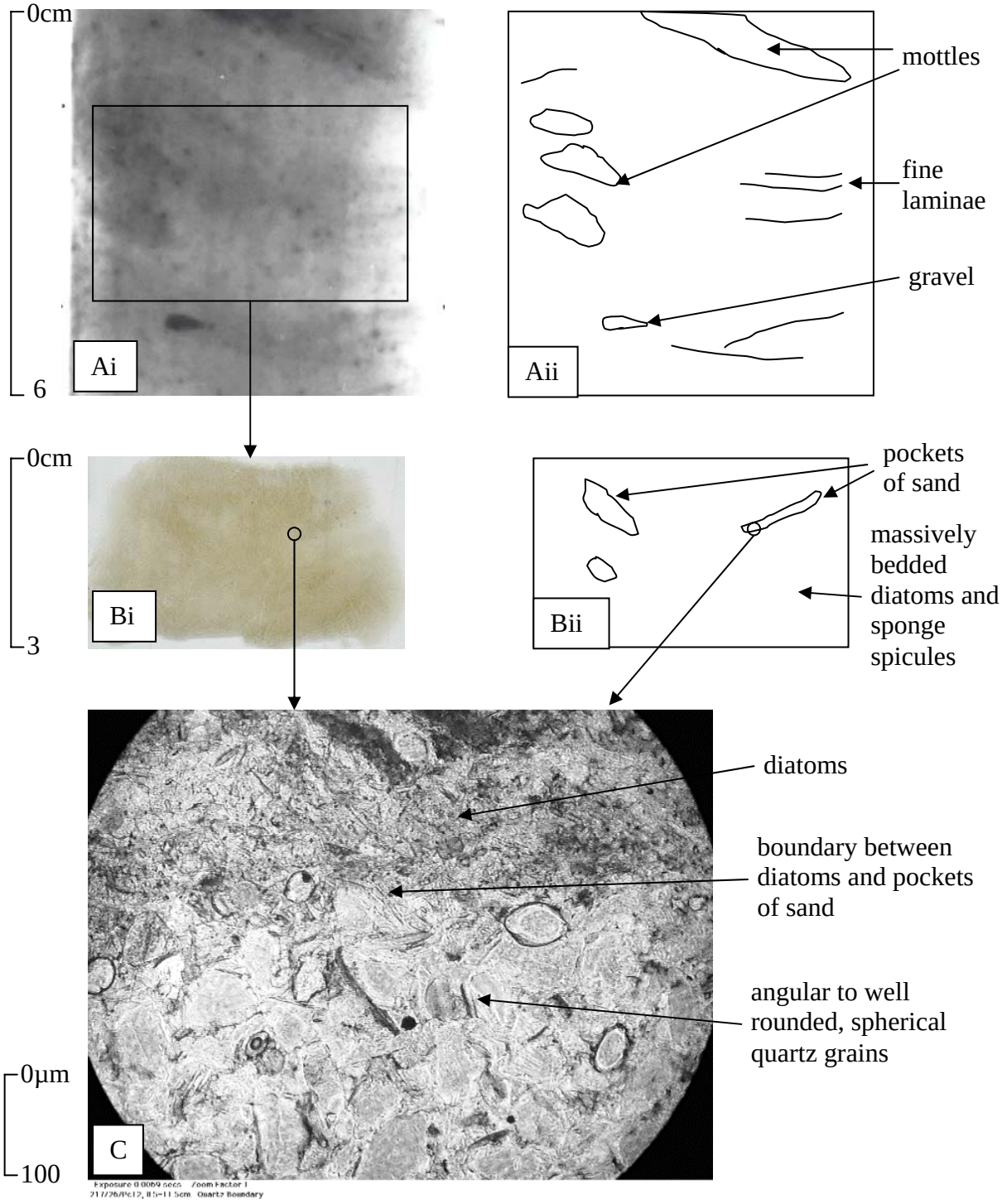

Figure 6.4 **Ai**&**Aii** = X-radiograph and line drawing showing dark-toned mottles, fine laminae and IRD gravel. **Bi**&**Bii** = photograph of thin section and line drawing (same scale) showing concentrations of fine to very fine grained sand that correlate with the mottles and laminae seen in the X-radiograph. **C** = photomicrograph showing close-up of the boundary between diatoms and a thin pocket of sand.

The microstructure of sediments in the thin section (Figure 6.4B) reveals small concentrations or pockets of fine to very fine grained sand scattered throughout the thin section. The sand consists of angular to well rounded, spherical quartz grains. Green pyroxene is also identified amongst the sand particles. The majority of sediments are massively bedded siliceous material such as diatoms, although many larger sponge spicules are also seen. Individual quartz grains are also present within the siliceous material. The photomicrograph in Figure 6.4C shows a distinct boundary between a concentration of quartz grains and overlying diatoms. Bioturbation in several pockets of sand is evidenced by bedding disruption by finer grained diatom material.

(2) Laminated SMO (sample depth 162-165 cm). The X-radiograph and equivalent depth thin section are presented in Figure 6.5A&B for comparison. The X-radiograph shows the horizontal light-and dark-toned laminae of laminated SMO facies. The photograph of the same depth thin section also reveals laminae that correlate with the structures in the X-radiograph (Figure 6.5A&B). Under microscope (Figure 6.5C), there is a distinct change between dark lamina and light lamina in the thin section. The dark lamina is more tightly packed with diatoms while the light lamina is matted and has more dispersed diatoms.

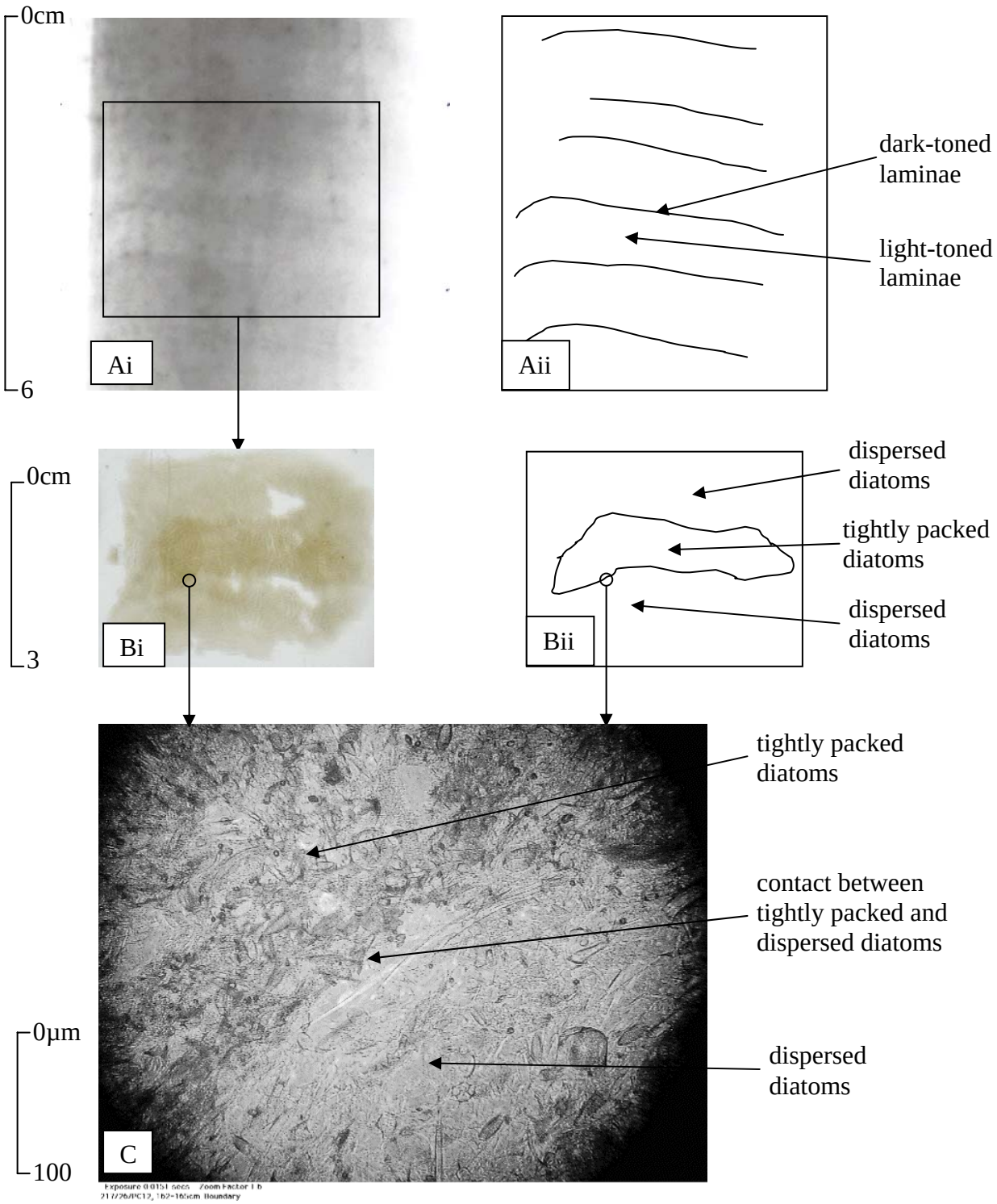

Figure 6.5 **Ai**&**Aii** = X-radiograph and line drawing showing light-and dark-toned laminae. **Bi**&**Bii** = photograph of thin section and line drawing (same scale) showing textural differences that correlate with the laminae seen in the X-radiograph. **C** = photomicrograph showing contact between tightly packed diatoms (upper half) and dispersed diatoms (lower half).

Under the microscope, diatoms dominate the sediment composition with no terrigenous contribution observed. The microstructure of the thin section reveals distinct variations how packed diatoms are within each lamina (Figure 6.5B). A mat of siliceous spines dominates the light lamina; believed to be derived from the diatoms of *Corethron criophilum* and vegetative spore *Chaetoceros* cells. The spines appeared to be somewhat aligned with the bedding of the lamina. *Corethron criophilum* valves, minus spines, and *Chaetoceros* resting spores are numerous in the light lamina. The centic diatom *Thalassiosira tumida* and the pennate diatom *Fragilariopsis curta* are also numerous. Very few desiccation cracks are observed within the light lamina due to the mesh-like linkage between diatom cells. In contrast, the dark lamina has many randomly oriented desiccation cracks, and appears to be more compact and diverse in diatom species. The dark lamina has a different assemblage of diatoms to the light lamina. *Chaetoceros* resting spores appear to be more common. The dark lamina lacks *Corethron criophilum* and siliceous spines. *Fragilariopsis kerguelensis* was generally the dominant pennate diatom observed. The photomicrograph in Figure 6.5C shows a distinct contact between the more densely packed diatom lamina and the underlying least dense lamina.

(3) Cross laminated SMO (sample depth 227-230.5 cm). Figure 6.6A&B displays a photograph of the thin section and X-radiograph of the same sample depth. The X-radiograph shows distinct light- and dark-toned laminae interpreted to be parallel foresets, inclined at 15˚ to the horizontal. When examined under the microscope, the thin section reveals faint dark and light lamina, which roughly correlate with the dark and light lamina of the X-radiograph. The dark lamina of the thin section reveals diatoms slightly more packed than in the light lamina. It was not possible to determine whether these light and dark lamina correspond with the contents of the light and dark lamina in the laminated SMO thin section. However, the dark lamina had a scattering of foraminifera in contrast to the light lamina, which had no foraminifer amongst the diatom matrix.

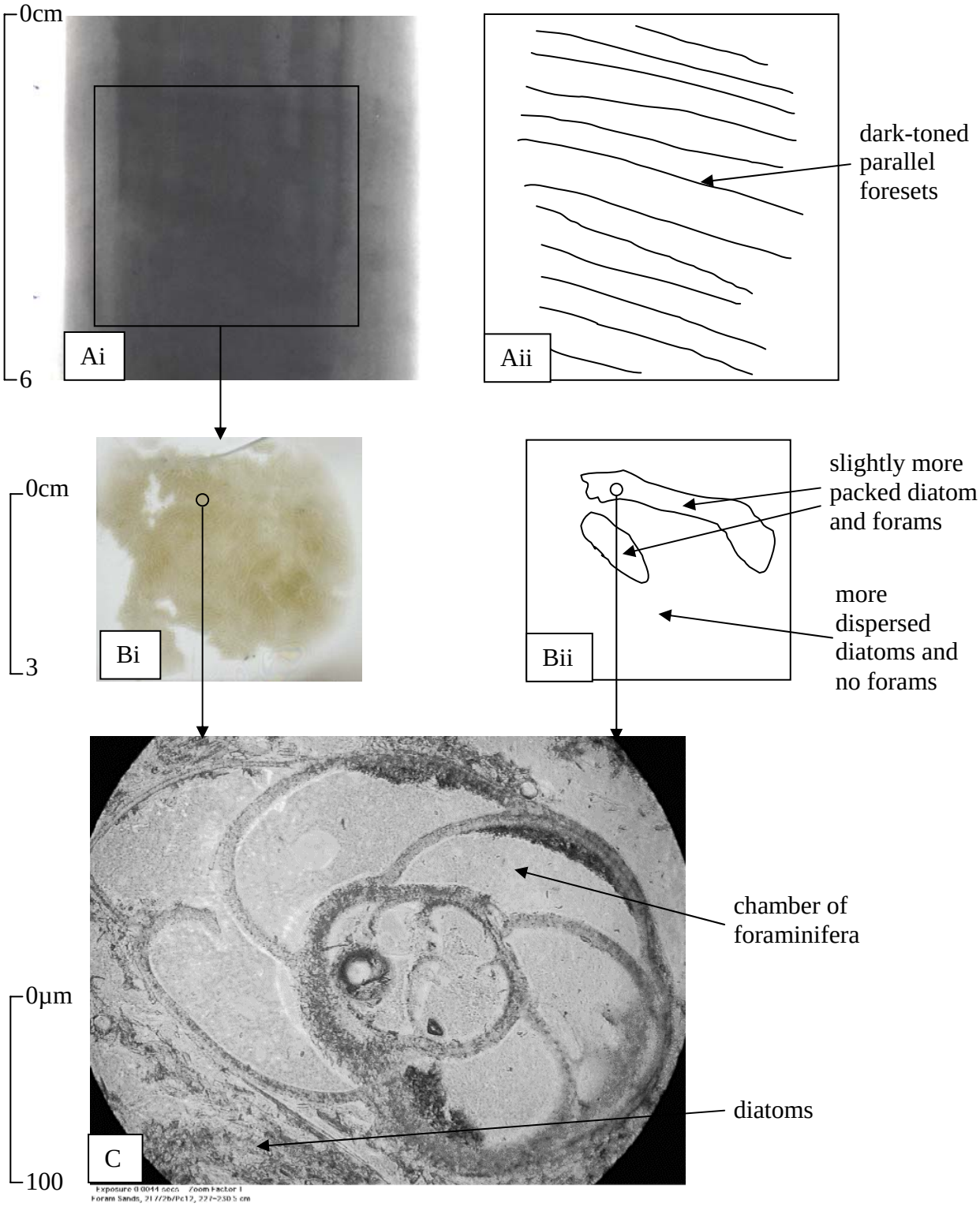

Figure 6.6 **Ai**&**Aii** = X-radiograph and line drawing showing dark-and light-toned parallel foresets at an angle of approximately 15˚. **Bi**&**Bii** = photograph of thin section and line drawing (same scale) showing faint dark lamina of more packed diatoms and foraminifera, overlying light lamina with slightly more dispersed diatoms and no foraminifera. The dark lamina of the thin section roughly correlates with the dark-toned lamina in the X-radiograph. **C** = photomicrograph of the benthic foraminifera *Globocassidulina crassa* from the dark lamina.

The microstructure of the thin section shows dark lamina that are slightly more packed in diatom material compared to the light lamina (Figure 6.6B). The dark lamina also has numerous benthic foraminifera, *Globocassidulina crassa*, surrounded by the diatom matrix. The calcium carbonate foraminifera were not corroded. The light lamina contain no foraminifera. Most diatoms show signs of frustule alignment, and a similar axis of orientation to the bedding of the light and dark lamina they lie in. Desiccation cracks formed during the preparation of the thin section have also followed the axis of orientation of the individual light and dark lamina. The photomicrograph of Figure 6.6C displays the relatively large (> 0.1 mm) *Globocassidulina crassa* in relation to the smaller (> 0.01 mm) diatoms, indicating the poorly sorted nature of the dark lamina.

(4) Cross laminated SMO (sample depth 237-240.5 cm). The X-radiograph and equivalent depth thin section are shown in Figure 6.7A&B for comparison. The structures within the X-radiograph show a 6 cm interval of cross laminae that is wavy and laterally discontinuous, bounded above and below with horizontal laminae. The thin section (Figure 6.7B) also confirms lamina with similar textural patterns to the X-radiograph. Lamina with more packed diatoms correspond to the dark-toned lamina of the X-radiograph, while the less packed diatom lamina correlate with the light-toned lamina of the X-radiograph. Again, it was not possible to determine whether these light and dark lamina correspond with the contents of the light and dark lamina in the laminated SMO thin section.

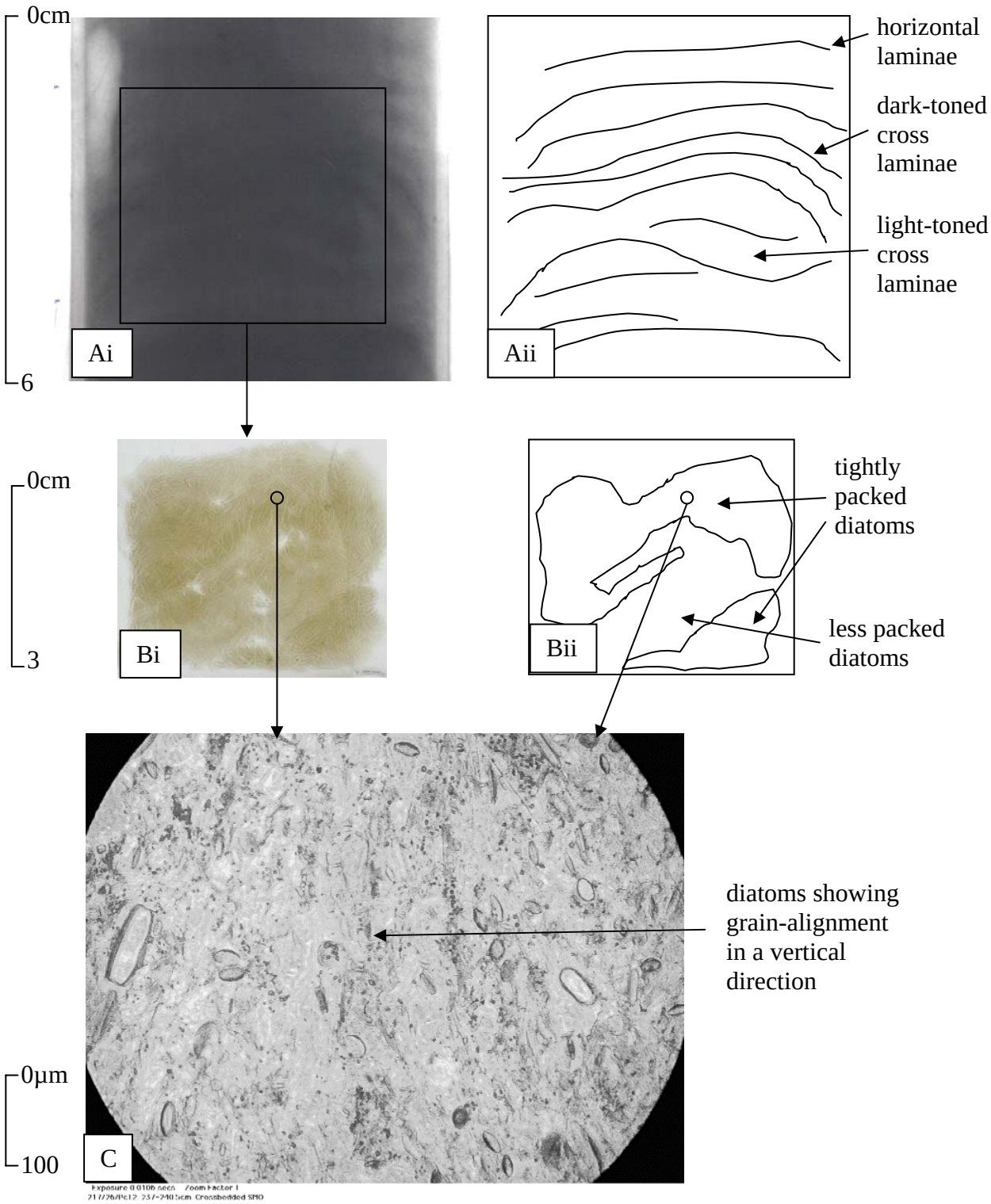

Figure 6.7 **Ai**&**Aii** = X-radiograph and line drawing showing dark-and light-toned cross laminae. **Bi**&**Bii** = photograph of thin section and line drawing (same scale) showing dark and light lamina that correlates with the dark-and light-toned cross lamina in the X-radiograph. **C** = photomicrograph showing a close-up of the oriented and aligned diatoms within the sediments. The diatoms in this example have a vertical grain-alignment only because shrinkage in the preparation of the thin section has folded the grains vertically. It is not indicative of vertical bedding of laminae.

The microstructure of this cross bedded SMO thin section reveals slight relative changes in the packing of diatoms within lamina corresponding with light and dark lamina (Figure 6.7B). Like the previous cross laminated SMO thin section, most diatoms show signs of frustule alignment, and a similar axis of orientation to the bedding of the light and dark lamina they lie in. The photomicrograph of Figure 6.7C shows a vertical alignment of diatoms within a denser lamina. Shrinkage during the preparation of the thin section has folded this section of diatoms vertically, and is not indicative of vertical bedding of lamina. Desiccation cracks formed during the making of the thin section have also followed the axis of orientation of the individual light and dark lamina.

6.4 Summary of Results

A comparison between structures within X-radiographs and thin sections show good correlation. Dark (dense) lamina in X-radiographs match dark lamina within thin sections that have increased diatom concentrations. Light (less dense) lamina in X-radiographs match more dispersed diatoms in light lamina of thin sections. Dark mottles in X-radiographs are also correlated with concentrations of quartz sand grains.

It was not possible to distinguish whether the composition of light lamina in laminated SMO and cross laminated SMO had the same diatom assemblage. The diatom assemblage from the light lamina of the laminated SMO is a mat of somewhat aligned siliceous spines derived from the diatoms of *Corethron criophilum* and vegetative spore *Chaetoceros* cells. Other numerous diatoms in light lamina of laminated SMO are *Corethron criophilum* valves, C*haetoceros* resting spores, *Thalassiosira tumida* and *Fragilariopsis curta*. The diatom assemblage of light lamina in cross laminated SMO had distinct frustule alignment parallel to the bedding of the lamina.

The presence of foraminifera was a noted difference in sediment composition between dark lamina of laminated and cross laminated SMO. It was not possible to determine a difference in diatom composition in the dark lamina of laminated and cross laminated SMO. The dark lamina of laminated SMO have a compact and

diverse diatom assemblage. *Chaetoceros* resting spores appear to be common and *Fragilariopsis kerguelensis* was the dominant pennate diatom observed. The dark lamina of laminated SMO lacks the *Corethron criophilum* and siliceous spines of the light lamina. The diatom assemblage of dark lamina in cross laminated SMO had distinct frustule alignment parallel to the bedding of the lamina.

Chapter 7. Discussion

7.1 Introduction

This study has three main aims. The first is to produce facies descriptions using visual core logs, multi-sensor core logger data and sedimentary structures revealed by X-radiographs of cores recovered from the Mertz Drift. This is in order to discover if there is an overall facies succession within the deposit, and whether the drift has some underlying pattern of deposition. The second aim is to use radiocarbon age data to explain the timing of any facies succession, and whether or not the Mertz Drift sediments do record a high resolution of palaeoenvironment change during the Holocene. A third aim was to conduct a microscope study of Mertz Drift sediments using thin sections. Analysis may reveal the source of biosiliceous material, and whether sediments are a hemipelagic drape, current lain or from gravity flows.

The discussion chapter covers the following related topics of relevance to the aims and hypotheses:

- The succession of environmental phases interpreted from the general pattern of facies in the deposit.
- A model of Mertz Drift formation.
- Sediment accumulation rates across the drift.
- The timing of post-LGM deposition in the George V Basin.
- Lamination couplets.
- The various physical controls on drift formation
- Does the Mertz Drift record bottom water formation?

7.2 Succession of Environments

The general succession of phases of depositional environment and units within a representative 500 cm core is presented in Figure 7.1 This study identifies a succession of four units in the Mertz Drift. Unit 1 is a diamicton, which underlies the drift deposit. Lying unconformably over the diamicton is Unit 2, a massively bedded

SMO. Overlying Unit 2 is a relatively thick Unit 3, consisting of laminated SMO interbedded with minor intervals of cross laminated and massively bedded SMO. Unit 4, a massively bedded fine sand/SMO, overlies the Mertz Drift as a drape. These units are described in turn to interpret the succession of environmental phases for the deposit.

(1) Sub-Ice Shelf Phase. The diamicton in core DF79-12 was interpreted as being deposited under a floating ice tongue, in a low energy, fjord-like environment (Domack 1982; Domack *et al.* 1991). This present study found Unit 1 to be a muddy diamicton with an erosional upper surface in X-radiographs of Mertz Drift cores that were sufficiently long to penetrate through the drift (Figure 7.1). The facies is very high in ice-rafted debris (IRD) gravel but was not quantified in this study as the focus was on the siliceous mud and diatom ooze (SMO) sediments of the drift. The diamicton sampled in this study is similarly interpreted as a sub-ice shelf, water-lain till.

The single corrected radiocarbon age of 24,589 yr BP, at the base of core 17PC02, reveals deposition during the Last Glacial Maximum (LGM). Deposition of diamicton during a glacial advance in the LGM is consistent with the findings of Harris and O'Brien (1998) who found a similar diamicton deposited during a glacial advance during the LGM on the Mac.Robertson shelf. During the last glacial advance, ice flow over the continental shelf off George V Land was from southeast to northwest (refer Chapter 5 - Figure 5.2; Domack *et al.* 1989). The combined Mertz and Ninnis Glacier Tongues were probably grounded on the outer shelf with restricted water circulation under the floating ice shelf. Sub-ice shelf till melted from beneath the glacier and combined with minor marine plankton at the western end of the George V Basin, where the Mertz Drift is located.

Modern phase with increased sea ice	Unit 4: **massively bedded fine sand/SMO 10%** (burrows 24% IRD 30%) *10 cm/kyr*
Climatic optimum phase with reduced sea ice	Unit 3: **laminated SMO 48%** (burrows 16% IRD 18%) *175, 293, 310 cm/kyr* plus **cross laminated SMO 4%** (burrows nil IRD 1%) *662 cm/kyr* plus **massively bedded SMO 13%**
Glacial retreat phase and transition to an open water environment	Unit 2: **massively bedded SMO 20%** (burrows 60% IRD 51%) *10 cm/kyr*
Sub-ice shelf phase	Unit 1: **diamicton 5%**

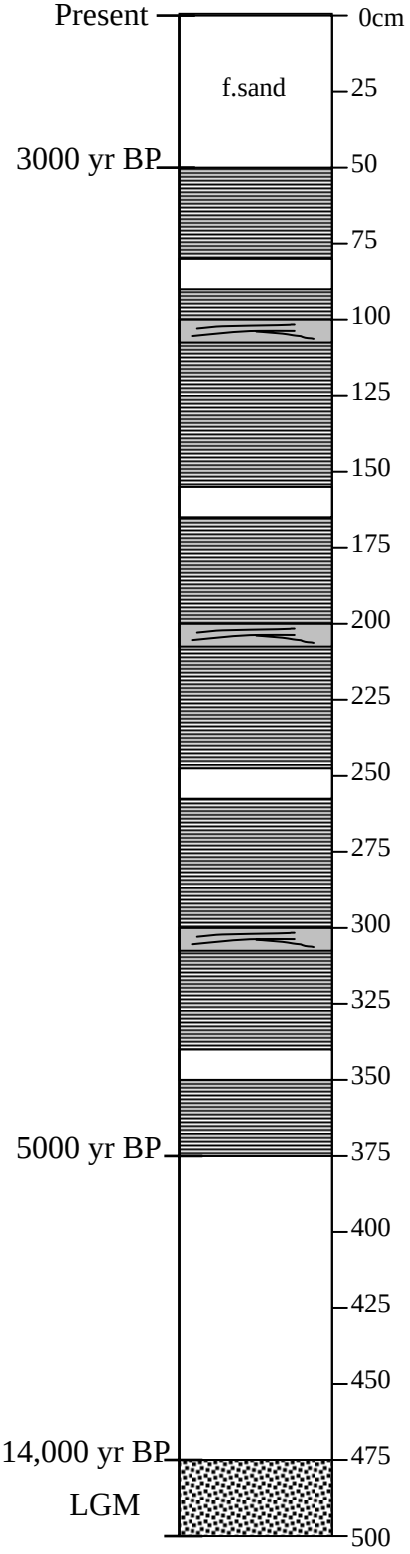

Figure 7.1 Mertz Drift succession of environmental phases and units with corrected radiocarbon ages within a representative 500 cm core. The percentages of facies in all cores are shown in bold. Percentages of all burrows and all IRD in each facies are shown within brackets. Average sediment accumulation rates for each facies are in italics. IRD = ice-rafted debris; LGM = Last Glacial Maximum. Refer to Appendix A - Figure A.1 for the facies legend.

(2) Glacial Retreat Phase. Domack *et al.* (1989) found a high IRD and bioturbated, massively bedded SMO at the base of core DF79-12, which was interpreted as a glacial retreat phase (refer Chapter 4 - Figure 4.1). This present study found a similar massively bedded SMO facies, comprising 20% of Mertz Drift sediments (Unit 2 in Figure 7.1). There was a high percentage of IRD gravel content (51% of all IRD) observed in X-radiographs of this facies. This study interprets that Unit 2 records a glacial retreat phase, and represents the transition from sub-ice shelf to open marine conditions. This interpretation is consistent with similar high IRD, massively bedded SMO facies, which represent sedimentation at the calving line of retreating glaciers (Domack *et al.* 1989; Domack and Harris 1998; Harris and O'Brien 1998). The high IRD in this facies is believed to be related to the concentration of icebergs by winds at the calving line (Domack and Harris 1998).

Ingolfsson *et al.* (1998) stated that ice retreat for the East Antarctic shelf area was underway by 11,000 to 10,000 yr BP, with deglaciation of some shallow inner shelf areas occurring between 10,000 to 5000 yr BP. Ingolfsson *et al.* (1998) also noted that by 5000 yr BP most Antarctic glaciers had retreated to or behind their present positions. The timing of Unit 2 conforms closely to the deglaciation period in the review by Ingolfsson *et al.* (1998). The timing for the onset of open marine conditions occurred about 14,000 yr BP based upon the corrected radiocarbon age at the base of core 26PC12. Thus, the end of the LGM is constrained between about 24,000 and 14,000 yr BP. This study found that the massively bedded SMO facies records a low sediment accumulation rate of about 10 cm/kyr. The extrapolated age at the top of this facies has a corrected radiocarbon age of about 5000 yr BP; thus Unit 2 represents deposition over a 9000 year period.

Domack and Anderson (1983) attributed the increased winnowing of sediments by impinging Circumpolar Deep Water (CDW) on the outer shelf for the increasing proportion of SMO within the lower section of core DF79-12. X-radiographs in this present study reveal a sharp contact whenever this diamicton/SMO boundary occurs. The sharp contact is possible evidence of the erosion that would be expected to occur as water masses intrude into the basin. The high proportion of burrows found within Unit 2 (60% of all burrows) may

demonstrate colonisation by benthic fauna on the Mertz Drift as a result of a retreating ice shelf. As the Mertz Glacier Tongue retreated, episodic deep basin currents may have provided the infrequent energy needed to produce low deposition rates, providing the substrate upon which benthic fauna found favourable for colonisation and bioturbation.

(3) Climatic Optimum Phase. Domack *et al.* (1989) interpreted the upward increase in biogenic material and three metre thick laminated SMO in core DF79-12 as the transition between proximal to distal ice tongue (refer Chapter 4 - Figure 4.1). In this present study, a similar facies succession overlies the massively bedded SMO, and comprised the bulk of Mertz Drift sediments (Unit 3 in Figure 7.1). Unit 3 consists of laminated SMO (48% of cores), interbedded with approximately three to four cross laminated SMO (4% of cores) and massively bedded SMO (13% of cores; Figure 7.1). For ease of discussion, Unit 3 is described as a laminated and cross laminated SMO succession. Both the laminated and cross laminated SMO facies record relatively low proportions of IRD gravel (18% and 1% of all IRD respectively). This study also interprets Unit 3 to represent an open marine environment with a distal ice tongue.

The Ingolfsson *et al.* (1998) review of post-LGM climatic history recorded a climate optimum in East Antarctica from about 4700 to 2000 yr BP. This period was warmer, wetter and had less sea ice than the present (Ingolfsson *et al.* 1998). The corrected radiocarbon ages from Mertz Drift cores with Unit 3 record this succession between about 5000 to 3000 yr BP. An important result of this study is that the period of deposition of the laminated and cross laminated SMO succession is close to the Ingolfsson *et al.* (1998) climatic optimum.

The average sediment accumulation rates for laminated SMO in cores 13GC05, 13GC06 and 26PC12 have high deposition rates (310, 293 and 175 cm/kyr respectively). The cross laminated SMO facies in the Mertz Drift records a deposition rate approximately double that of the laminated SMO facies at 662 cm/kyr. Sediment accumulation rates for Unit 3 are over an order of magnitude greater than the rate for the underlying Unit 2. It is unlikely that an increase in productivity over the shelf of

greater than 20 times can account for the thick Unit 3. Instead, enhanced bottom current activity is believed responsible for concentrating the laminated SMO facies into a drift deposit during this climate optimum phase. Furthermore, cross laminated SMO may represent short periods of rapid sedimentation and higher velocity bottom current activity relative to velocities responsible for deposition of laminations. Another study of cross laminated SMO from marine cores obtained from the Nielsen Shelf Valley, near Prydz Bay, also supports this interpretation, and the mid-Holocene timing of enhanced bottom current activity (Harris, submitted).

The low proportion of burrows observed within the laminated and cross laminated SMO facies (16% and 0% of all burrows respectively) may prove that the environment of deposition was not suitable for colonisation by benthic fauna. A large influx of fine grained biogenic material such as occurred during this sedimentary succession would make colonisation difficult, which could explain the reduced bioturbation in the X-radiographs and the excellent preservation of laminae. Alternatively, the rate of bioturbation is much less than the sediment accumulation and current reworking so no record is preserved during this period.

It is possible that the high sediment accumulation rates in Unit 3 may have reduced the concentration of IRD gravel deposited over the Mertz Drift even if IRD sedimentation was constant since the LGM. A reduced proportion of IRD gravel may also infer a reduction in glacial calving due to a change in palaeoclimate and/or glacial retreat. The lack of IRD gravel in the laminated SMO of core DF79-12 was also noted as unusual by Domack and Anderson (1983) given the glacial setting of the region and observed debris zones in icebergs. It was not possible in this study to calculate accurate figures to prove or disprove that a high sedimentation rate alone was responsible for the low IRD in this unit, even if the IRD rate was constant.

Analysis of a thin section of laminated SMO revealed a distinct change of diatom assemblage between lamina. The light lamina is a mat of somewhat aligned siliceous spines and numerous *Fragilariopsis curta*, a sea ice associated diatom. The dark lamina is a compact and apparently diverse diatom assemblages, with numerous *Fragilariopsis kerguelensis*, an open water associated diatom. Thus, these limited

observations confirm Domack's (1988) initial findings of a relative change in sea ice diatom assemblage to open water diatom assemblage observed within lamination couplets of core DF79-12. The relative dominance of sea ice diatoms to other diatoms in each couplet is interpreted in this present study as representing the initial pelagic flux of diatoms induced by melting sea ice, while the overlying laminae represents primary productivity during the remainder of the summer season. Sediment trap data are required to confirm this assumption.

Relatively shallow, impinging Circumpolar Deep Water (CDW) over the outer shelf is responsible for transporting fine grained sediment towards the coast (Domack 1988). As SMO is not found anywhere in the eastern half of the George V Basin (Harris 2000), then this study proposes that bottom currents associated with high salinity Shelf Water (HSSW; refer Chapter 2 - Figure 2.5) sweep northwesterly along the length of the basin, and collect falling pelagic material brought into the inner shelf by CDW. The HSSW then concentrates the sediment into the Mertz Drift at the western end of the George V Basin.

Analysis of cross laminated SMO thin sections reveals diatoms with a distinct axis of orientation and grain-alignment. The alignment of individual elongate grains suggests they were emplaced individually and not as clasts and faecal pellets. The sediment within the cross laminated SMO appears to be current-lain, and is consistent with the interpretation by Harris (submitted) that cross laminated SMO may represent higher velocity bottom current activity relative to velocities responsible for deposition of laminations. Additionally, the burial of the relatively large foraminifera *Globocassidulina crassa* and the much smaller diatom matrix is an indication of a poorly sorted sediment that would be expected if bottom current energy increases. As calcium carbonate material can experience dissolution at depths greater than 500 m on the shelf (Domack 1988), the lack of corrosion observed in the foraminifera could be further evidence of the high sedimentation rate recorded in cross laminated SMO facies and burial before dissolution could occur.

(4) Modern Phase. Domack *et al.* (1989) noted a significant increase in sand percentage occurring in the upper 60 cm of core DF79-12 (refer Chapter 4 - Figure

4.2), and was interpreted as reduced biogenic input during the late-Holocene (Domack *et al.* 1991). This present study found a similar massively bedded fine sand/SMO facies, deposited as a drape over the Mertz Drift (Unit 4 in Figure 7.1). The massively bedded fine sand/SMO comprises approximately 10% of Mertz Drift cores, and has a relatively high proportion of IRD gravel content (30% of all IRD). Unit 4 is also interpreted in this study as representing deposition of sediments during modern (late-Holocene) oceanographic conditions. Thus, Unit 4 has been deposited as a drape over the Mertz Drift during a period when the continental shelf in the region undergoes long periods of sea ice cover each year with a short but productive summer.

Seismic profiles from the WEGA expedition show this surface layer to be significantly different from the underlying laminated SMO facies (Figure 7.2). Datasonics chirper data reveal an acoustically thin and dark layer overlying the Mertz Drift, which is believed to represent the massively bedded fine sand/SMO facies (Brancolini and Harris 2000).

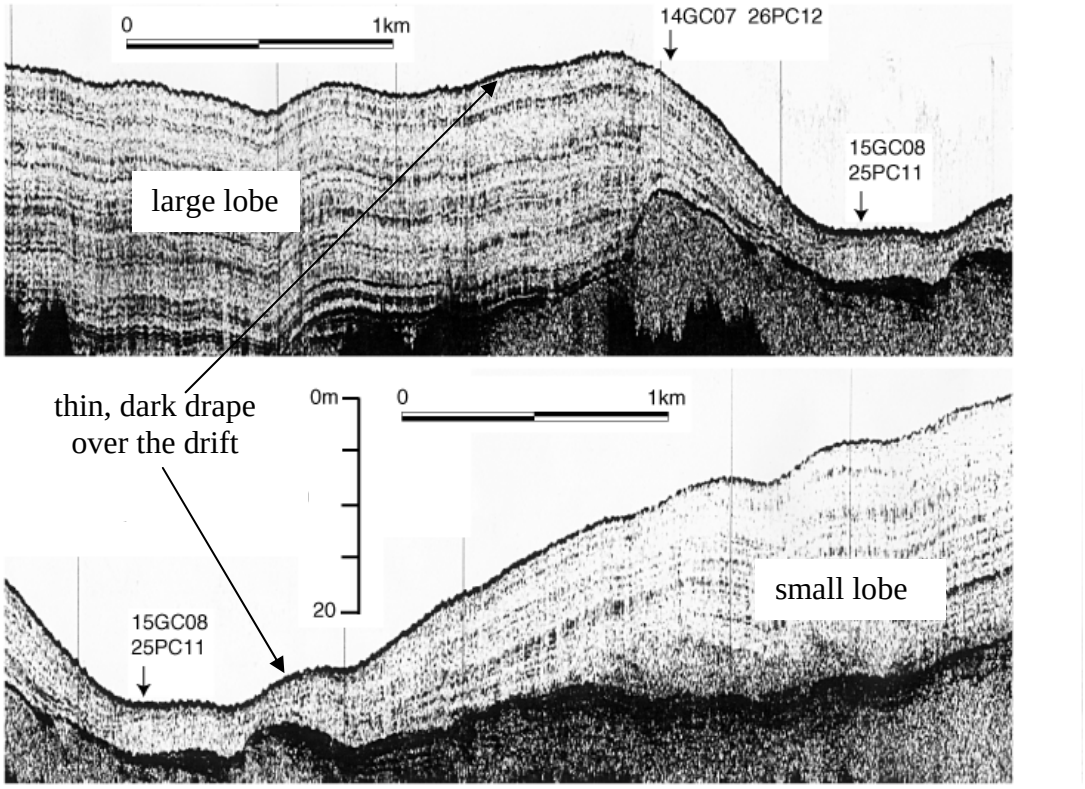

Figure 7.2 Chirper data showing the details of internal acoustic bedding across the large and small lobes of the Mertz Drift, separated by a channel in the vicinity of core 25PC11 (source: Brancolini and Harris 2000). Note the thin and dark drape over the drift, interpreted to be Unit 4 - the massively bedded fine sand/SMO facies.

A distinct climatic deterioration occurred in East Antarctica after 2000 yr BP, with colder, drier conditions, and more sea ice (Ingolfsson *et al.* 1998; Roberts *et al.* 2000). There has since followed a subsequent warming to present (Ingolfsson *et al.* 1998; Roberts *et al.* 2000). The mean of four corrected radiocarbon ages at the base of Unit 4 show deposition commenced about 3000 yr BP to the present. An important finding of this study is that deposition of the drape commenced close to the time when the climatic deterioration occurred.

Unit 4 has similarities with Unit 2, the massively bedded SMO facies at the bottom of Mertz Drift cores. Both facies record massive and convoluted structures within X-radiographs. Both units show a relatively high proportion of burrows and IRD gravel content, and record the same relatively low sediment accumulation rate (10 cm/kyr). The lower Unit 2 is interpreted as being deposited in a warming environment after a glacial, and the upper Unit 4 is also interpreted as reflecting deposition during a cooler environment that is warming. Therefore, bottom current activity during the period 3000 yr BP to the present is considered similar to that interpreted for the period 14,000 to 5000 yr BP.

Episodic deep basin currents may have provided the infrequent energy needed to produce low deposition rates, providing the substrate upon which benthic fauna found favourable for colonisation, as observed in seafloor photographs. The photographs at one site on the drift record sponge communities and Anthozoa on a substrate interpreted to be massively bedded fine sand/SMO (refer Chapter 4 - Figure 4.11). Deep basin sponge communities survive in soft, predominantly muddy surfaces, and may live on the few boulders large enough to provide a stable substrate, which are high enough to prevent significant sediment accumulation on their surface (Barthel and Gutt 1992). The numerous sponge spicules observed in the thin section possibly confirm a significant colonisation of the Mertz Drift by deep water sponge communities, as recorded in seafloor photographs. There is also evidence for bioturbation in the thin section, which confirms the observation that Unit 4 has a relatively high proportion of burrows in X-radiographs (24% of all burrows).

7.3 Model of Mertz Drift Formation

A summary model describing the formation of the Mertz Drift in three discrete post-LGM phases is shown in Figure 7.3. The physical controls on drift formation are discussed in more detail later in this chapter. The following is a description of each phase:

(1) Glacial Retreat Phase - 14,000 to 5000 yr BP (Figure 7.3A). Eustatic sea level rise followed by subsequent regional warming resulted in a rapid retreat of the Mertz Glacier Tongue to produce an open water, marine environment over the George V Basin. Short periods of episodic, relatively shallow Circumpolar Deep Water (CDW) over the outer shelf, swept sediments into the inner shelf. Corresponding pulses of deep basin, high salinity Shelf Water (HSSW) concentrated sinking fine grained material into a drift. Sediments contain high ice-rafted debris (IRD) gravel, and the substrate was colonised by benthic fauna.

(2) Climate Optimum Phase - 5000 to 3000 yr BP (Figure 7.3B). A mid-Holocene climatic optimum resulted in less extensive sea ice in the region. Longer periods of seasonal open water and air-sea interaction allowed correspondingly longer periods of CDW to be upwelled over the outer shelf. Upwelled CDW transported greater volumes of fine grained material into the George V Basin. CDW over the basin cooled and sank to help produce HSSW and more energetic bottom currents, which in turn concentrated sediments into the drift. High sedimentation rates reduced the concentration of IRD gravel, and created an environment unsuitable for colonisation by benthic fauna.

(3) Modern Phase - 3000 yr BP to present (Figure 7.3C). Regional cooling caused seasonally more extensive sea ice. During episodic, relatively shorter periods, upwelled CDW swept lower volumes of fine grained sediments into the George V Basin. Pulses of deep basin HSSW concentrated material as a thin drape over the drift. A low deposition rate resulted in high IRD gravel, and the substrate was recolonised by benthic fauna.

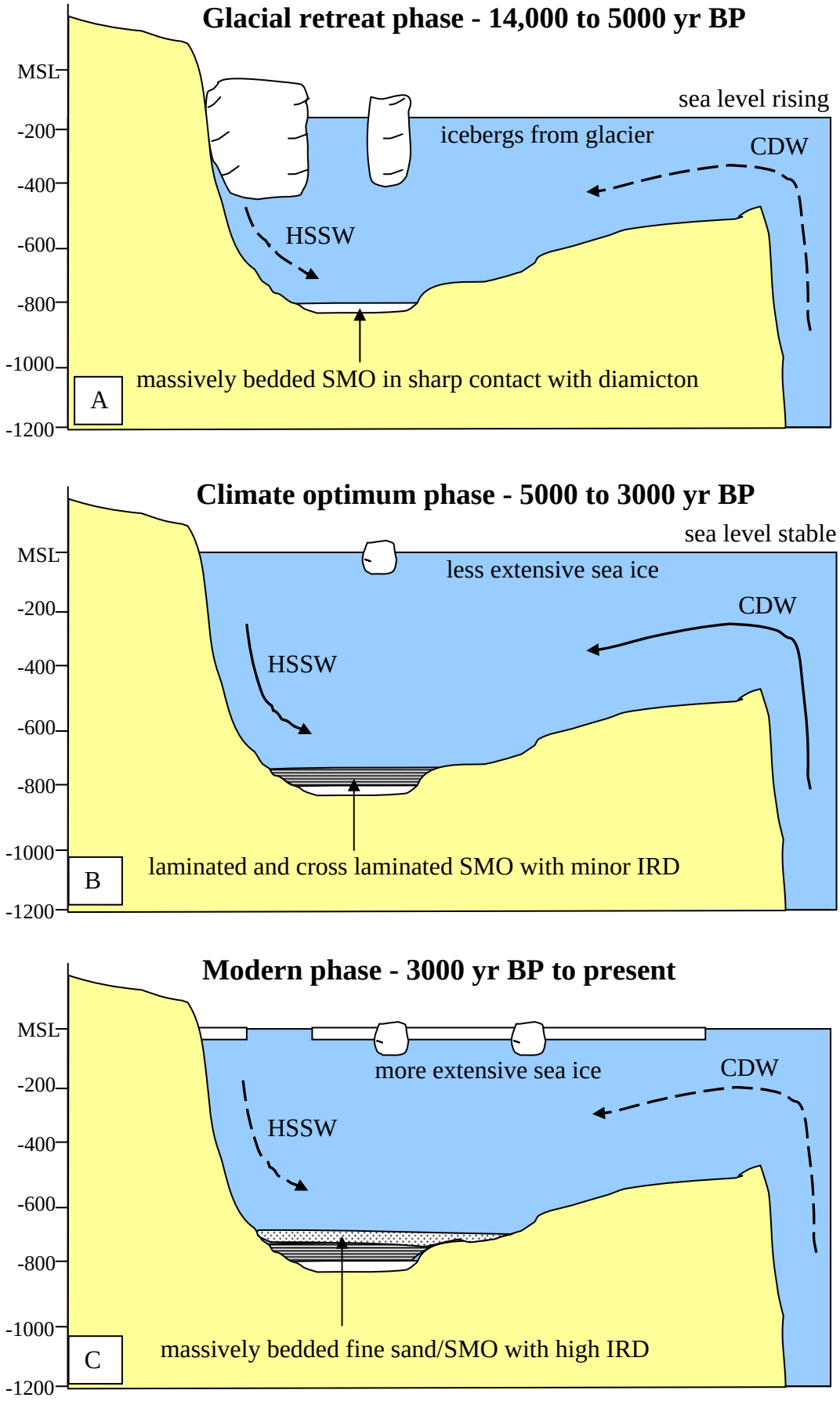

Figure 7.3 Model of Mertz Drift formation using a cross section of the shelf. **A** = Glacial retreat phase; **B** = Climatic optimum phase; **C** = Modern phase. CDW = Circumpolar Deep Water; HSSW = high salinity Shelf Water; MSL = mean sea level.

7.4 Sediment Accumulation Rates

A new finding, in addition to the aims of this study, is that sediment accumulation rates across the Mertz Drift have not been constant over the same time scale. This finding is evidenced by a lower sediment accumulation rate of 175 cm/kyr within laminated SMO from core 26PC12, compared to 293 and 310 cm/kyr for laminated SMO in cores 13GC05 and 13GC06 respectively. The difference between the rates appears to correspond with the morphology of the drift. Figure 7.4 shows that the thickest part of the drift of about 35 m occur in the vicinity of cores 13GC05 and 13GC06, while core 26PC12 was obtained from the edge of the large lobe where acoustic strata thin and pinch out. Radiocarbon ages from core 16PC01 on the small lobe (Figure 7.4) would be a useful test for a high sediment accumulation rate similar to cores 13GC05 and 13GC06, however, no radiocarbon ages were available from core 16PC01. The sediment accumulation rates across the Mertz Drift are likely to vary depending on where the current preferentially deposits sediment over the drift. Topography is likely to be an important factor in the current flow regime in this region.

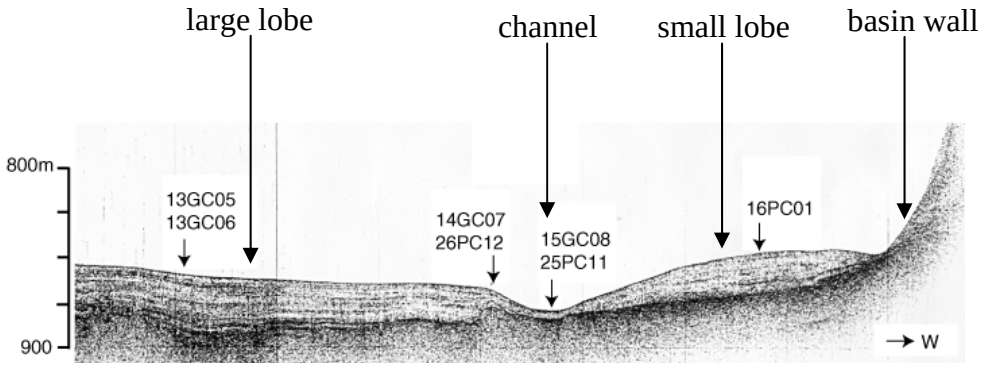

Figure 7.4 East/west 3.5 kHz seismic profile across the large and small lobes of the Mertz Drift (source: Brancolini and Harris 2000). Cores 13GC05 and 13GC06 lie at the thickest part of the drift on the large lobe, and have relatively high sedimentation rates within laminated SMO. Core 26PC12 is positioned on the edge of the large lobe where acoustic strata thins and pinches out, and has a lower sedimentation rate within the laminated SMO of this core.

7.5 Timing of Post-LGM Deposition in the George V Basin

The timing of the Last Glacial Maximum (LGM) around Antarctica is believed to have coincided with the timing of lowest global sea levels around 20,000-18,000 yr BP (Ingolfsson *et al.* 1998). The sub-ice shelf phase of deposition for the Mertz Drift was around 24,000 yr BP based upon the single radiocarbon age from diamicton in this study. Diamicton (Unit 1) in the western end of the George V Basin (i.e. Mertz Drift area) was thus deposited as a result of a glacial advance during the LGM, and not during a mid-Holocene glacial advance as proposed by Domack *et al.* (1991). Similarly, the timing of the onset of open marine conditions in this present study (Unit 2 - 14,000 to 5000 yr BP) is in contrast to, and older than, the Domack *et al.* (1991) estimate of mid- to late-Holocene timing of open marine conditions following glacial retreat off George V Land. The climatic optimum phase (during which the laminated and cross laminated SMO succession (Unit 3) of this study was deposited) lasted from 5000 to 3000 yr BP. The equivalent laminated SMO within core DF79-12 recorded corrected radiocarbon dates of between about 2400 to 1000 yr BP (Domack *et al.* 1991).

The younger Domack *et al.* (1991) ages for core DF79-12 may be the result of using a surface age of 5020 years to correct radiocarbon ages, nearly double the surface ages used to correct Mertz Drift cores in this study. Thus, the assumptions about reservoir correction for core DF79-12 made by Domack *et al.* (1991), and the surface age used to correct core DF79-12 appear to be in error. A recalculation of Domack *et al.*'s (1991) corrected radiocarbon ages (refer Chapter 5 - Table 5.1) using the mean surface radiocarbon age of 2643 years from this present study, results in a close match of radiocarbon ages for the laminated and cross laminated SMO: 5000 to 3000 yr BP (this study) versus about 4200 to 3000 yr BP (core DF79-12). However, there was a poor match between the massively bedded SMO at the base of the Mertz Drift: 14,000 to 5000 yr BP (this study) versus about 4700 to 4200 yr BP (core DF79-12). No explanation can be given for the relatively poor match in radiocarbon ages for the massively bedded SMO.

7.6 Lamination Couplets

A hypothesis of this study is that Mertz Drift sediments largely result from cyclical, high productivity diatom blooms due to annual seasonal changes in sea ice cover. This hypothesis was based upon the Domack (1988) productivity model to explain the development of laminated SMO facies in shelf basin sediments (refer Chapter 1 - Figure 1.3). This present study finds evidence in the laminated SMO thin section for a cycle of sea ice diatoms to open water diatoms. Based on the Domack (1988) model, this cycle is interpreted as representing the initial pelagic flux of diatoms induced by melting sea ice, while the overlying lamina represents primary productivity during the remainder of the summer season.

Calculations of the mean deposition time of lamination couplets in cores 13GC05 and 26PC12 indicate periods of between 2.6 and 4.3 years respectively. These figures appear to disprove the hypothesis that Mertz Drift sediments result from diatom blooms due to annual seasonal changes in sea ice cover. Yet the errors involved in calculating the mean deposition time of lamination couplets in cores 13GC05 and 26PC12 suggest caution in disproving the annual productivity hypothesis of this study. This study identifies that the mean deposition time of lamination couplets is most likely to be multiyear but not decadal. The relevance of multiyear cycles recorded in lamination couplets is that the laminated SMO of the Mertz Drift thus records a high resolution history of sea ice versus open water production over the George V Basin. A downcore comparison of sea ice versus open water diatoms within a long piston core from the drift would be useful in understanding this history.

Combining the interpretation of formation of laminae from thin section analysis with the finding of a mean deposition time of between 2.6 and 4.3 years leads to a revised hypothesis that Mertz Drift laminated sediments result from cyclical, high productivity diatom blooms due to seasonal changes in sea ice cover. The lamination couplets could reflect events that take between 2.6 to 4.3 years to occur, such as the changes in sea ice extent as has recently been seen in the Weddell Sea, coherent with observed passages of the Antarctic Circumpolar Wave (Cosimo and Gordon 1998).

7.7 Physical Controls on Drift Formation

Domack (1988) hypothesised that the thicker SMO sediments at the western end of the George V Basin (i.e. the area Mertz Drift lies in) should contain a greater proportion of gravity flow muds than the uniform and draped layers as recovered in core DF79-12. An aim of this project was to conduct thin section analysis, which may reveal whether sediments were a hemipelagic drape, current lain or from gravity flows. Thin sections did reveal sediments to be a possible continuum between drape and current lain deposits, but no evidence for gravity flows was observed. In addition, the criteria to distinguish debris flow from high and low concentration turbidites, such as upper or lower sharp contacts and upward fining of beds (Wright *et al.* 1983), do not appear within any Mertz Drift X-radiographs. As no sharp contacts were obvious from the X-radiographs within this thick laminated and cross laminated SMO succession, it is difficult to support the Domack (1988) gravity flow hypothesis. If gravity flows were an important feature of the Mertz Drift then seismic profiles would show wedge-shaped acoustic reflections. Instead, profiles reveal a mounded and constructional feature, consistent with the depositional architecture indicative of a 'confined drift' as defined by Faugeres *et al.* (1999).

7.7.1 Oceanography

This study proposes that two separate currents are responsible for the construction of the Mertz Drift. The two water masses responsible for the currents are:

(1) Circumpolar Deep Water (CDW). Relatively shallow, impinging CDW transports fine grained biogenic material from the water column and terrigenous material winnowed from the outer shelf banks towards the coast, and over the George V Basin. This process is well accepted within Antarctic glacial-marine models, in that fine grained material is swept from the outer shelves by upwelled CDW, and transported southerly towards the inner shelf (Domack 1988; Harris and O'Brien 1998). Most of the sediments within the Mertz Drift were probably derived from the outer shelf except for any ice-rafted debris (IRD) and diatoms falling from above.

(2) High Salinity Shelf Water (HSSW). Deep basin bottom currents derived from HSSW (separate from southerly-flowing CDW) sweep northwesterly along the length of the basin, and collect falling fine grained biogenic and terrestrial material brought into the inner shelf by CDW. These sediments are then concentrated into the Mertz Drift at the western end of the basin. The geomorphology of the drift suggests a bottom current from the southeast, which will be argued in the following paragraphs based upon recent oceanographic information, and other physical processes such as seafloor bathymetry and Coriolis effect.

Recent oceanographic studies have yet to resolve the current flows at the western end of the George V Basin but there are some initial results from acoustic doppler current profiler data for northwesterly-flowing deep basin currents reflective of HSSW (Williams 2000). Bindoff and Williams (submitted) state that a major source for the brine contributing to the cold, dense HSSW originates from the Mertz polynya at the eastern end of the George V Basin. This information forms the basis for the proposal that the deep basin bottom current responsible for concentrating sediments into the Mertz Drift is derived from HSSW, flowing from the eastern end of the George V Basin towards the western end of the basin (i.e. in the vicinity of the Mertz Drift), then northward over the sill as Antarctic Bottom Water (AABW; refer Chapter 2 - Figure 2.5).

7.7.2 Bathymetry

It is possible that the bathymetric form of the basin may explain sedimentation into a drift deposit. Any water mass with fine grained sediments in a suspension load must experience a reduction in velocity to allow settling at the western end of the George V Basin. The bathymetric map of the continental shelf off George V Land displays a 'peanut' shaped George V Basin (refer Chapter 1 - Figure 1.4). There is a low ridge at about longitude 144˚ east that separates the western arm of the basin from the deeper east section (Harris 2000). Any northwesterly-flowing HSSW must encounter this ridge then flow down into the western end of the basin before being deflected north towards the sill. In effect, a gyre is likely to have been produced over the western end of the basin where fine grained sediments settle in a drift deposit

when the velocity drops. The proposed general flow of HSSW within the George V basin is displayed in Figure 7.5.

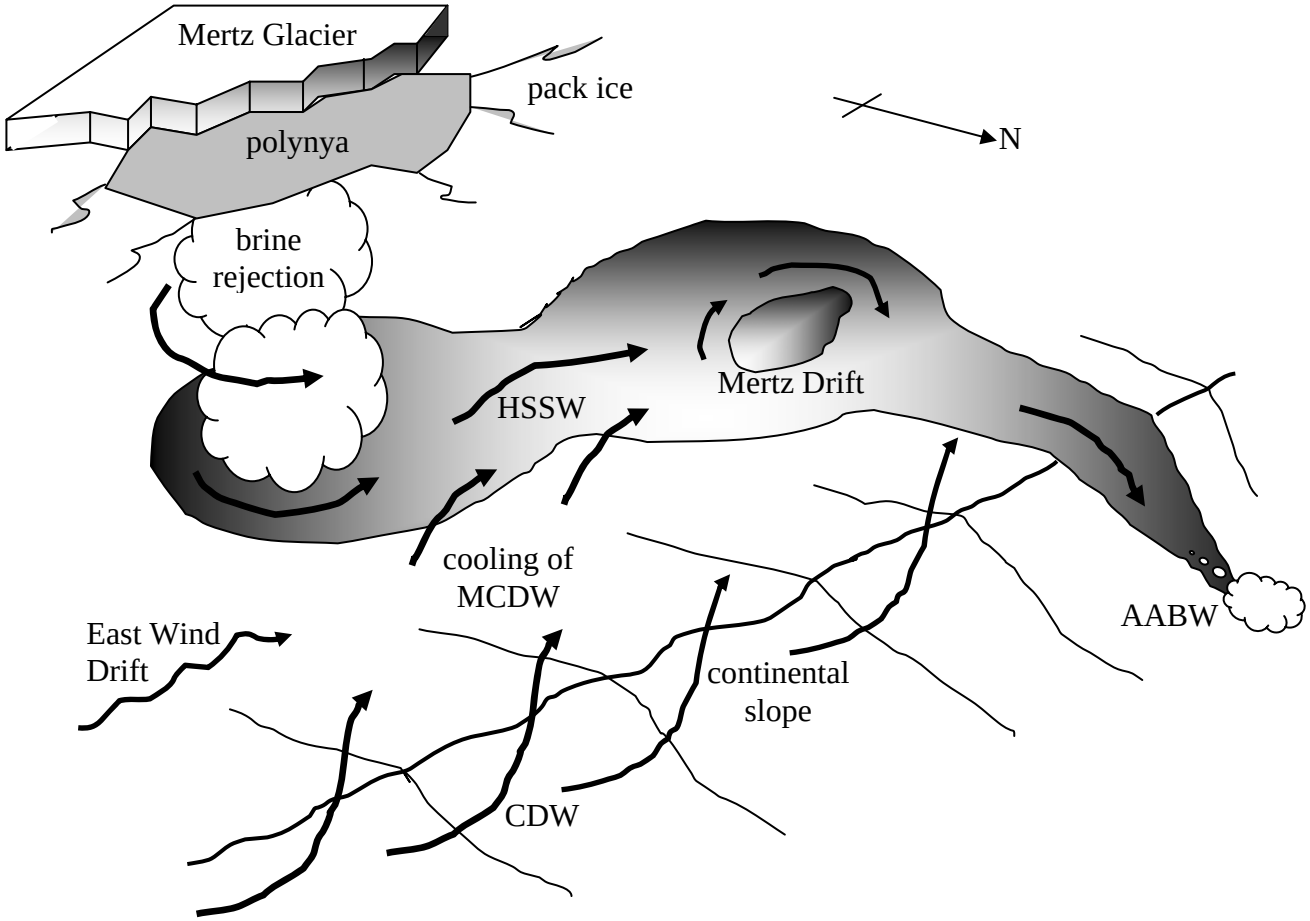

Figure 7.5 Diagram showing brine rejection and/or cooling of impinging Modified Circumpolar Deep Water (MCDW) to produce westerly flowing high salinity Shelf Water (HSSW) and Antarctic Bottom Water (AABW) within the George V Basin (modified from: Baines and Condie 1998). Note the proposed gyre effect over the western end of the basin believed responsible for the concentration of sediments into the Mertz Drift.

7.7.3 Geomorphology and Coriolis Effect

The review of deep sea drift deposits or contourite drifts by Faugeres *et al.* (1999) states that as a general rule, deep sea sediment bodies of any type tend to migrate according to a number of principal factors: the flow direction, the Coriolis effect and the bathymetric framework. Firstly, whatever the type of current, drift deposits tend to migrate downstream. Secondly, the Coriolis effect influences the current regime and lateral migration of drifts. In the Southern Hemisphere, if current flow is from east to west, the Coriolis effect deflects the flow to the left, effectively

constraining the flow against any slope. Being so constrained, the current flow intensifies, erosion occurs and a channel develops. Lower velocities to the right of a east to west current flow favour deposition and drift construction, with the drift tending to migrate upslope as well as prograde alongslope. Current flows are also significantly affected by bottom morphology. A change in steepness of the slope may cause initiation or cessation of deposition and drift construction by a bottom current. An examination of the isopach map (refer Chapter 3 - Figure 3.1) and seismic profiles of Figures 7.2 and 7.4, reveal features consistent with the factors described above, which explain a bottom current from the southeast. These features are displayed diagrammatically in Figure 7.6.

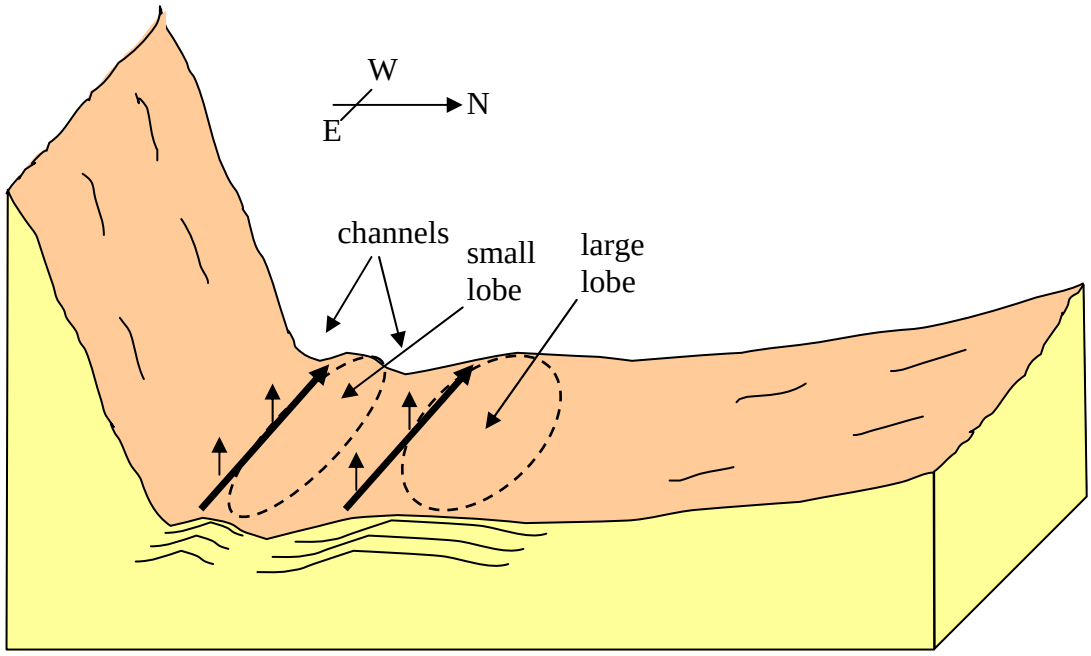

Figure 7.6 Diagram illustrating the possible relationships between factors responsible for sediment deposition of the Mertz Drift (modified from: Faugeres *et al.* 1999). Thick black arrows show split currents from the southeast, and flow restriction causing channels to the left of lobes as a result of Coriolis effect.

In assessing the proposed concept of sediment transport from the southeast, both the large and small lobes of the Mertz Drift have a southeast to northwest orientation, in keeping with a downstream direction of current flow (Figure 7.6). Additionally, the drift also displays a deep channel separating the large and small lobes. Cores obtained from this position of the drift (e.g. cores 15GC08 and 25PC11) attest to the 'soupy' and overturned nature of sediments within the deep channel. There is also a smaller dip or channel separating the small lobe from the basin wall

(refer to Figure 7.4). Thus, current flow appears to split at a finer-scale over the drift to erode and create two channels. Both channels are consistent with flow restriction to the left as a result of Coriolis effect. A topographic high underlying the Mertz Drift on the west side of the large lobe (under core 26PC12 in Figure 7.2) may explain why currents have split at this finer scale. Deposit zones to the right of the split currents explain the development of the two lobes, and possibly the varying sediment accumulation rates across the Mertz Drift. Faugeres *et al.* (1999) also describes progradation towards the slope for drifts in the southern hemisphere as a result of the Coriolis effect. The internal acoustic structure of the Mertz Drift displays this feature. From seismic profiles, Brancolini and Harris (2000) note that acoustic reflectors from the small lobe dive beneath the reflectors of the large lobe. This may reflect progradation toward the side of the basin in keeping with the Faugeres *et al.* (1999) model of drift deposition, and provide further proof that current flow is from the southeast.

7.8 Does the Mertz Drift Record Bottom Water Formation?

This study proposed that it was unlikely that an increase in productivity over the shelf of greater than 20 times could account for the high deposition rates during the climatic optimum phase (Unit 3). Primary productivity is dependent on the presence of sunlight, carbon dioxide, nutrient salts and water, whilst the rate is controlled by the levels of these factors and by the ambient temperature (Walton 1987). With the arrival of spring and summer, the sea ice breaks up, exposing the water to light. Within days a phytoplankton bloom develops as a result of rapid multiplication of resting spores brought to the surface and also released from the fragmenting ice layer (Walton 1987). However, studies show that highest numbers of diatom species occurred with the melting of the sea ice then dropped off during the remainder of summer when open water prevailed (Knox 1994). The implication is that regardless of the period of favourable light and temperature each season, phytoplankton blooms occur only during a brief period at the beginning of summer and reduces thereafter. It is difficult to believe that a climatic optimum would change the relative productivity to a level to produce the high sedimentation rates recorded in the Mertz Drift, based upon the behaviour of diatom blooms under present conditions.

Even if primary productivity, and possibly IRD sedimentation, has been relatively constant since the Last Glacial Maximum (LGM), the only mechanism to explain the high sedimentation rates in the Mertz Drift are physical processes such as enhanced bottom currents. A surge in the local current regime in the George V Basin may possibly concentrate greater volumes of fine grained material into a drift deposit during the climate optimum phase. A relative reduction in bottom current intensity during the glacial retreat phase (Unit 2) and modern phase (Unit 4) therefore will not lead to transporting the same volume of fine grained material, and result in lower deposition rates.

Evidence for enhanced bottom current activity during the climatic optimum are the lateral accretion surfaces, parallel foresets, wavy or laterally discontinuous laminae observed in X-radiographs of cross laminated SMO from the Mertz Drift. Cross laminations are believed to represent short periods of rapid sedimentation and higher velocity bottom current activity relative to velocities responsible for deposition of laminations. Thin sections of cross laminated SMO show current-lain diatom frustule alignment, rapid sedimentation in the form of uncorroded foraminifera and poorly sorted sediments. Similarly, thin sections of laminated SMO show evidence of current transport with somewhat aligned siliceous spines in the light laminae.

This study thus proposes that Mertz Drift sediments do record bottom water formation. The deep basin bottom current believed to be responsible for concentrating sediments into the deposit is derived from high salinity Shelf Water (HSSW), which fills the George V Basin, and eventually overflows the sill at the shelf edge to become Antarctic Bottom Water (AABW; Rintoul 1998). The interpretation of environments from this study therefore implies three distinct periods of HSSW, and hence AABW production, since the LGM. The massively bedded SMO (Unit 2) was deposited by relatively less energetic bottom currents from 14,000 to 5000 yr BP. This period occurred during glacial retreat as sea level rose and the climate warmed (Ingolfsson *et al.* 1998). The laminated and cross laminated SMO succession (Unit 3) was deposited during a surge in the local bottom current regime from 5000 to 3000 yr BP. This period is close to a climatic optimum when East Antarctica was warmer, wetter and had less sea ice than the present (Ingolfsson *et al.* 1998). A climatic deterioration in

East Antarctica with colder, drier conditions, and more sea ice (Ingolfsson *et al.* 1998), resulted in relatively less energetic, episodic bottom currents depositing massively bedded fine sand/SMO (Unit 4) from 3000 yr BP to present.

As two separate water masses and the resulting currents are believed responsible for the Mertz Drift (i.e. the relatively shallow CDW and deep basin HSSW), this study proposes that a possible factor linking the two water masses to changes in local current regime is the change in sea ice cover over the shelf. Relative changes in sea ice cover have been highlighted in the Ingolfsson *et al.* (1998) review of Antarctic glacial and climatic history since the LGM. Less extensive sea ice in the region during a climatic optimum would allow winds such as from cyclonic storms to interact with the sea and draw CDW onto the shelf. This interaction would occur in the same manner that causes upwelling of oceanic water masses on lower latitude continental shelves (Press and Seiver 1986).

Recent oceanographic studies in the region found CDW peaks in flow over the outer shelf in summer when the sea ice has melted (Williams 2000). Therefore, a longer period of seasonal open water during a climatic optimum may allow a correspondingly longer period of time for the upwelling of CDW over the outer shelf and towards the coast. As CDW is linked to the production of modified Circumpolar Deep Water (MCDW), then HSSW through brine rejection, and ultimately AABW as it flows off the shelf (Rintoul 1998; Bindoff and Williams, submitted), a longer period of upwelled CDW may be the oceanographic key that enhances bottom current activity. The resulting surge in local bottom currents as HSSW fills the basin would, in turn, focus the higher volumes of fine grained sediments into the Mertz Drift, and produce more AABW during a climatic optimum. The relative changes in deposition are important because of the implications for the non-steady-state of bottom water production proposed by Broecker *et al.* (1998).

Another important implication from the results of this study is the role of the Mertz Drift as a carbon sink. Antarctic deep shelf basins have been suggested as potential carbon sinks by Harris *et al.* (1999). This is because sediments are presently accumulating within the shelf valleys and basins, which represent approximately 10%

of the shelf surface area compared to the 90% of the area that is essentially erosional in character (Harris and O'Brien 1996). This present study calculated a carbon content within the Mertz Drift of approximately 78 million tonnes (Mt). This is approximately seven times the carbon content calculated for the Andvord Drift, the only other drift deposit found on the Antarctic shelf to date (11 Mt; Harris *et al.* 1999). When averaged over the entire drift formation period of approximately 14,000 years, the 78 Mt of carbon calculated within the Mertz Drift may only represent a low carbon deposition rate of 5.6 kt C/yr. However, when about 65% (the calculated percentage of Unit 3) of that 78 Mt, or 45.5 Mt, is deposited between 5000 and 3000 yr BP, during a period of enhanced bottom current, the carbon deposition rate climbs to about 25 kt C/yr. As there are over 19 deep basins along the Australian Antarctic Territory alone, with the majority unstudied, then any drift deposits which may be in these basins could play an important role in the carbon cycle of the Antarctic shelf.

Chapter 8. Conclusions

8.1 Conclusions

This present study has developed a new model to explain the origin of the Mertz Drift. This study draws upon models of drift deposits by Faugeres *et al.* (1999), and previous models of Antarctic glacial-marine sediments by Anderson *et al.* (1983), Domack (1988), Domack and Harris (1998), and Harris and O'Brien (1998).

A study of X-radiographs, visual core logs and multi-sensor core logger data from 18 gravity and piston cores collected by the WEGA research expedition on the Mertz Drift, defines five facies:
(1) massively bedded siliceous mud and diatom ooze (SMO)
(2) massively bedded fine sand/SMO,
(3) laminated SMO,
(4) cross laminated SMO, and
(5) diamicton.

A comparison of facies interpretation logs of all cores, the application of radiocarbon ages to cores, thin section analysis and seafloor photographs of the Mertz Drift allow interpretation of the five facies into four generalised phases of environmental history. The diamicton corresponds to sub-ice shelf, water-lain till deposition during the Last Glacial Maximum (LGM). Unconformably overlying the diamicton is a massively bedded SMO with a high proportion of ice-rafted debris (IRD). This unit represents a period of glacial retreat of the ice shelf and a transition to an open marine environment, commencing about 14,000 yr BP. Low sedimentation rates during this period last for about 9000 years. A thick succession of laminated and cross laminated SMO follows, deposited during a mid-Holocene climate optimum from 5000 to 3000 yr BP. Overlying the Mertz Drift as a drape is a massively bedded fine sand/SMO with a high proportion of IRD, deposited from 3000 yr BP to present. This drape reflects modern oceanographic conditions commencing from a time of climatic deterioration in the region.

This study found large relative changes in sediment accumulation rates between the glacial retreat phase, climatic optimum phase and modern phase. A comparison of sediment accumulation rates across the Mertz Drift also reveals that rates have not been constant over the same time scale. Radiocarbon ages from Mertz Drift cores show diamicton was deposited as a result of a glacial advance during the LGM, and not during a Domack *et al.* (1991) mid-Holocene glacial advance over the George V Basin. The timing of the onset of open marine conditions in this study is in contrast to, and older than, the Domack *et al.* (1991) mid- to late-Holocene timing of open marine conditions in the area.

As a consequence of this study, the three hypotheses proposed at the start of the thesis are mostly supported. However, this study was not able to confirm that Mertz Drift sediments largely result from cyclical, high productivity diatom blooms due to annual seasonal changes in sea ice cover. In contrast, observations of lamina revealed cyclical changes in diatom assemblages within lamination couplets with mean deposition times of between 2.6 to 4.3 years.

Mertz Drift sediments are concentrated and reworked by episodic, deep basin currents. The two currents believed responsible for the construction of the drift are the relatively shallow, upwelled Circumpolar Deep Water (CDW), transporting fine grained sediments southwards towards the inner shelf, and deep high salinity Shelf Water (HSSW) flowing northwesterly along the basin, focusing sinking sediments into a drift deposit. A gyre is likely to have been produced over the western end of the basin where fine grained sediments settle in a drift deposit when the velocity drops. Coriolis effect and seafloor topography are two physical processes that are likely to be important factors in the current flow regime in this area.

Mertz Drift sediments record a high resolution record of bottom current intensity during the Holocene, and hence palaeoenvironment, off George V Land. Bottom currents are associated with the formation of HSSW, which in turn becomes Antarctic Bottom Water (AABW). The relative reduction of seasonal sea ice cover during a climatic optimum is believed to be a key factor in allowing longer periods of CDW over the shelf, which leads to a surge in bottom currents and the concentration

of greater volumes of sediment into the Mertz Drift. Calculation of carbon deposition rates in the Mertz Drift shows that drift deposits may play an important role in the carbon cycle of the Antarctic shelf.

The sediments of the Mertz Drift reflect dramatic and rapid changes in the palaeoenvironment during the Holocene. There is currently a global anthropogenic warming trend influencing sea ice distribution around Antarctica. Ice cores show that warming over the past three decades is the most pronounced in over four centuries. The results from this study predicts that: *if the warming trend and sea ice reduction continue, then the energetic current environment, observed during the mid-Holocene climatic optimum, will develop*. However, the proviso for this scenario will only occur if sea ice reduces significantly from the extensive area it currently occupies around Antarctica during most of the year. This study also has important implications for oceanographers as the results suggest a non-steady-state of Antarctic Bottom Water production during the Holocene.

8.2 Recommendations for Further Research

To help resolve the issue of lamination couplet origin and period of cyclicity, sediment trap data would be required to confirm diatom assemblage successions. A longer piston core at the site of the thickest section of the drift would provide a detailed record of past environmental conditions from a relatively unknown region of the East Antarctic shelf. This record would provide a comparison for other better studied locations such as the Nielsen Shelf Valley and Prydz Bay. The aim would be to develop an East Antarctic Holocene palaeoclimatology, as one of key strategic questions underpinning Australian Antarctic research is - What geological and geophysical processes have shaped the continent and the surrounding ocean, and what has been their effect on the present and past Antarctic climate?

The findings from this present study can now be compared with the Dome C ice core onshore. This was one of the aims for the WEGA expedition. The correlation of sedimentary and glacial records would contribute to the understanding of temporal and spatial constraints of the glacial/interglacial stages and late-Quaternary

palaeoclimatic fluctuations. The comparison of sedimentary and glacial records would also permit the linkage of atmospheric processes and the response of the marine system.

Future research with the existing WEGA cores could involve obtaining more radiocarbon dates to 'fine-tune' the corrected ages to the various facies. Radiocarbon ages from core 16PC01, on the small lobe, would be a useful test for a high sediment accumulation rate similar to cores 13GC05 and 13GC06, from the large lobe. A study of variability in sea ice versus open water diatom assemblages within individual laminae would be very useful. Techniques would involve individual diatom species counts and a detailed thin section analysis. In addition, an overall downcore comparison of sea ice versus open water diatoms within a long piston core would be useful for helping understand the history of sea ice versus open water production on the continental shelf off George V Land.

References

Anderson, J.B., Domack, E.W. and Kurtz, D.D. (1980). Observations of sediment-laden icebergs in Antarctic waters: implications to glacial erosion and transport. *Journal of Glaciology* Vol. 25, No. 23: 387-396.

Anderson, J.B., Brake, C., Domack, E.W., Myers, N. and Wright, R. (1983). Development of a Polar Glacial-Marine Sedimentary Model from Antarctic Quaternary Deposits and Glaciological Information. In: Molnia, B.F. (editor). *Glacial-Marine Sedimentation*. New York: Plenum Press: 233-263.

Antarctic CRC (2000), Antarctic CRC Home Page [www.antcrc.utas.edu.au], [cited February 25, 2000]. Available from Internet: <URL:http://www.antcrc.utas.edu.au/sediment_web/collab/wega/wega.html>.

Arntz, W.E. and Gallardo, V.A. (1994). Antarctic Benthos: Present Position and Future Prospects. In: Hempel, G. (editor). *Antarctic Science, Global Concerns*. Berlin: Springer-Verlag: 243-277.

Ashley, G.M. and Smith, N.D. (2000). Marine sedimentation at a calving glacier margin. *GSA Bulletin* Vol. 112, No. 5: 657-667.

Australian Antarctic Division (2000), Australian Antarctic Division Home Page [www.antdiv.gov.au], [cited August 27, 2000]. Available from Internet: <URL:http://www.antdiv.gov.au/resources/atlas/>.

Baines, P.G. and Condie, S. (1998). Observations and Modelling of Antarctic Downslope Flows: a Review. In: Jacobs, S.S. and Weiss, R.F. (editors). *Ocean, Ice and Atmosphere: Interactions at the Antarctic Continental Margin. Antarctic Research Series Volume 75*. Washington D.C.: American Geophysical Union: 29-49.

Baroni, C. and Orombelli, G. (1991). Holocene raised beaches at Terra Nova Bay, Victoria Land, Antarctica. *Quaternary Research* 36: 157-177.

Barthel, D. and Gutt, J. (1992). Sponge associations in the eastern Weddell Sea. *Antarctic Science* 4(2): 137-150.

Berkman P.A. and Forman S.L. (1996). Pre-bomb radiocarbon and the reservoir correction for calcareous marine species in the Southern Ocean. *Geophysical Research Letters* Vol. 23, No. 4: 363-366.

Berkman, P.A., Andrews, J.T., Bjorck, S., Colhoun, E.A., Emslie, S.D., Goodwin, I.D., Hall, B.L., Hart, C.P., Hirakawa, K., Igarashi, A., Ingolfsson, O., Lopez-Martinez, J., Lyons, W.B., Mabin, M.C.G., Quilty, P.G., Taviani, M. and Yoshida, Y. (1998). Circum-Antarctic coastal environmental shifts during the Late Quaternary reflected by emerged marine deposits. *Antarctic Science* 10 (3): 345-362.

Bindoff, N.L. and Williams, G.D. (submitted). Sea-ice growth and water mass modification in the Mertz Glacier Polynya during winter. *Annals of Glaciology*.

Brancolini, G. and Harris, P.T. (2000). AGSO Record No. 2000/19 Post-cruise Report: Joint Italian/Australian Marine Geoscience Expedition Aboard the R.V. *Tangaroa* to the George Vth Land Region of East Antarctica during February-March, 2000.

Broecker, W.S., Peacock, S.L., Walker, S., Weiss, R., Fahrbach, E., Schroeder, M., Mikolajewicz, U., Heinze, C., Key, R., Peng, T.H. and Rubin, S. (1998). How much deep water is formed in the Southern Ocean? *Journal of Geophysical Research Vol*. 103 No. C8: 15,833-15,843.

Buchsbaum, R., Buchsbaum, M., Pearse, J. and Pearse, V. (1987). *Animals Without Backbones*. Chicago: The University of Chicago Press: 76.

Colhoun, E.A. (1997). A Review of Geomorphological Research in Bunger Hills and Expansion of the East Antarctic Ice Sheet during the Last Glacial Maximum. In: Ricci, C.A. (editor*). The Antarctic Region: Geological Evolution and Processes. Proceedings of the VII International Symposium on Antarctic Earth Sciences*. Siena: Terra Antarctica Publication: 801-807.

Cosimo, J.C. and Gordon, A.L. (1998). Interannual Variability in Summer Sea Ice Minimum, Coastal Polynyas and Bottom Water Formation in the Weddell Sea. In: Jefferies, M.O. (editor). *Antarctic Sea Ice: Physical Processes, Interactions and Variability. Antarctic Research Series Volume 74*. Washington DC: American Geophysical Union: 293-315.

Cunningham, W.L, Leventer, A., Andrews, J.T., Jennings, A.E. and Licht, K.J. (1999). Late Pleistocene-Holocene marine conditions in the Ross Sea, Antarctica: evidence from the diatom record. *The Holocene* 9.2: 129-139.

Domack, E.W., Fairchild W.W. and Anderson J.B. (1980). Lower Cretaceous sediment from the East Antarctic continental shelf. *Nature* 287: 625-626.

Domack, E.W. (1982). Sedimentology of glacial and glacial marine deposits on the George V - Adélie continental shelf, East Antarctica. *Boreas* 11: 79-97.

Domack, E.W. and Anderson J.B. (1983). Marine Geology of the George V Continental Margin: Combined Results of Deep Freeze 79 and the 1911-14 Australasian Expedition. In: Oliver, R.L., James, P.R. and Jago, J.B. (editors). *Antarctic Earth Science*. Canberra: Australian Academy of Science: 402-406.

Domack, E.W. (1988). Biogenic Facies in the Antarctic glacimarine environment: basis for a polar glacimarine summary. *Palaeogeography, Palaeoclimatology, Palaeoecology* 63: 357-372.

Domack, E.W., Jull, A.J.T., Anderson, J.B., Linick, T.W. and Williams, C.R. (1989). Application of Tandem Accelerator Mass-Spectrometer dating to late

Pleistocene-Holocene sediments of the East Antarctic continental shelf. *Quaternary Research* 31: 277-287.

Domack, E.W., Jull, A.J.T. and Nakao, S. (1991). Advance of East Antarctic outlet glaciers during the Hypsithermal: implications for the volume state of the Antarctic ice sheet under global warming. *Geology* Vol. 19: 1059-1062.

Domack, E.W. and Harris, P.T. (1998). A new depositional model for ice shelves, based upon sediment cores from the Ross Sea and the Mac.Robertson shelf, Antarctica. *Annals of Glaciology* 27: 281-184.

Edgar, G.J. (1997). *Australian Marine Life*. Kew, Victoria: Reed Books: 112.

Emslie, S.D., Fraser, W., Smith, R.C. Walker, W. (1998). Abandoned penguin colonies and environmental change in the Palmer Station area, Anvers Island, Antarctic Peninsula. *Antarctic Science* 10 (3): 257-268.

Faugeres, J.C., Stow, D.A.V., Imbert, P. and Viana, A. (1999). Seismic features diagnostic of contourite drifts. *Marine Geology* 162: 1-38.

Fitzsimons, S.J. and Colhoun, E.A. (1995). Form, structure and stability of the margin of the Antarctic ice sheet, Vestfold Hills and Bunger Hills, East Antarctica. *Antarctic Science* 7: 171-179.

Goodwin, I.D. (1996). A mid to late Holocene readvance of the Law Dome ice margin, Budd Coast, East Antarctica. *Antarctic Science* 8 (4): 395-406.

Gowlett-Holmes, K. (2000). Dr. K. Gowlett-Holmes, CSIRO Marine Research [personal communication, 10 July 2000].

Hampton, M.A., Kravitz, J.H. and Luepke, G. (1987). Geology of Sediment Cores from the George V Continental Margin, Antarctica. In: Eittreim, S.L. and Hampton, M.A. (editors). *The Antarctic Continental Margin: Geology and*

Geophysics of Offshore Wilkes Land, CPCEMR Earth Science Series Volume 5A. Houston: Circum-Pacific Council for Energy and Mineral Resources: 151-174.

Harris, P.T., O'Brien, P.E., Sedwick, P. and Truswell, E.M. (1996). Late Quaternary history of sedimentation on the Mac.Robertson shelf, East Antarctica: problems with ^{14}C-dating of marine sediments. *Papers and Proceedings of the Royal Society of Tasmania* Vol. 130(2): 47-53.

Harris, P.T. and O'Brien, P.E. (1996). Geomorphology and sedimentology of the continental shelf adjacent to Mac.Robertson Land, East Antarctica: a scalped shelf. *Geo-Marine Letters* 16:287-296.

Harris, P.T. and O'Brien P.E. (1998). Bottom currents, sedimentation and ice-sheet facies successions on the Mac.Robertson shelf, East Antarctica. *Marine Geology* 151: 47-72.

Harris, PT., Domack, E.W., Manley, P.L., Gilbert, R. and Leventer, A. (1999). Andvord drift: A new type of inner shelf, glacial marine deposystem from the Antarctic Peninsula. *Geology* Vol. 27, No. 8: 683-686.

Harris, P.T. (2000), Dr. P.T. Harris, Antarctic CRC, University of Tasmania [personal communication, 25 August 2000].

Harris, P.T. (submitted). Ripple cross-laminated sediments on the East Antarctic shelf: evidence for episodic bottom water production during the Holocene? *Marine Geology*.

Heine, J.C. and Speir, T.W. (1989). Ornithogenic soils of the Cape Bird Adélie penguin rookeries, Antarctica. *Polar Biology* 10: 89-99.

Ingolfsson, O., Hjort, C., Berkman, P.A., Bjorck, S., Colhoun, E., Goodwin, I.D., Hall, B., Hirakawa, K., Melles, M., Moller, P and Prentice, M.L. (1998).

Antarctic glacial history since the Last Glacial Maximum: an overview of the record on land. *Antarctic Science* 10(3): 326-344.

Joyner C.C. (1988). The Antarctic legal regime and the Law of the Sea. *Oceanus* 31 No.2: 22-27.

Knox, G.A. (1994). The Biology of the Southern Ocean. Cambridge: Cambridge University Press: 15.

Leventer, A. (1992). Modern distribution of diatoms in sediments from the George V Coast, Antarctica. *Marine Micropaleontology* 19: 315-332.

Massom, R.A., Harris, P.T., Michael, K.J. and Potter, M.J. (1998). The distribution and formative processes of latent-heat polynyas in East Antarctica. *Annals of Glaciology* 27: 420-426.

Mawson, D. (1997). *The Home of the Blizzard*. Kent Town, S.A.: Wakefield Press.

McMinn, A. (2000). Late Holocene increase in sea ice extent in fjords of the Vestfold Hills, eastern Antarctica. *Antarctic Science* 12 (1): 80-88.

Parish, T.R and Bromwich, D.H. (1987). The surface windfield over the Antarctic ice sheets. *Nature* Vol. 328: 51-54.

Press, F. and Seiver, R. (1986). *Earth*. New York: W.H. Freeman and Co.: 291.

Rintoul, S.R. (1998). On the Origin and Influence of Adélie Land Bottom Water. In: Jacobs, S.S. and Weiss, R.F. (editors). *Ocean, Ice and Atmosphere: Interactions at the Antarctic Continental Margin. Antarctic Research Series Volume 75*. Washington DC: American Geophysical Union: 151-171.

Roberts, D. and McMinn, A. (1999). A diatom-based palaeosalinity history of Ace Lake, Vestfold Hills, Antarctica. *The Holocene* Vol. 9: 401-408.

Roberts, D., McMinn, A. and Zwartz, D. (2000). An initial palaeosalinity history of Jaw Lake, Bunger Hills based on a diatom-salinity transfer function applied to sediment cores. *Antarctic Science* 12(2): 172-176.

Verkulich, S.R and Hiller, A. (1994). Holocene deglaciation of the Bunger Hills revealed by ^{14}C measurements on stomach oil deposits in snow petrel colonies. *Antarctic Science* 6(3): 395-399.

Walton, D.W.H. (1987). *Antarctic Science*. London: Cambridge University Press.

Whitworth III, T., Orsi, A.H., Kim, S.J., Nowlin Jr., W.D. and Locarnini, R.A. (1998). Water Masses and Mixing Near the Antarctic Slope Front. In: Jacobs, S.S. and Weiss, R.F. (editors). *Ocean, Ice and Atmosphere: Interactions at the Antarctic Continental Margin. Antarctic Research Series Volume 75*. Washington D.C.: American Geophysical Union: 1-27.

Williams, G.D. (2000), G.D. Williams, Antarctic.CRC, University of Tasmania [personal communication, 1 September 2000].

Wong, A.P.S., Bindoff, N.L. and Forbes, A. (1998). Ocean-Ice Shelf Interaction and Possible Bottom Water Formation in Prydz Bay, Antarctica. In: Jacobs, S.S. and Weiss, R.F. (editors). *Ocean, Ice and Atmosphere: Interactions at the Antarctic Continental Margin. Antarctic Research Series Volume 75*. Washington D.C.: American Geophysical Union: 173-187.

Wright, R., Anderson, J.B. and Fisco, P.P. (1983). Distribution and Association of Sediment Gravity Flow Deposits and Glacial/Glacial-Marine Sediments Around the Continental Margin of Antarctica. In: Molina, B.F. (editor). *Glacial-Marine Sedimentation*. New York: Plenum Press: 265-300.

Figure A.1 Facies legend for Mertz Drift cores. SMO = siliceous mud and diatom ooze.

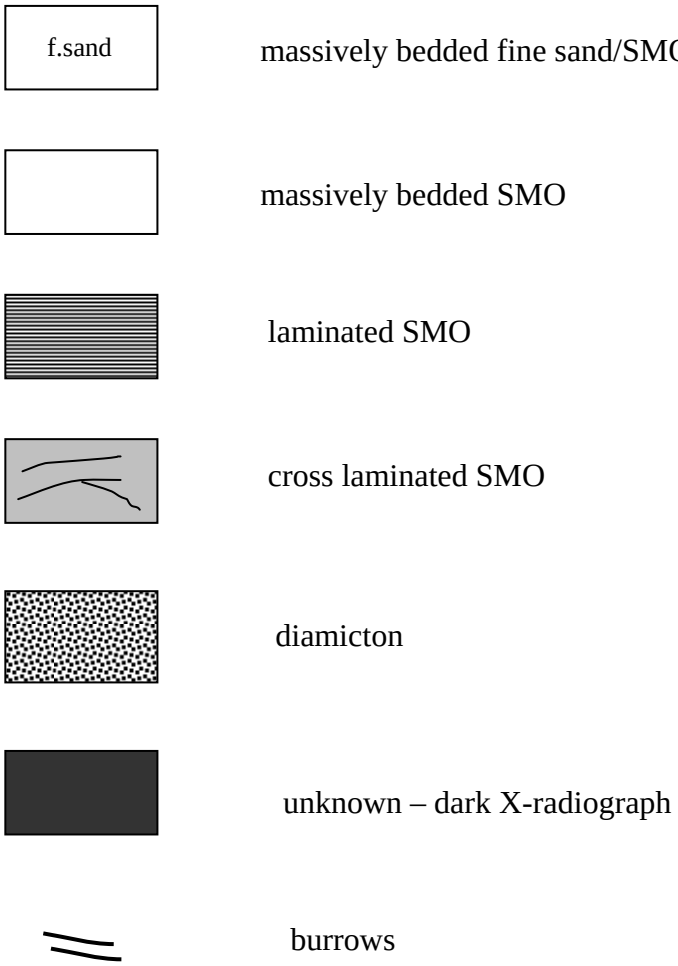

Figure A.2 Facies interpretation log and gravel content of core 11GC02.

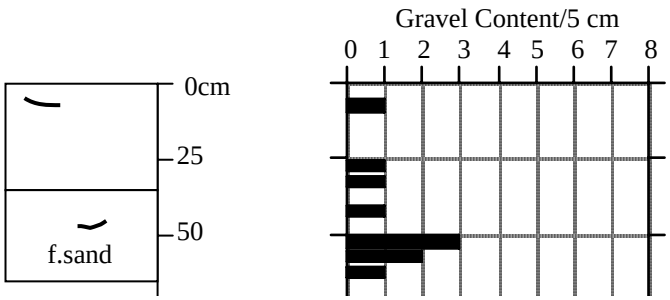

Figure A.3 Facies interpretation log and gravel content of core 11GC03.

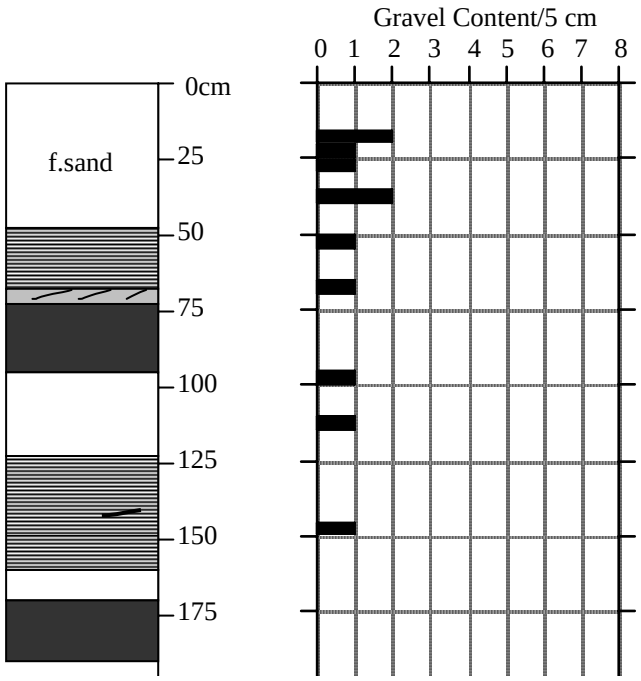

Figure A.4 Facies interpretation log and gravel content of core 12GC04.

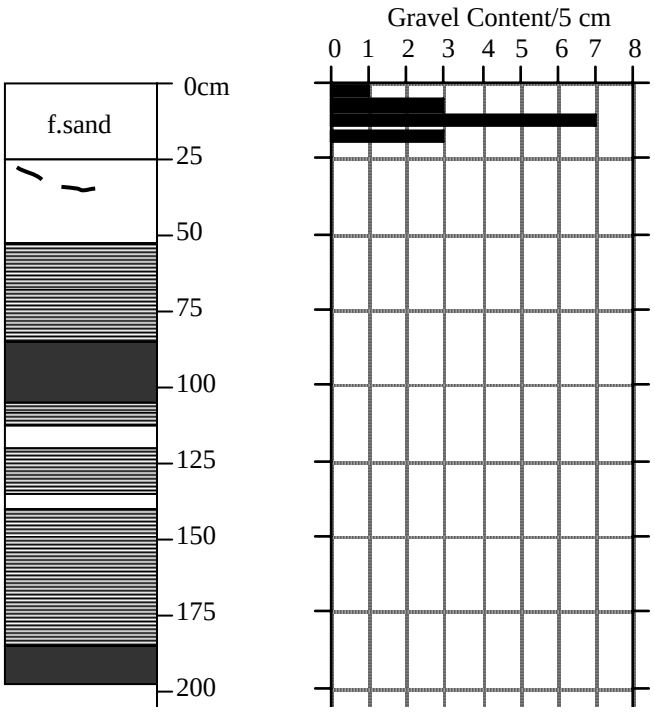

Figure A.5 Facies interpretation log (with uncorrected radiocarbon ages) and gravel content of core 13GC05.

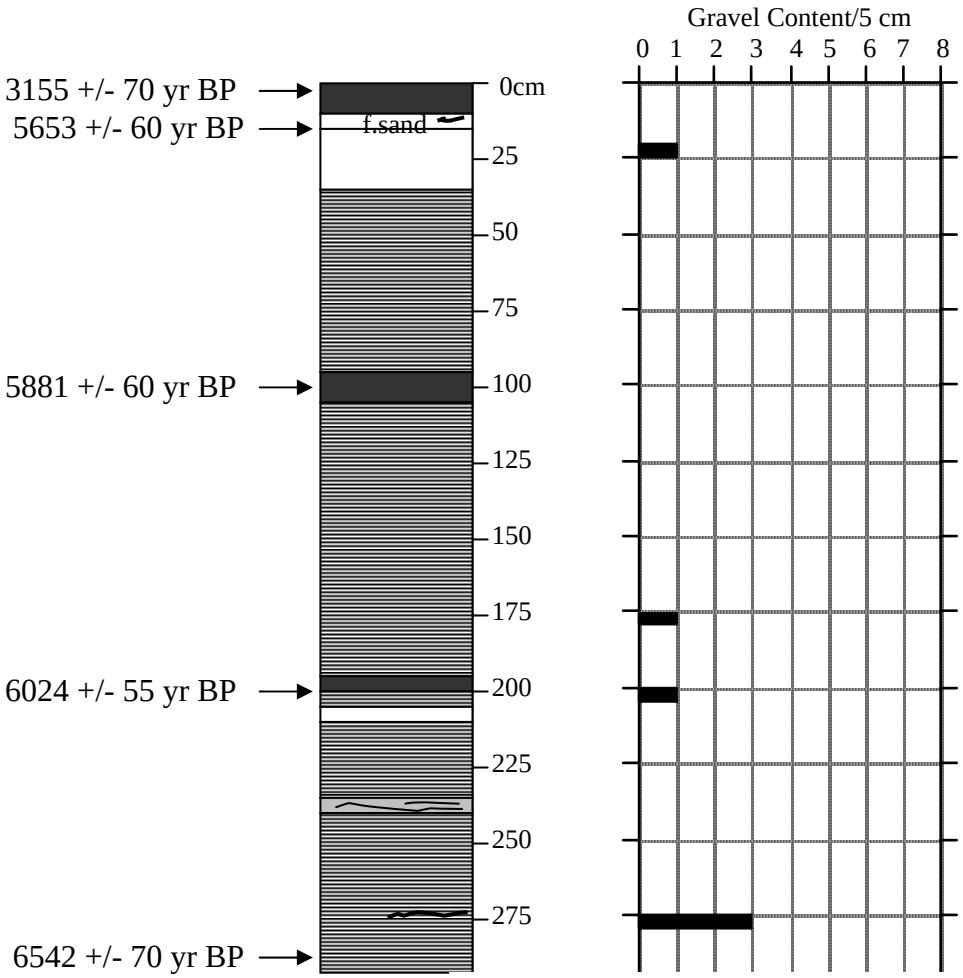

Figure A.6 Facies interpretation log (with uncorrected radiocarbon ages) and gravel content of core 13GC06.

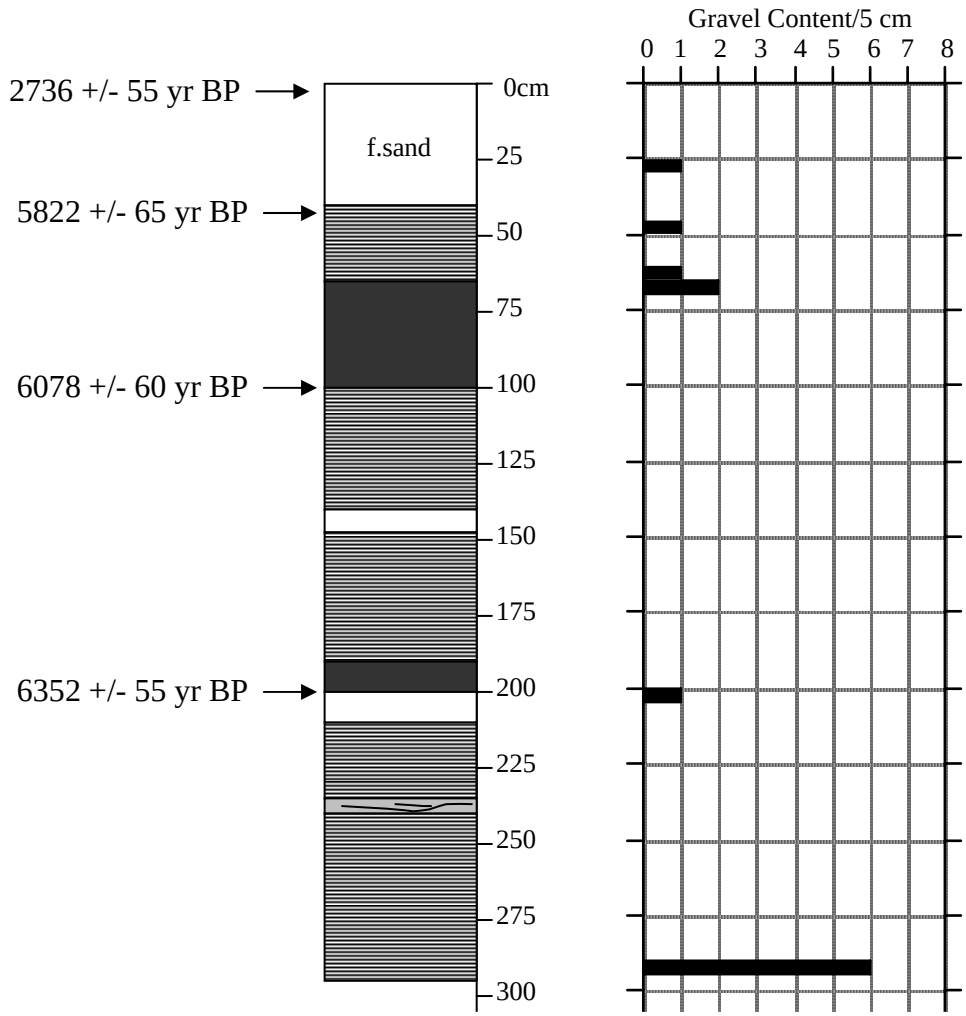

Figure A.7 Facies interpretation log (with uncorrected radiocarbon ages) and gravel content of core 14GC07.

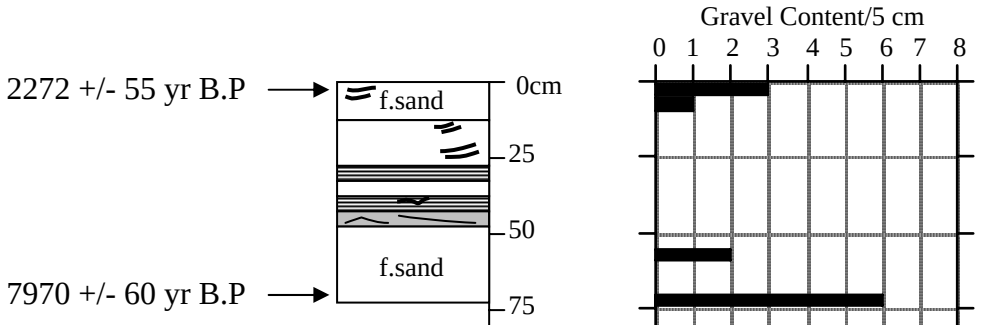

Figure A.8 Facies interpretation log and gravel content of core 15GC08.

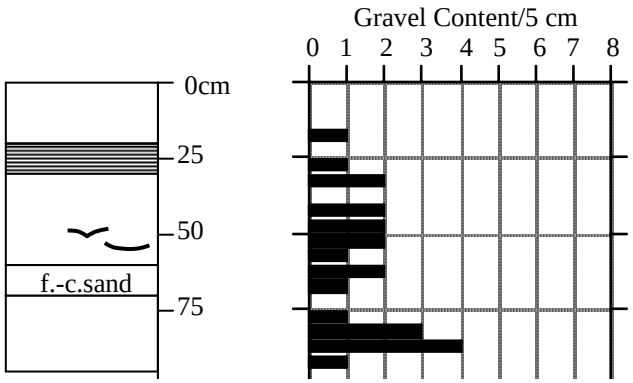

Figure A.9 Facies interpretation log (with uncorrected radiocarbon ages) and gravel content of core 15GC09.

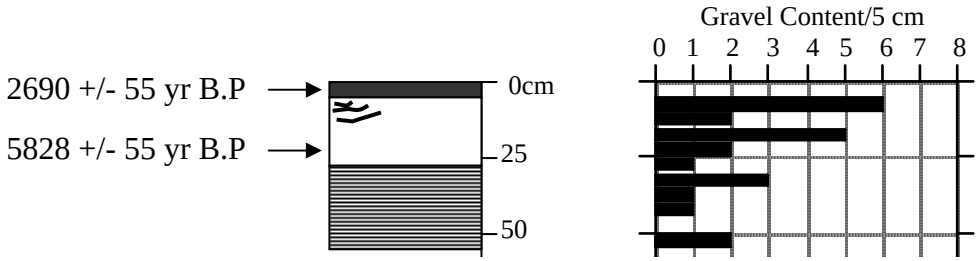

Figure A.10 Facies interpretation log and gravel content of core 16PC01.

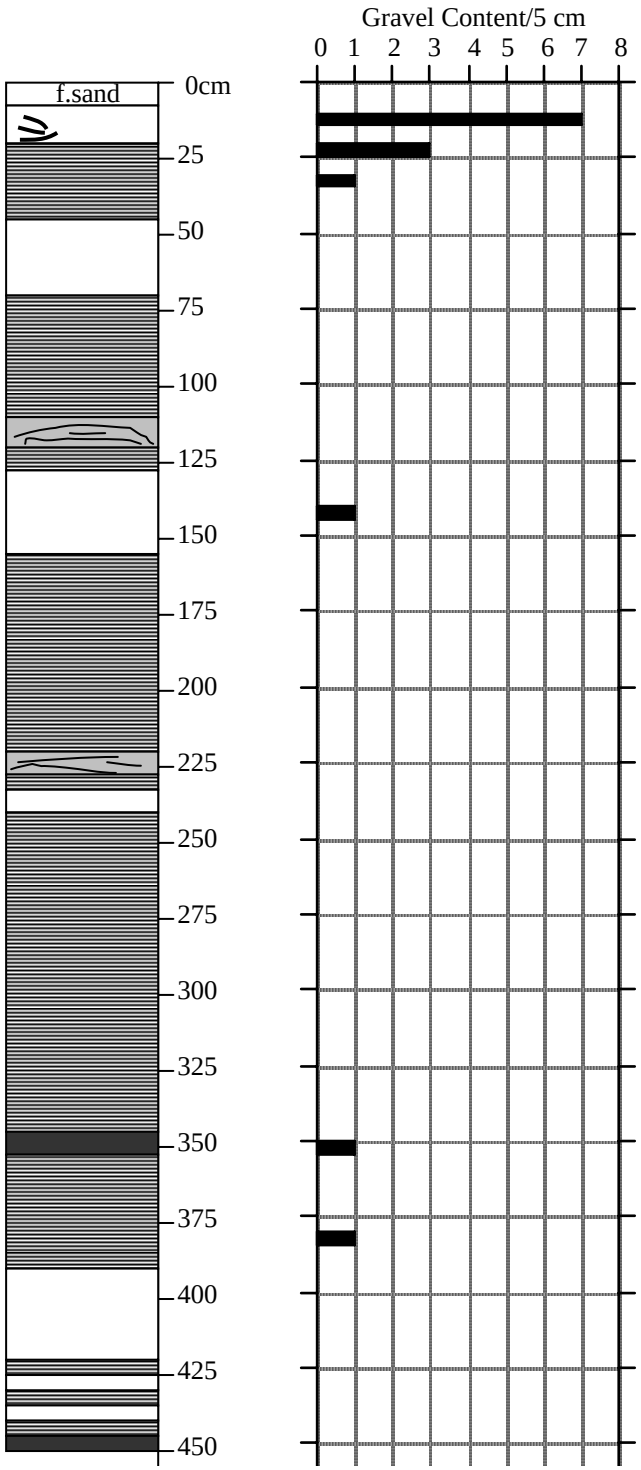

Figure A.11 Facies interpretation log (with uncorrected radiocarbon ages) and gravel content of core 17PC02.

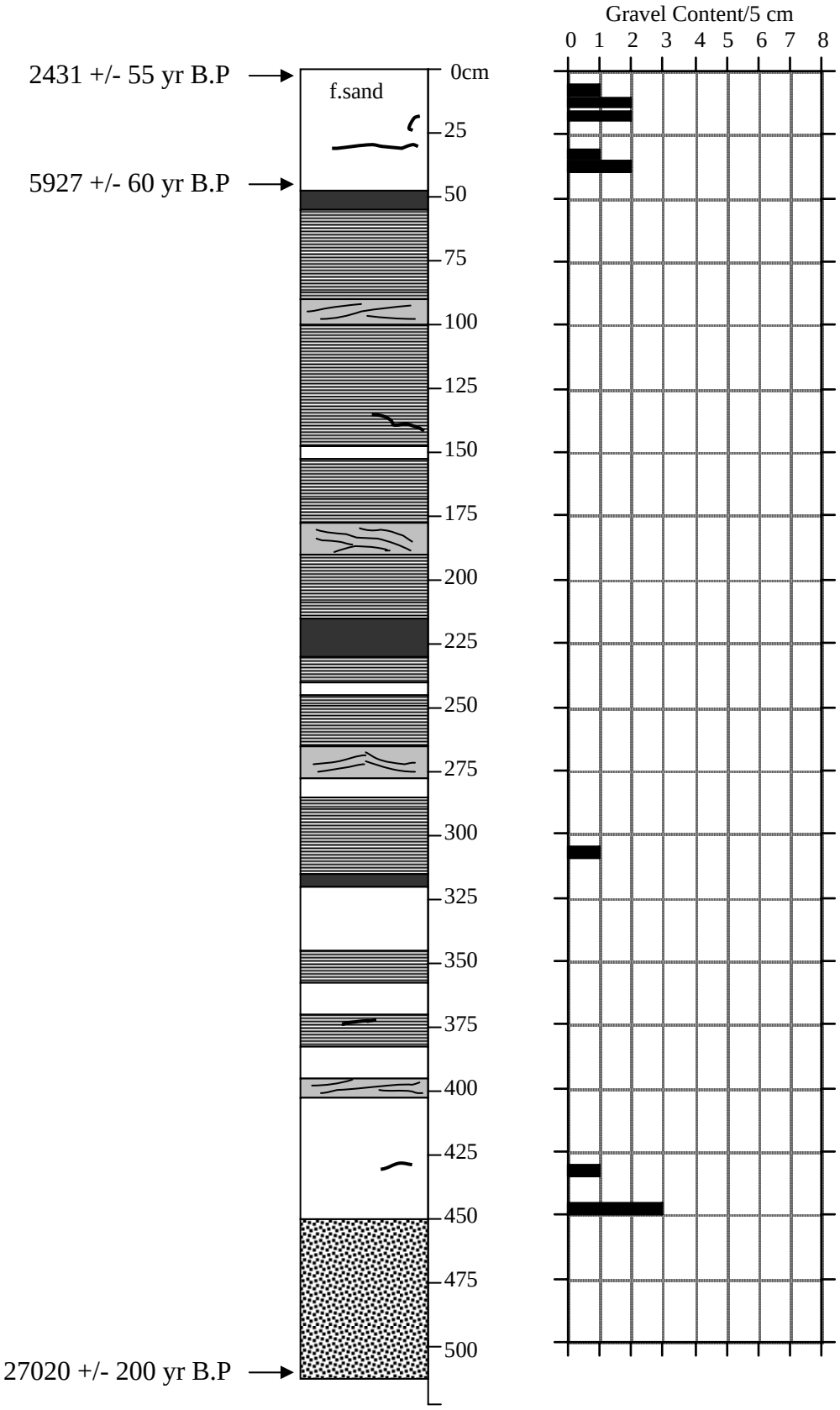

Figure A.12 Facies interpretation log and gravel content of core 18PC03.

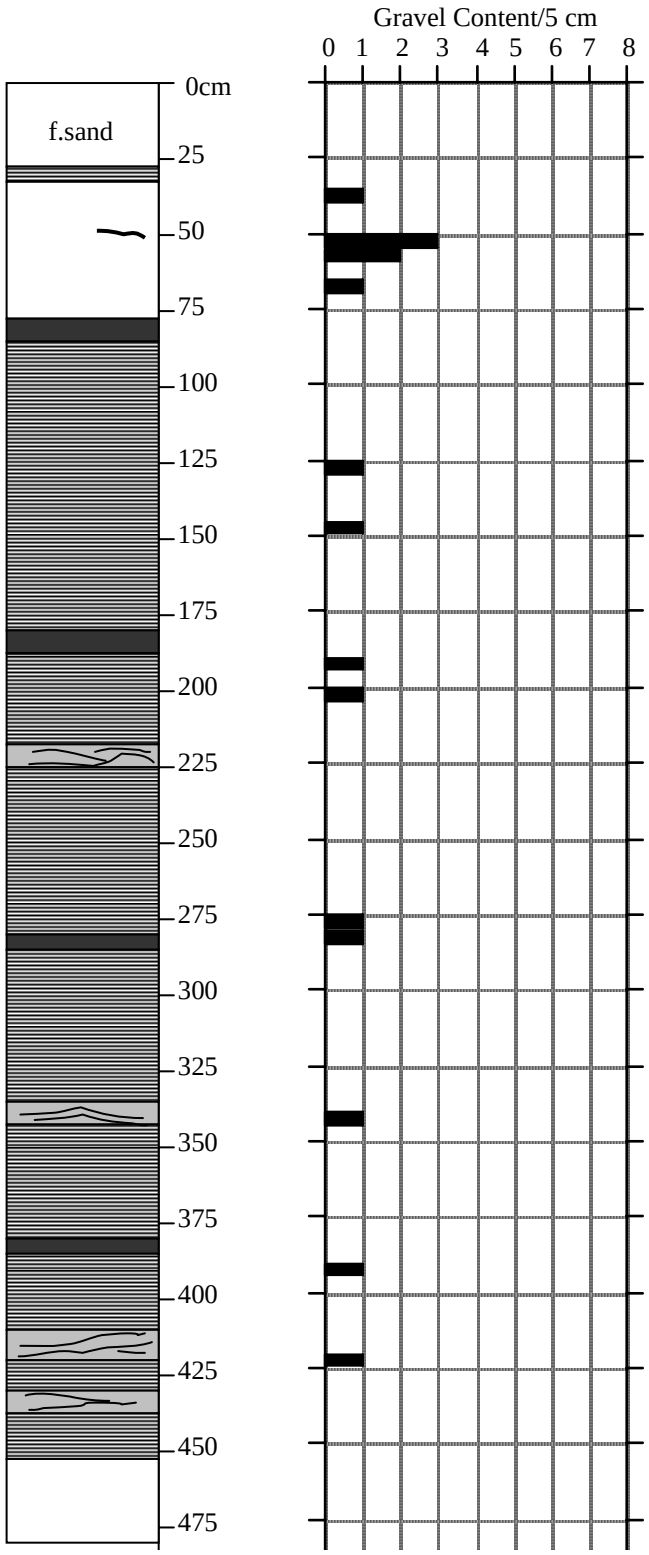

Figure A.13 Facies interpretation log and gravel content of core 19PC04.

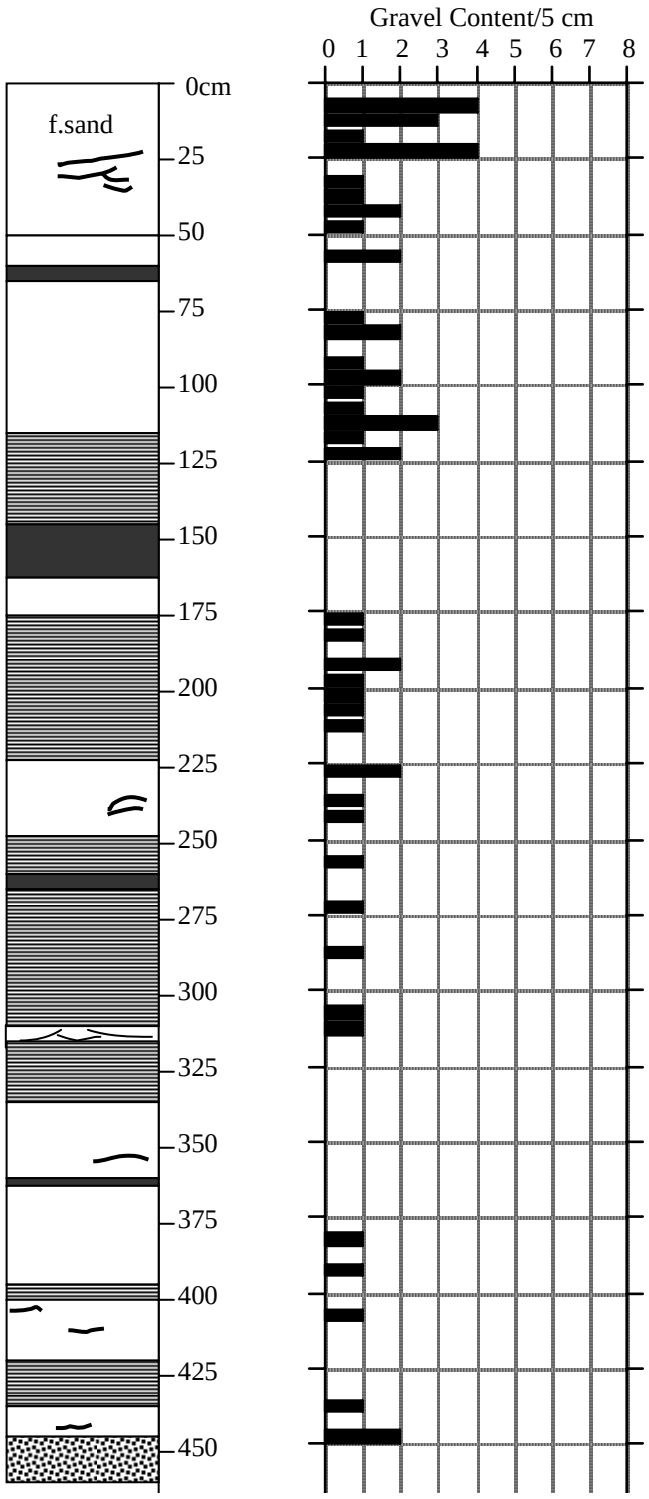

Figure A.14 Facies interpretation log and gravel content of core 20PC05.

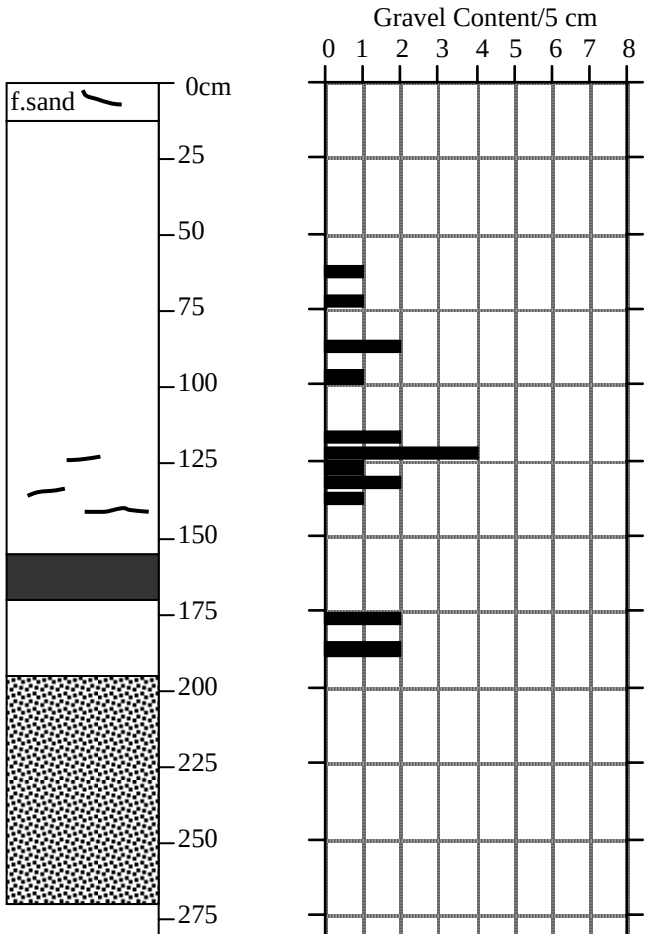

Figure A.15 Facies interpretation log and gravel content of core 23PC09.

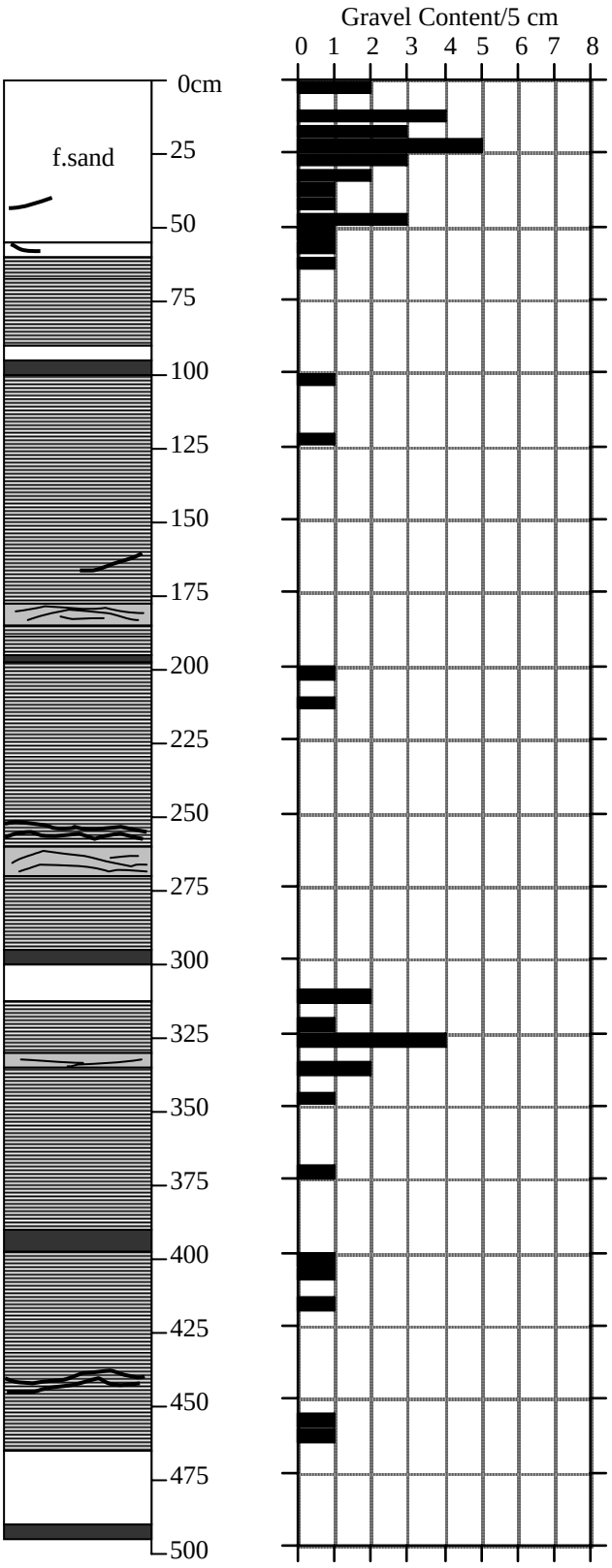

Figure A.16 Facies interpretation log and gravel content of core 24PC10.

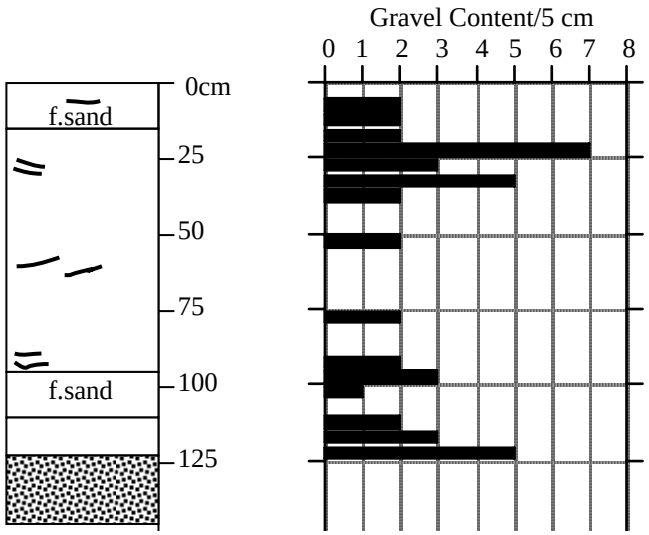

Figure A.17 Facies interpretation log (with uncorrected radiocarbon ages) and gravel content of core 25PC11.

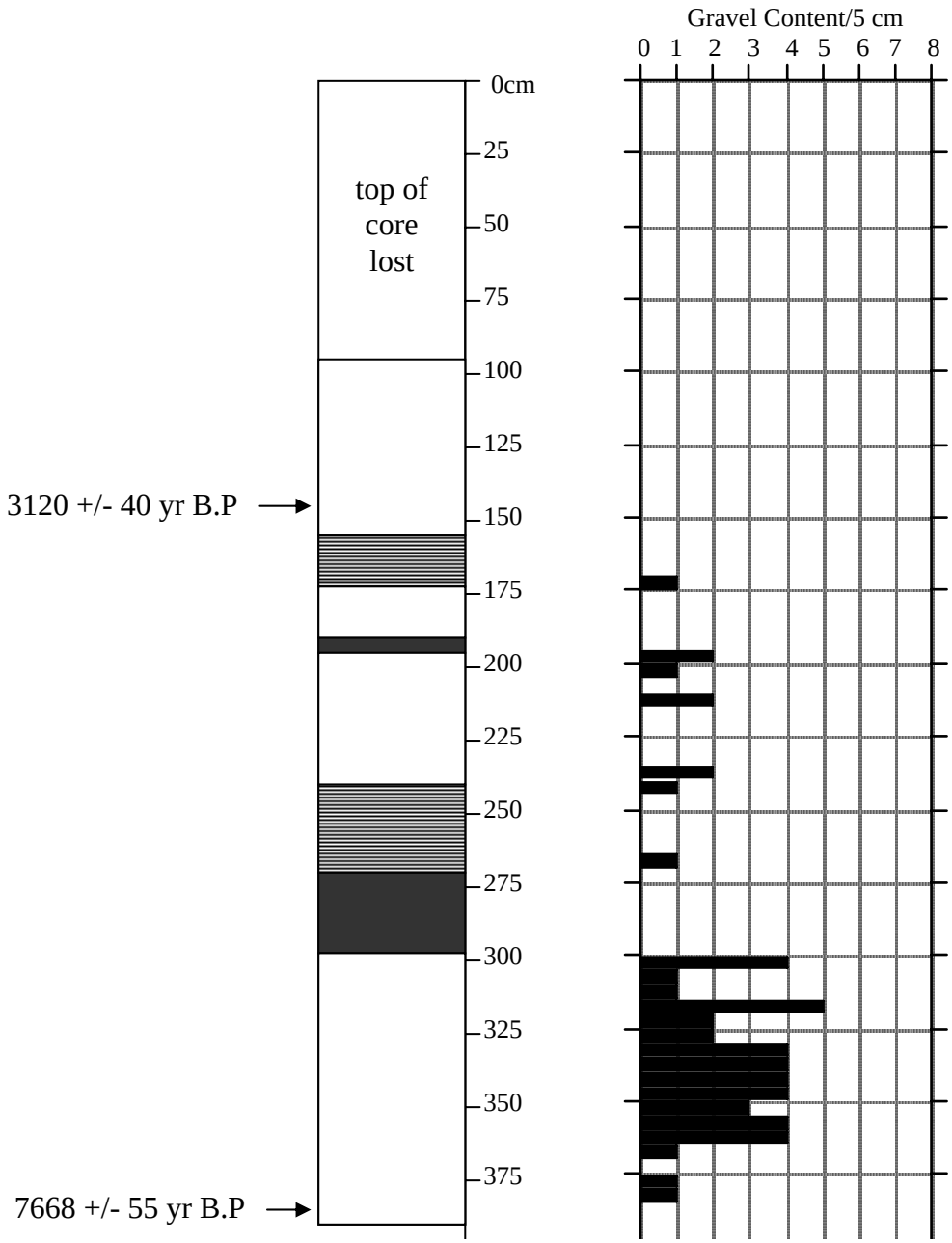

Figure A.18 Facies interpretation log (with uncorrected radiocarbon ages) and gravel content of core 26PC12.

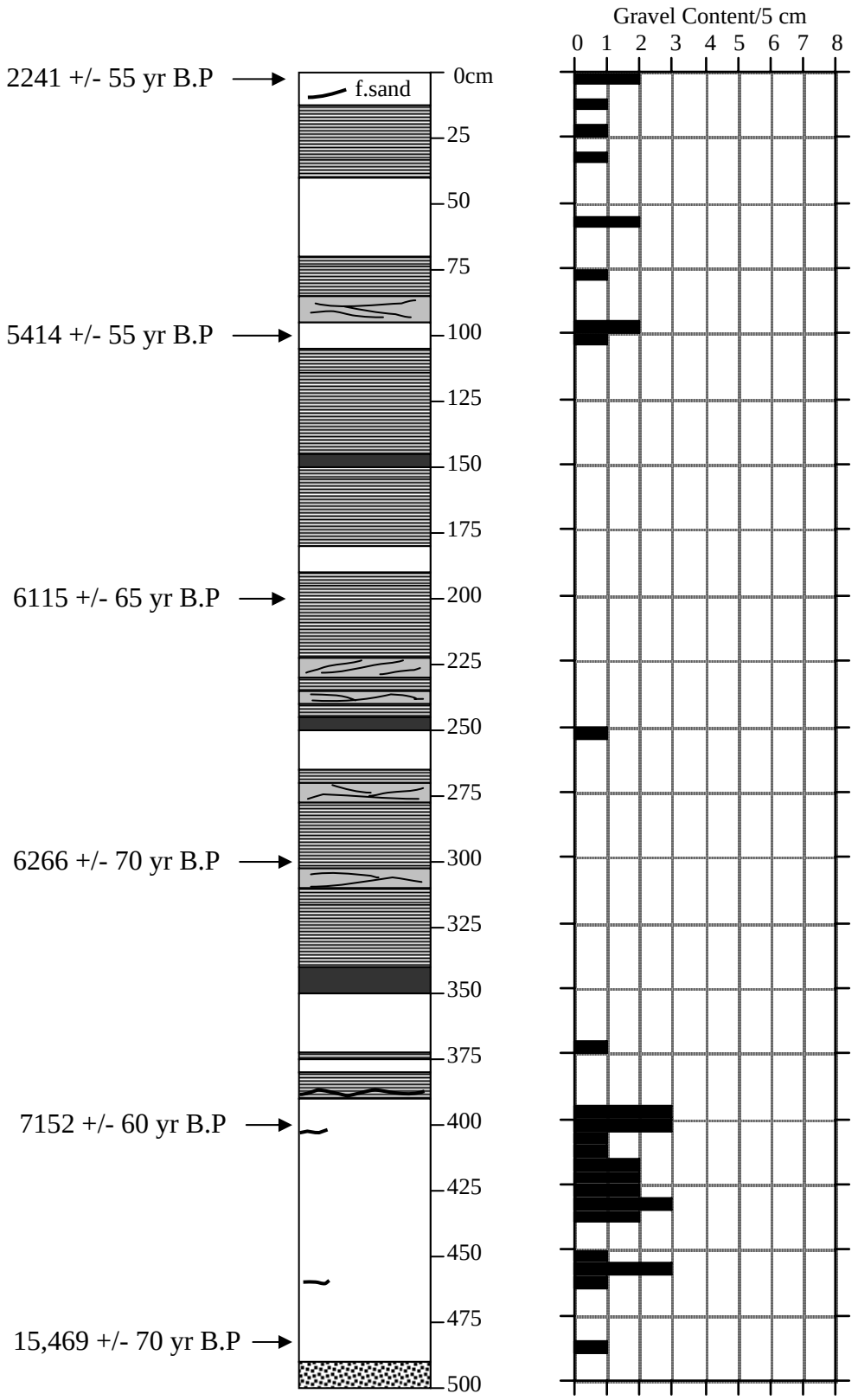

Figure A.19 Facies interpretation log and gravel content of core 27PC13.